RNA medicines *in vivo*: delivery of mRNA, siRNA, PMOs and Cas9 mRNA/sgRNA

von Jana Pöhmerer

Inaugural-Dissertation zur Erlangung der Doktorwürde der
Tierärztlichen Fakultät der Ludwig-Maximilians-Universität
München

RNA medicines *in vivo*: delivery of mRNA, siRNA, PMOs and Cas9 mRNA/sgRNA

von Jana Pöhmerer
aus Neustadt an der Aisch

München 2024

Aus dem Veterinärwissenschaftlichen Department der Tierärztlichen Fakultät
der Ludwig-Maximilians-Universität München

Lehrstuhl für Molekulare Tierzucht und Biotechnologie

Arbeit angefertigt unter der Leitung von Univ.-Prof. Dr. Eckhard Wolf

Angefertigt am: Lehrstuhl für Pharmazeutische Biotechnologie, Fakultät für
Chemie und Pharmazie der Ludwig-Maximilians-Universität München

Mentor: Univ.-Prof. Dr. Ernst Wagner

Gedruckt mit Genehmigung der Tierärztlichen Fakultät
der Ludwig-Maximilians-Universität München

Dekan: Univ.-Prof. Dr. Reinhard K. Straubinger, Ph.D.

Berichterstatter: Univ.-Prof. Dr. Eckhard Wolf

Korreferenten: Univ.-Prof. Dr. Kaspar Matiasek

Tag der Promotion: 06. Juli 2024

Für meine Eltern

TABLE OF CONTENTS

ABBREVIATIONS

°C	degree Celsius
µg, µL	microgram(s), microliter(s)
18PA	1,2-dioleoyl-sn-glycero-3-phosphate
Ago	argonaute
ALT	alanine aminotransferase
APC	antigen presenting cell
ApoE	apolipoprotein E
ASO	antisense oligonucleotide
ASGPR	asialoglycoprotein receptor
AST	aspartate aminotransferase
bp	base pairs
BUN	blood urea nitrogen
Cas9	CRISPR (*see below*) associated protein 9
cDNA	copy/complementary DNA
cf.	confer
CLAN	cationic lipid-assisted nanoparticles
CNS	central nervous system
CPP	cell penetrating peptide
Crea	creatinine
CRISPR	clustered regularly interspaced short palindromic repeats
Ctrl	control (group)
DBCO	dibenzocyclooctyne
DC	dendritic cell
DMD	Duchenne muscular dystrophin
DMEM	Dulbecco's modified Eagle's medium
DMG-PEG	2-dimyristoyl-sn-glycerol-methoxy polyethylene glycol
DNA	deoxyribonucleic acid
DODAP	1,2-dioleoyl-3-dimethylaminopropane
DOPE	1,2-dioleoyl-sn-glycero-3-phosphoethanolamine
DOTAP	1,2-dioleoyl-3-trimethylammonium-propane
DOTMA	N-[1-(2,3-dioleyloxy) propyl]-N, N, N-trimethylammoniumchloride
DSB	double stand break
dsDNA	double-stranded DNA
DSPC	distearoyl phosphatidylcholine
eGFP	enhanced green fluorescent protein
EDTA	edetate calcium disodium
EPR	enhanced permeability and retention
FBS	Fetal bovine serum
FVII/FVIII	factor VII/VIII
siVII/siVIII	siRNA targeting FVII/FVIIII

FELASA	Federation of European Laboratory Animal Science Associations
FDA	Food and Drug Administration
g	gram
G	Birmingham gauge (parameter for needle diameter)
GalNAc	N-acetylgalactosamine
h	hour(s)
hATTR	hereditary transthyretin amyloidosis
HBG	HEPES buffered glucose
HC	hepatocyte
HDR	homology directed repair
HIV	human immunodeficiency virus
i.a.	*inter alia*
i.e.	*id est* (that is)
i.m.	intramuscular(ly)
INDEL	insertion (and/or) deletion
i.v.	intravenous(ly)
IVT	*in vitro* tanscribed
KC	Kupffer cell
LAF	lipo-amino fatty acid
LDL(R)	low density lipoprotein (receptor)
LNP	lipid nanoparticle
LSEC	liver sinusoidal endothelial cell

Luc	luciferase
MAC	macrophage
MFI	mean fluorescence intensity
mg, mm	milligram(s), millimeter(s)
miRNA	micro RNA
mRNA	messenger RNA
n	number of samples
NHEJ	non-homologous end joining
N/P	polymer nitrogen to nucleic acid phosphate ratio
NA	nucleic acid
NPC	non-parenchymal cell
OAA	oligoaminoamide
ORF	open reading frame
p.i.	*post injectionem* (after injection)
PAM	proto-spacer adjacent motif
PBS	phosphate-buffered-saline
PCR	polymerase chain reaction
pDNA	plasmid DNA
PEG	polyethylene glycol
Ph.D.	Doctor of Philosophy
PLL	poly(*L*- lysine)
PM	polyplex micelle
PMN	polymorphonuclear leukocytes/neutrophils

PMO	phosphorodiamidate morpholino oligomer
pre-mRNA	precursor mRNA
RES	reticuloendothelial system
RISC	RNA-induced silencing complex
RLU	relative light units
RNA	ribonucleid acid
RNAi	RNA interference
RNP	ribonucleoprotein
rpm	rounds per minute
RT-PCR	reverse transcription - polymerase chain reaction
S	spike
s.c.	subcutaneous(ly)
S.E.M.	standard error of the mean
SARS-CoV-2	severe acute respiratory syndrome-related coronavirus 2
SD	standard deviation
sec	second
SC	stellate cell
sgRNA	single guide RNA
siRISC	small interferring RISC
siRNA	small interferring RNA
SMA	spinal muscular atrophy
SPF	specific pathogene-free
SOPF	specific and opportunistic pathogen-free
SORT	selective organ targeting
SPAAC	strain-promoted alkyne-azide cycloaddition
SPPS	solid-phase peptide synthesis
SSO	splice-switching oligonucleotide
Stp	succinoyl tetraethylene pentaamine
TALEN	transcription activator-like effector nuclease)
TIDE	tracking of indels by decomposition
TTR	transthyretin
Tf	transferrin
UTR	untranslated region
XP	xenopeptide
ZAL	zwitterionic amino lipid
ZFN	zink finger nuclease

I. INTRODUCTION

In this chapter, a brief introduction should facilitate convenient access to the topic of RNA medicines and different delivery strategies in vivo. Thereby, especially aspects of importance for the main parts of the thesis are highlighted and other areas of the wide field of nucleic acid therapies are not included.

1. Intracellular delivery of nucleic acid based nanoagents

Addressing the disease right by its root, can be seen as the basic idea of genetic engineering approaches which were highly discussed already during the 1960s [1, 2]. Here, genetic transfer was accomplished by *e.g.* simple proteins to increase the infectivity of viral ribonucleic acid (RNA) [3]. Since then, the field of nucleic acid therapy has evolved into a revolutionary area of next-generation medicine for personalized treatment of life-threatening diseases such as cancer [2] and other intractable, hereditary diseases [4].

1.1. Nucleic acid medicines

By introducing genetic material into a host organism, gene therapy focuses, *i.a.*, on increasing the expression of beneficial and inhibition of pathogenic proteins for therapeutic purposes. [5]. This concept has its origins more than 50 years ago [6] and symbolizes the clinical potential of nucleic acid drugs. Unlike small-molecule or antibody-based drugs, RNA therapeutics involve more precise and effective strategies for reaching even so-called undruggable target sites [7, 8]. In 1978, Stephenson *et al*. [9] proved inhibition of viral RNA by nucleic acids and only 12 years later, Wolff *et al.* [10] demonstrated one of the first *in vivo* transfers of vector-free RNA and deoxyribonucleic acid (DNA) constructs into the skeletal muscle of mice. Since then, enormous progress has been made in the rapidly developing field of nucleic acid medicine: To date, a total of 29 RNA therapeutics and 30 gene therapies, including genetically modified cell therapies, have reached the market. Of these, 8 RNA-based and 6 gene therapies were approved in the last year alone [11].

The high versatility of nucleic acid medicines refers to the possibility to exploit biological mechanisms of cells and following gain-of-function as well as loss-of function strategies [2]. In this way, RNA therapeutics can be used

at various stages of the molecular process of transferring genetic information into proteins. [12]. This suggests that cellular gene expression can be enhanced by the direct introduction of exogenous copies of mutated endogenous genes or messenger RNA (mRNA) on the one hand. On the other hand, the production of target molecules can be suppressed by RNA interference (RNAi) or gene knock-out by programmable nucleases [5]. In addition, nucleic acid medicine has the unique ability to keep pace with rapidly evolving changes in diseases, such as cancer mutations or sudden viral pandemics [13].

According to their mode of action and target site (**Figure 1**), nucleic acid-based drugs can be classified into different categories [2]. At first, mRNA drugs represent a straightforward approach of genetic transfer by introducing protein transcripts into various cell types, even in a non-dividing state, and without the risk of integration into the host genome, unlike DNA therapies. Therefore, mRNA-based medicines only need to reach the cytosol of the cell [14]. However, effective ribosomal translation is restricted to poor bioavailability of the negatively charged, synthetic RNA [15]. That is why, chemical modulation of the *in vivo* transcribed (IVT) mRNA is one major effort to improve this gain-of-function strategy [14] (*see below*). On the other side, loss-of-function approaches can be enforced by the insertion of *e.g.* small interfering RNA (siRNA) which specifically targets cellular mRNA and induces its degradation. This technology also does not require nuclear entry, but is based on an endogenous mRNA cleavage complex, the RNA-induced silencing complex (RISC) with a central argonaute (Ago) protein [16]. In order to further precisely modulate gene expression, another specific way of interfering with cellular mechanisms is represented by antisense oligonucleotides (ASOs). These are nucleic acid oligomers that target the endogenous mRNA by complementary Watson-Crick base pairing [17]. Of this group, phosphorodiamidate morpholino oligomers (PMOs) are representatives of splice-switching oligonucleotides (SSOs), designed to block cellular target sites of pre-mRNA splicing and consequently induce exon skipping in the nuclear compartment of cells. In this way, it is possible to restore the normal splicing mechanisms of functional proteins [18]. Finally, the way in which genetic information is

expressed can also be influenced one step earlier by directly modifying the genomic DNA. Therefore, a widely used and revolutionary technology is the so-called clustered regularly interspaced short palindromic repeats (CRISPR) – associated protein 9 (Cas9), which triggers cellular repair mechanisms through a double-strand break (DSB) in the vicinity of mutated DNA sequences. In this way, either functioning gene sequences can be restored or the expression of harmful counterparts can be suppressed [5]. Co-delivery of Cas9 mRNA and single guide RNA (sgRNA) enables rapid Cas9 protein translation and subsequent sgRNA-mediated targeting to the intranuclear site of action, where the ribonucleoprotein (RNP) complex acts as a programmable endonuclease.

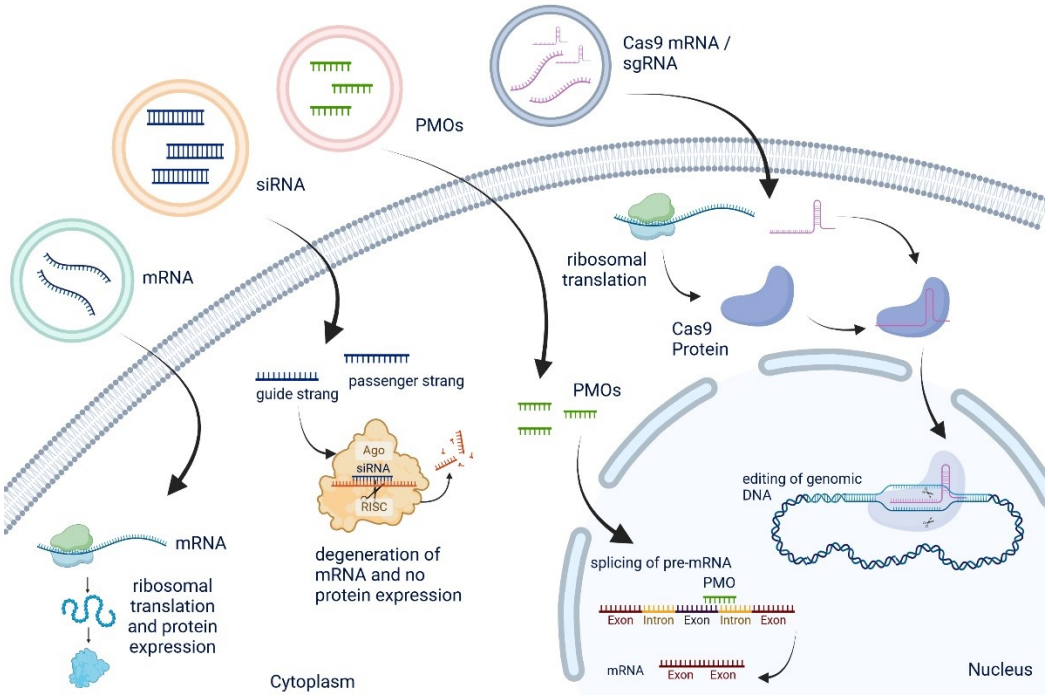

Figure 1. Overview of the biological mechanism of action and the intracellular target site of selected RNA therapeutics. Different nucleic acid cargos, compacted into nanocarriers (coulored circles), reach specific intracellular target sites: mRNA (green nanocarrier) and siRNA (yellow nanocarrier) stay in the cytosol, whereas PMOs (red nanocarrier) and Cas9 mRNA/sgRNA (blue nanocarrier) require intranuclear transport. At the ribosome, mRNA is translated into proteins. However, siRNA, loaded into the RISC complex with a central Ago protein, triggers gene silencing via mRNA degeneration. In the nucleus, PMOs interfere with splicing mechanisms of the pre-mRNA and the CRISPR Cas9 RNP complex induces genome editing of the double strand DNA. This figure was created with Biorender.com.

In summary, the molecular tools mentioned above represent only a selection of the many different nucleic acid-based therapeutic approaches that have been the basis for the success of gene therapy drugs in recent years. Plasmid DNA (pDNA), for example, is also an important therapeutic approach that was primarily explored in the early years of gene therapy [19] and still plays an important role in the field of *i.a.* cancer vaccines [20]. However, the focus of the present work will be on RNA therapies, where a key difficulty is to ensure precise and effective delivery of the therapeutic payload [7].

1.2 Delivery systems/carriers

Due to their size and surface charge, unmodified RNA-based therapeutics are unlikely to cross lipid bilayers in order to reach intracellular target sites and are prone to degradation by ubiquitous RNases [7, 13]. The compaction of RNA into nanocarriers [21] is therefore essential for efficient transfer of nucleic acid into cells, also known as transfection [22, 23]. By taking advise from nature, early delivery systems were designed with a high degree of similarity to viruses [24]. Because of optimized nucleic acid compaction and penetration into the cells, virus-based nanocarriers act as dynamic [25] delivery agents with high transfection efficiency [26] and recent impact in cell-based gene therapy [27, 28]. However, significant drawbacks such as immunogenicity [29] and limited loading capacity [30] of viral vectors restrict their clinical applicability and therefore require an alternative non-viral approach. The synthetic carrier landscape includes organic and inorganic structures, where organic carriers with lipid components can build micelles, liposomes and lipid nanoparticles (LNPs), and polymer-based systems (so-called polyplexes) compromise *i.a.* complexes of polyethylenimine (PEI), poly(*L*- lysine) (PLL), or polyamidoamine (PAMAM) dendrimers [31]. The early beginnings of lipid-based synthetic nanocarriers were made with the discovery that phospholipids form spontaneous bilayer structures in aqueous environment [32]. The resulting liposomes can transport both hydrophilic nucleic acids and hydrophobic small molecules, making them an early platform for the first US Food and Drug Administration (FDA)-approved anticancer nanodrug DOXIL®, and thus a successful transition from theory

to practice [33, 34]. Based on the assumption that transfer across the negatively charged cell membrane is easier for cationic nanoparticles, positively charged lipids or polymers were directly formulated with nucleic acid, allowing stable and effective compaction of the cargo into lipoplexes or polyplexes [22, 35]. However, since permanently cationic carrier systems can exhibit harmful side effects by unspecific interactions with biological membranes and blood components [36], the development of more complex LNPs with ionizable lipids has been pursued, which are currently among the most advanced delivery systems [37].

What all synthetic carriers have in common is that they have to meet the requirements of both, the compaction and protection of the condensed nucleic acid [38] and the desired mode of administration [39]. As far as nanomedicine for intravenous cancer treatment is considered, the delivery process can be subdivided into five consecutive stages: (blood) circulation, (organ) accumulation, (tissue) penetration, (cell) internalization and (intracellular) release [40]. This so-called CAPIR cascade can be used to describe the requirements for an ideal nanocarrier, which should simultaneously exhibit stability and lability properties [41] as well as responsiveness to biological stimuli [42]. When nanoparticles come into contact with biological fluids, *e.g.* blood components, such as erythrocytes, can interact with the carriers [43] and certain plasma proteins are likely to form a specific protein corona on the surface [44]. This can have a significant impact on the (patho)physiological properties of the vector and its transport pathway within the host organism [45]. To prevent non-specific cellular uptake, clearance by the reticuloendothelial system (RES) and to prolong circulation time in the blood [46], shielding agents such as polyethylene glycol (PEG) can facilitate stable protection of the nanoparticle and payload [47]. In this way, the enhanced permeability and retention (EPR) effect can simultaneously achieve an accumulation of the nanocarrier in the vicinity of the target organ, which is mainly due to the increased extravasation of macromolecules of a certain size from the leaky vasculature and poor lymphatic drainage within the tumor tissue [48, 49]. While this mechanism is known as passive targeting, active targeting is usually achieved by using ligands, such as transferrin (Tf) [49, 50] or folate

[51], which are bound to the nanoparticle surface and mediate even higher accumulation by specific interaction with cellular receptors. In the case of LNPs, intravenously (i.v.) or intramuscularly (i.m.) administered particles often end up in the liver due to apolipoprotein E-low density lipoprotein-mediated (ApoE-LDL-mediated) uptake into hepatocytes [51, 52]. The reason for this can be explained by the physicochemical properties of LNPs, such as particle size or surface charge [53]. To increase the versatility of target organs, a selective organ targeting (SORT) strategy [54] has been developed to reach other extra-hepatic tissues for therapeutic purposes. When, for example, the molar ratio of the cationic lipid 1,2-dioleoyl-3-trimethylammonium propane (DOTAP) was changed to 50% or 30% of the anionic 1,2-dioleoyl-sn-glycero-3-phosphate (18PA) were added to the LNP formulation, the delivered nanoparticles were directed away from the liver to the lung or spleen, respectively. After reaching the target organ, penetration into deeper tissue complexes is a critical step in the delivery, especially for solid tumors that are not located near blood vessels. Active targeting strategies mentioned above as well as prolonged circulation time may be beneficial in this context, but nanoparticle size and pathological features of the tumor microenvironment are still the limiting factors [55]. Subsequent cellular uptake (internalization) can occur either via a passive endocytosis pathway, *e.g.* through clathrin [56] in the case of LNPs, or via an active receptor binding mechanism, *e.g.* mediated by ligands such as antibodies [57]. For complete transfection, a high correlation of intracellular release of nucleic acid from the surrounding vector system with prior escape from the endosome is also dependent on the endosomolytic potential of the nanocarrier [58]. The endosomal escape of lipoplexes is triggered by transient pore formation in the endosomal membrane and membrane fusion processes by LNPs, whereas polyplexes are said to escape at least partly according to the proton sponge effect [59]. This phenomenom describes an osmotic swelling of the endosome due to, *e.g.* high proton buffering capacitis of polymers such as PEI or PAMAM. However, the final rupture of the endosome is also induced by direct interactions of cationic polyplexes and polymers with endosomal membranes by promoting needle-like holes [58, 60].

Our research group, headed by Prof. Dr. Ernst Wagner (*Chair of Pharmaceutical Biotechnology; LMU, Munich*), focuses on sequence- and topology-defined xenopeptides (XP) as carriers for various nucleic acids. Definition by sequence is thereby strongly orientated towards nature, where peptides are also designed in a sequence-based manner of natural amino acids to determine their biological identity [61]. This strategy has been applied to the optimization of xenopeptides, composed of both, cationic natural amino acids with excellent carrier properties, such as lysine (for nucleic acid binding) and histidine (for endosomal buffering), and artificial building blocks with high chemical versatility, following chemical and molecular evolution approaches [39]. Using solid-phase peptide synthesis (SPPS) for simplified and precise peptide optimization, artificial oligoaminoethylene amino acids, such as succinoyltetraethylene pentaamine (Stp), were first incorporated into oligoaminoamides (OAA) to take advantage of their PEI-like proton sponge capacity [62, 63]. Thus, oligomers with defined sequences and various architectures were furthermore expanded with hydrophobic domains of fatty acids to improve the stability of, *e.g.* T-shape topologies for potent siRNA delivery. These lipo-OAAs form so-called lipopolyplexes with nucleic acids, which define an intermediate complex of cationic polymers and lipids [22, 62]. By systematically modifying the structural motifs and investigating the relationships between transfection efficiency and physicochemical properties of the nanocarriers [64], a huge library with over 1800 sequence-defined xenopeptides is now established in our group. Adapted to the requirements of the intracellular transport process as well as of different nucleic acid payloads [41, 65-67], additional ligands, shielding or moieties for enhanced cellular entry promoted transfection properties of dynamic synthetic carriers [68]. In our recent studies, we focus on the optimization of double pH-responsive lipo-xenopeptides with a molecular chameleon character [69]. This novel class of highly potent, non-viral nanocarriers combines polar cationizable Stp units and at least two apolar reversibly cationizable lipo-amino fatty acids (LAFs) with a pH-tunable polarity. This means that at neutral pH, the LAFs are hydrophobic and become hydrophilic in the acidic milieu of the endosome. Incorporated into both, polyplexes and LNPs, they exhibit favorable properties for highly efficient

delivery of various nucleic acids with fast transfection kinetics at ultra-low doses *in vitro* and *in vivo* [69, 70].

2. Selection of nucleic acid cargos

Smaller molecules such as siRNA or ASOs do not necessarily require complex nanocarriers, but can be molecularly modified to increase stability as well as delivered as *e.g.* simple peptide conjugates. Larger carriers such as mRNA or DNA, on the other hand, must be encapsulated in stable vector systems to ensure successful transfection [31]. In the following, a selection of nucleic acid carriers and their intracellular delivery strategies are briefly discussed to provide a better understanding of the applied systems of the experimental thesis part.

2.1. Protein expression by messenger RNA

Nanocarriers encapsulating mRNA have proven their potential over the last couple of years, mainly since mRNA-based vaccines have been emerged for clinical approval during the COVID-19 pandemic in 2020 [71-73]. Moreover, mRNA-based therapeutics have become an advanced field for a variety of treatment options, such as vaccinations, cancer immunotherapy, genetic disorder treatments or protein replacement [14, 74, 75]. However, there are still some hurdles to overcome regarding the delivery process, as unmodified mRNA lacks sufficient stability in the biological environment [76]. Basically, IVT mRNA is composed of different structural elements, like its eukaryotic counterpart. The largest sequence is the open reading frame (ORF), which contains the protein transcript and is surrounded by a 5' and 3' untranslated region (UTR). In addition, both ends of the single-stranded RNA molecule are flanked by non-coding structural features of a 5' 7-methylguanosine cap and a 3' poly(A) tail, consisting of a long chain of adenine nucleotides [15]. By optimizing non-coding structural features, such as phosphorothiolate cap analogues [77] or poly(A) tail extension [78], the stability and translational efficiency of the mRNA can be improved, while the immunogenicity of the exogenous protein transcript is strongly attributed to the presence of nucleoside modifications, such as methyladnosine or thiouridine [79]. Nevertheless, the concern of immunogenity can be seen as a double-edged sword,

because antigen-directed cellular and humoral immune responses are particularly desirable for vaccination applications [71, 80]. Besides the optimization of the mRNA transcript, appropriate delivery systems are essential for efficient transfection of *i.e.* antigen encoding mRNA, ranging from LNPs [81] and lipopolyplexes [82], to polyplexes [83], block copolymer micelles [84], and exosomes [85]. As in the case of approved anti-COVID-19 mRNA vaccines, Comirnaty® (Tozinameran, Pfizer/BioNTech) and Spikevax® (Elasomeran, Moderna), LNPs are currently the most commonly used nanocarriers for mRNA vaccines [73]. After intramuscular injection, these RNA therapeutics, which contain the transcript for the spike (S) glycoprotein of severe acute respiratory syndrome-related coronavirus 2 (SARS-CoV-2) [86], are taken up by myocytes, dendritic cells (DCs) as part of the antigen presenting cell (APC) group, as well as by resident immune cells of lymph nodes [87]. For subsequent endosomal escape and efficient intracellular release of the mRNA payload, certain structural features of the LNP are advantageous such as the pH-dependent reversible protonation of the ionizable lipid, promoting efficient mRNA release and sufficient cellular protein expression levels, which can be addressed by optimizing the composition of the ionizable lipid [88]. Moreover, improved biocompatibility for chronic administration applications and robust immune responses, *e.g.* for i.m. vaccinations, can be achieved with improved toxicity due to biodegradable ionizable lipids. [89, 90].

2.2. RNA interference by small interfering RNA

As a loss-of-function strategy for potentially harmful proteins, the cellular mechanism of RNAi plays a critical role in the treatment of gene-associated diseases [91]. More than 20 years ago, double-stranded RNAs (dsRNAs) with homologous sequences to the target gene were discovered in a Nobel Prize-winning study of nematodes and shortly afterwards demonstrated as a natural process of gene silencing in mammalian cells [92, 93]. In contrast to mRNA, non-coding RNAs for RNAi, namely exogeneous siRNA and genome-derived microRNA (miRNA), are shorter RNA duplexes with important functions in posttranscriptional gene regulation processes and therefore high therapeutic potential, especially regarding non-druggable targets [94, 95]. As mentioned above, synthetic siRNAs utilize the cellular

machinery of specific mRNA cleavage, in which the catalytic RISC protein Ago2 mediates the activation of the guide strand through the specific binding of a ribose 2'-OH group and the small interfering RISC (siRISC) induces complementary binding to the mRNA target [96, 97]. Therefore, mRNA-like chemical modifications must be precisely performed to avoid potential adverse effects of double-stranded synthetic siRNA and to improve the stability and efficiency of therapeutic siRNA. [98, 99]. Additional neutralization of the total surface charge improves the transferability of naked siRNA, but due to the poor bioavailability of intracellular siRNA, transport vehicles are still required for efficient transfection [13].

Out of five FDA-approved siRNA-therapeutics only Patisiran (Onpattro, 2018) [100] is systemically delivered by hepatocyte-directed LNPs, whereas Givosiran (Givlaari 2019) [101], Lumasiran (Oxlumo, 2020) [102], Inclisiran (Leqvio, 2021) [103] and Vutrisiran (amvuttra, 2022) [104] are conjugated to N-acetylgalactosamine (GalNAc) for subcutaneous injections. In addition to the known success of LNPs for gene regulation in the liver [105], the use of GalNAc delivery systems represents an effective and simple strategy for targeting in the liver based on the specific binding of the polymer to the asialoglycoprotein receptors (ASGPR) on hepatocytes, but requires highly stabilized siRNA [106, 107]. LNPs, on the other hand, represent a more complex carrier system, composed of different lipidic components, which are under permanent optimization to *i.a.* efficiently target neuronal or cancer cells with improved safety profile [108, 109].

2.3. PMOs for splicing modulation

The process of precursor mRNA (pre-mRNA) splicing is an important mechanism of endogenous gene expression and is therefore highly regulated [110]. In general, the spliceosome, an endogenous ribonucleoprotein is responsible for constitutive splicing, in which each non-coding intron is removed and coding regions, called exons, are ligated. The alternative splicing mechanism involves the additional excision of one or more exons and plays a critical role in the diversity of protein phenotypes

that result from a single genotype [111, 112]. However, mutations in splicing processes are known to cause several diseases, ranging from neuromuscular disorders, such as spinal muscular atrophy (SMA) [113], to neurodegenerative tauopathies [114] and tumorgenesis [115]. Using Watson-Crick base pairing, single-stranded oligonucleotides target sequences of , *i.a*., certain splice sites and subsequently block harmful splicing mechanisms of the mRNA transcript [116]. In 1998, the ASO drug fomivirsen (Vitravene) became the first nucleic acid-based drug to be approved for blockage of viral protein translation [117]. Since then, tremendous progress has been made in the field of splice-switching SSOs, another class of ASOs, but intracellular delivery of the nuclear target remains a bottleneck [118, 119]. Although the uncharged PMO molecule can be delivered in a vector-free approach, peptide conjugation improves efficiency of cellular uptake [120] and local injections support treatment approaches for hard-to-reach targets, such as the central nervous system (CNS) [121].

2.4. CRISPR Cas9 genome editing

At the current stage, huge advances of the Nobel Prize winning CRISPR Cas9 genome editing strategies [122] are on the rise regarding clinically approved CasGevy technologies [123] and progressed clinical trials for NTLA-2001 treatment [124, 125].

CRISPR was first discovered by *Ishino et al*. (1987) in *Escherichia coli* and later revealed as a bacterial defense mechanism against viral invasion [126, 127]. Despite further improvements in exploiting the therapeutic efficacy of various CRISPR-Cas9 applications (pDNA, mRNA, RNP), the process of Cas9 mRNA/sgRNA delivery faces critical hurdles. The joint transport of two macromolecules must ensure that both, the mRNA-Cas9 protein transcript and the sgRNA, are present in the cellular compartment in sufficient concentration to enter ribosomal translation and subsequently activate the Cas9 endonuclease[13, 31]. In addition, this protein complex can only be effective for genetic manipulation if it successfully enters the nuclear compartment. One approach to overcome these challenges is cell-based *ex vivo* genome editing, which is already being explored for several

therapeutic targets, including human immunodeficiency virus (HIV) type 1, cancer immunotherapy, and Duchenne muscular dystrophy (DMD) [128]. Nevertheless, *in vivo* delivery by non-viral vectors represents an urgent approach of reduced off-target and enhanced on-target effects of Cas 9 [129]. Apart from polymeric delivery systems, such as cationic lipid-assisted nanoparticles (CLANs) [130] and polyplex micelles (PMs) [131], LNPs are the most suitable and widely used non-viral nanocarrier for co-loaded Cas9 mRNA/sgRNA. Highly advanced components, *i.a.*, range from bioreducible lipid-like particles, so-called lipidoids [132] over zwitterionic amino lipids (ZALs) [133] to SORT LNPs [134], and also the aforementioned NTLA-2001 system in late clinical development consists of a Cas9 mRNA/sgRNA LNP targeting the transthyretin (TTR) gene [124]

3. Aims of this thesis

This thesis aimed to investigate the significant potential of different established carriers in polyplexes and LNPs for *in vivo* delivery of nucleic acids (mRNA, siRNA, PMO and CRISPR Cas9 mRNA/sgRNA) into the target cell.

3.1. Lipoamino bundle LNPs for efficient mRNA transfection

In our group, recently synthesized LAF carriers [69] showed promising transfection results in the form of lipopolyplexes even in the presence of high serum as well as at low doses *in vivo.* The current work should evaluate LNPs as beneficial *in vivo* delivery platforms including the new generation of sequence – defined lipo-XP carriers.

Based on promising *in vitro* screening results, selected lipo-XPs formulated as mRNA LNPs were to be tested intravenously in tumor-bearing mice in comparison to commercially available standard ionizable lipids SM-102 (as used in the SpikeVax vaccine of Moderna) and MC3-DLin-DMA (as used in the Onpattro formulation). Luciferase mRNA as a reporter cargo was to be used, and the resulting in expression patterns *in vivo* were to be determined. A follow-up study should evaluate which exact cell types of liver, spleen and lungs could be addressed by the XP carriers in comparison to SM-102.

3.2. Targeting of liver endothelial cells with LAF siRNA LNPS

Inspired by the promising results of mRNA LNPs (as discussed in the first chapter), a further experimental setup was to be designed with the best performing LAF-Stp-LNPs as delivery systems for siRNA. Herein, the gene silencing of blood coagulation factors VII (FVII) and VIII (FVIII) was to be performed to investigate the efficient targeting of hepatocytes (HCs) and liver sinusoidal endothelial cells (LSECs), using best-performing lipoamino bundle LNPs in direct comparison to FDA-approved DLin-MC3-DMA-based LNPs.

3.3. DMD exon skipping with xenopeptide-PMOs

In another study, splicing modulation of mRNA was to be adressed, introducing a specific class of SSOs, named PMOs. Therefore, the most potent PMO carrier, T-shape **1395**-PMO, identified in a library screening of aminoethylene-lipopeptide PMO-conjugates, performed in a previously designed reporter cell model (Anna-Lina Lessl, LMU PhD-thesis 2024), had to be tested for *in vivo* application. For this purpose, a simple non-transgenic mouse model was defined in order to appraise the *in vivo* biodistribution and splicing modulation of the DMD exon 23 in various organs and muscle tissue [135].

3.4. Xenopeptide polyplexes for CRISPR Cas9 based gene editing

Above mentioned LAF-Stp carriers had been successfully introduced for codelivery of CRISPR-Cas9 mRNA / sgRNA as polyplexes or LNPs resulting in efficient genome editing in cell culture at very low dose within high serum to imitiate *in vivo* conditions (LMU PhD thesis Janin Germer, 2024). The next aim was to evaluate genome editing efficiencies of DMD exon 23 in BALB/C mice, either upon systemic intravenous or local intramuscular delivery. As a pre-experiment, intramuscular administration of luciferase mRNA should verify transfection efficiencies of potent sequence-defined XPs after local application [136].

II. MICE, MATERIALS AND METHODS

1. Mice

1.1. Mouse strains

1.1.1. A/J mice

Female A/JOlaHsd mice were purchased from Envigo RMS GmbH (Düsseldorf, Germany). This albino inbred strain is mainly common in behaviour studies as well as in the research of carcinogenesis and shows small intra-strain aggression [137]. In the current studies, A/JOlaHsd mice were used as a syngeneic animal model for N2a neuroblastoma tumors.

1.1.2. BALB/C mice

Female BALB/cJRj albino mice were received from Janvier Labs (Le Genest-St-Isle, France). This inbred strain is difficult to rear and is found in the research area of cardiovascular diseases, immunology, and oncology [138]. In our animal facility, specific and opportunistic pathogen-free (SOPF) BALB/C mice are also used as sentinel animals for regularly health monitoring investigations because of their functional innate and adaptive immune system.

1.2. Housing conditions

At the age of 5 weeks, mice arrived at the facility and were left to adjust to their new environment for at least 7 days before the start of experiments. On a daily basis, the welfare of the animals was controlled and documented referring to §11 of the German Animal Welfare Act [139]. The mice were kept in isolated ventilated cages (IVC type II long, Tecniplast, Hohenpeißenberg, Germany) in an air-conditioned room and under specific pathogen-free (SPF) conditions. The lightning did not surpass an intensity of 200 Lux and followed a 12-hours day and night rhythm. The room temperature was kept between 24-26 °C, and the air humidity was between 40-60%. Both parameters were also recorded daily. Feed (Ssniff Spezialdiäten, Soest, Germany) and water was provided *ad libitum* and both were autoclaved before getting in touch with the animals. Moreover, cages, dust-free bedding (ABEDD Vertriebs GmbH, Vienna, Austria) and enrichment materials (plastic houses, wooden tunnels and paper towels) were exchanged every week after being sterilized by an autoclave as well.

1.3. Health monitoring

In order to guarantee a specific pathogen-free environment, quaterly health analysis of two SOPF BALB/C mice were performed according to the Federation of European Laboratory Animal Science Associations (FELASA) guidelines. These examinations were done by an external laboratory (mfd Diagnostics GmbH, Wendelsheim, Germany) and always resulted in negative reports during the recent studies. The animals were ordered from the same breeder (Janvier Labs, Le Genest-St-Isle, France) and housed under equal conditions compared to those of the experimental mice. However, when it came to weekly changing of the cages and equipment, sentinel mice were exposed to 50% of used feed and bedding of the experimental mice.

2. Materials

2.1. Cell culture

Material	Source
Neuro-2a (N2a) cells (murine neuroblastoma cells)	American Type Cell Collection (ATCC) (Manassas, VA USA)
antibiotics	Sigma Aldrich (Taufkirchen, Germany)
FBS (Fetal bovine serum)	Sigma Aldrich (Taufkirchen, Germany)
HEPES	Biomol GmbH (Hamburg, Germany)
DMEM	Sigma Aldrich (Taufkirchen, Germany)

2.2. Buffers and chemicals

Material	
PBS (phosphate-buffered-saline)	136.89 mM sodium chloride, 2.68 mM potassium chloride, 8.10 mM sodium phosphate dibasic heptahydrate, 1.47 mM potassium dihydrogen phosphate, pH 7.4
HBG	20mM HEPES, 5% glucose
LAR Buffer	20 mM glycylglycine; 1 mM $MgCl_2$; 0.1 mM ethylene-diaminetetraacetic acid; 3.3 mM dithiothreitol; 0.55 mM adenosine 5′-triphosphate; 0.27 mM coenzyme A, pH 8-8.5

Cell culture 5x lysis buffer	Promega (Mannheim, Germany)
D-Luciferin	Promega (Mannheim, Germany)
Protease and Phospatase Inhibitor Cocktail	Sigma Aldrich (Taufkirchen, Germany)
RNAlater solution	Thermo Fisher Scientific (Schwerte, Germany)

2.3. Lipoamino xenopeptides

The oligomers **1621**, **1752**, **1762, 1611** and **1612** were synthesized by Melina Grau (PhD student at Pharmaceutical Biotechnology, LMU, Munich).

ID	Topology	Sequence	Stp/LAF ratio
1621	Bundle 2	K[K(8Oc)$_2$]$_2$-Stp	1:4
1752	Bundle 2	K[K(12Bu)$_2$]$_2$-Stp	1:4
1762	Bundle 2	K[K(10Oc)$_2$]$_2$-Stp	1:4
1611	U-shape 1	K(12Oc)-Stp-K(12Oc)	1:2
1612	U-shape 3	K(12Oc)$_2$-Stp-K(12Oc)-K (12Oc)	1:4

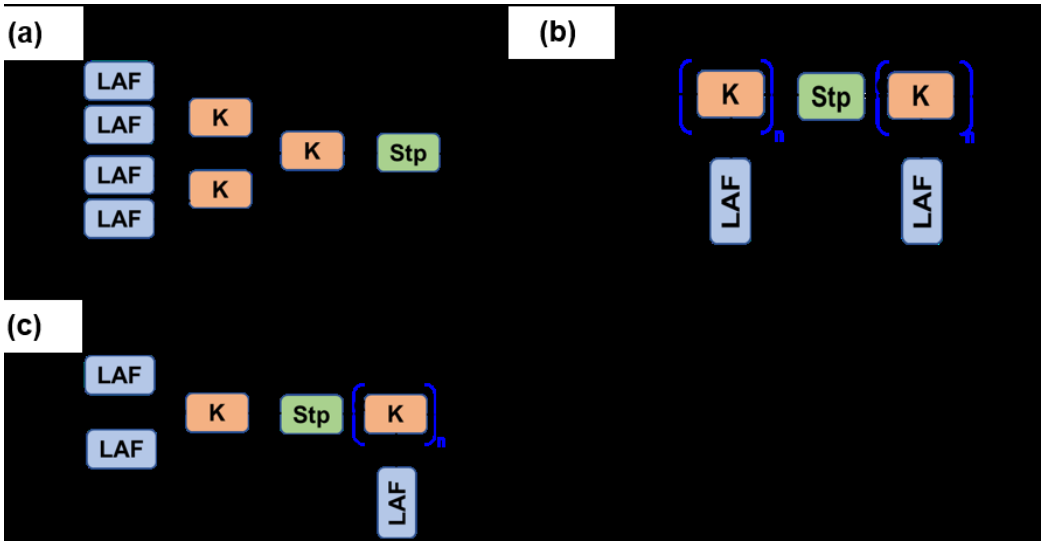

Figure 2. Characteristics of LAF-oligomers. a) Scheme of a Bundle 2 structure. b) Scheme of a U-shape 1 structure. c) Scheme of a U-shape 3 structure. (K, lysine; Stp, succinoyl tetraethylene pentamine; LAF, lipo-amino fatty acid; 8Oc,

LAF based on 8-aminooctanoic acid and two octyl chains; 12Bu, LAF based on 4-aminobutanoic acid and two dodecyl chains; 10Oc, LAF based on 8-aminooctanoic acid and two decyl chains; 12Oc, LAF based on 8-aminooctanoic acid and two dodecyl chains). Figure provided by Melina Grau (PhD student at Pharmaceutical Biotechnology, LMU, Munich).

The oligomer **1395** (illustrated in **Figure 3**) was synthesized by Anna-Lina Lessl (PhD student at Pharmaceutical Biotechnology, LMU, Munich).

ID	Backbone characteristic	Fatty acid	Sequence (N → C)
1395	H-Stp-H	OleA (C18:1)	$K(N_3)$-Y_3-H-Stp-H-$K(K(OleA)_2)$-H-Stp-H-Y_3

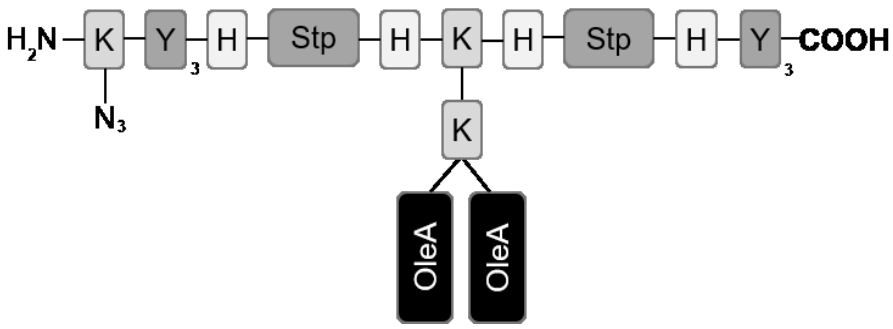

Figure 3. Schematic illustration of the xenopeptide 1395 architecture according to the ionizable backbone "H-Stp-H". K, lysin; Y, tyrosine; H, histidine; Stp, succinoyl tetraethylene pentamine; OleA, Oleic Acid (C18:1).

2.4. Nucleic acids

Nucleid acid	Source
mRNA CleanCap® FLuc mRNA (5moU)	Trilink Biotechnologies (San Diego, CA USA)
mRNA CleanCap® eGFP mRNA (5moU)	Trilink Biotechnologies (San Diego, CA USA)
siFVII Ambion™ In Vivo Factor VII siRNA	Thermo Fisher Scientific (Schwerte, Germany)

siFVIII ON-TARGETPlus SMARTpool siRNA	GE Healthcare Dharmacon, Inc. (Lafayette, CO, USA)
PMO (705); PMO (Ex23)	Gene Tools, LLC (Philomath, OR, USA)
Cas9 mRNA Clean Cap® Cas9mRNA (5moU)	Trilink Biotechnologies (San Diego, CA USA)

PMOs

Both PMOs contained a 3´-primary amine (PMO-NH2) for dibenzocyclooctyne (DBCO) functionalization. PMO (705) and PMO (Ex23) were chemically modified with DBCO-NHS or in case PMO (705) also with DBCO-NHS and AF647 conjugation.

Nucleic acid	**Sequence**	**Target**
PMO (705)	CCTCTTACCTCA GTTACAATTTATA	G point mutation at position 705 in intron 2 of the human β-globin gene (IVS2-705)
PMO (Ex23)	GGCCAAACCTCGGC TTACCTGAAAT	Donor splice site of DMD intro 23

Capital letters: standard RNA ribonucleotides (A, Adenylate; G, Guanylate; C, Cytidylate, U, Uridylate)

sg RNAs

sgRNAs were chemically modified (2' O-methyl modification on the first 3 and last 3 RNA bases) and purchased from Integrated DNA Technologies (Coralville, IA USA).

Nucleic acid	**Sequence**
sgDMDEx23 Target site / PAM	ATTTCAGGTAAGCCGAGGTT / TGG
sgDMDEx23 full RNA sequence	5'mA*mU*mU*UCAGGUAAGCCGAGGUUGU UUUAGAGCUAGAAAUAGCAAGUUAAAAUA AGGCUAGUCCGUUAUCAACUUGAAAAAGUG GCACCGAGUCGGUGCmU*mU*mU*U

Capital letters: standard RNA ribonucleotides (A, Adenylate; G, Guanylate; C, Cytidylate, U, Uridylate); Modification pattern: 'm_' = 2'-O-methyl RNA bases e.g. 'mA*'; '_*' = phosphorothioated RNA bases e.g. 'A*

2.5. *In vivo* experiments

	Source
Rycarfa®	TAD Pharma GmbH (Cuxhaven, Germany)
Bepanthen®	Bayer Vital GmbH (Leverkusen, Germany)
Isoflurane CP®	CP-Pharma (Burgdorf, Germany)
Syringes	B. Braun (Melsungen, Germany)
Cannulas	Henke-Sass, Wolf GmbH (Tuttlingen, Germany); BD Diagnostics (Heidelberg, Germany)
Citrate blood sample tube	Sarstedt AG & Co. KG (Nümbrecht, Germany)
EDTA blood sample tube	KABE Labortechnik GmbH (Nümbrecht-Eisenroth, Germany)

2.6. *Ex vivo* evaluation

	Source
BIOPHEN™ FVII kit	HYPHEN BioMed (Neuville-sur-Oise, France)
BIOPHEN™ FVIII:C kit	HYPHEN BioMed (Neuville-sur-Oise, France)
peqGOLD Total RNA Kit qScript™	VWR International (Darmstadt, Germany)
total RNA Kit qScript™ cDNA SuperMix	Quanta Biosciences (Gaithersburg, MD, USA)
qScript cDNA synthesis kit	Quanta Biosciences (Gaithersburg, MD, USA)
QIAquick® PCR purification kit	QIAGEN (Hilden, Germany)

QIAMP DNA Mini Kit	QIAGEN (Hilden, Germany)
QIAquick Gel Extraction Kit	QIAGEN (Hilden, Germany)

2.7. Instruments

Instrument	Source
Caliper DIGI-Met	Preisser (Gammertingen, Germany)
Cordless animal shaver GT 420 ISIS	Aesculap Suhl GmbH (Suhl, Germany)
Centro LB 960 plate reader Luminometer	Berthold Technologies GmbH & Co. KG (Bad Wildbad, Germany)
Centrifuge 5415 D	Eppendorf SE (Hamburg, Germany)
Homogenizer FastPrep-24™ Classic	MP Biomedicals Germany GmbH (Eschwege, Germany)

2.8. Software

	Provider
Graph Pad Prism 9 software	Graph Pad Software (San Diego, CA USA)
Biorender.com	Biorender.com
TIDE web tool	https://tide.nki.nl/

3. Methods

3.1. Cell culture

The murine neuroblastoma cell line Neuro2A (N2a) was cultured in Dulbecco's modified Eagle's medium (DMEM)-low glucose (1 g/L glucose), supplemented with 10% (v/v) fetal bovine serum (FBS), 4 mM of stable L-glutamine, 100 U/mL of penicillin, 100 µg/mL of streptomycin and cultured at 37° C and 5% CO_2 in an incubator at a relative humidity of 95% [70]. Prior to inoculation into mice, the cells were grown in antibiotic free medium for at least three passage numbers.

3.2. *In vivo* experiments

All animal experiments were approved by the district government of Upper-Bavaria (file number: ROB-55.2-2532.Vet_02-19-19, ROB-55.2-2532.Vet_02-19-20) and were in accordance with the guidelines of the German Animal Welfare Act [139].

For tumor inoculation, the cells were suspended in 150µL PBS and injected subcutaneously with a 25 G cannula into the left flank of mice anaesthetized by inhalation of isoflurane. The anesthesia was induced with 3 %, maintained with 2.5 % of isoflurane and an oxygen rate of flow of 2.5 L/min. Using a caliper, the tumor size was measured daily and calculated with the well-established formula of [$V= (W^2 \times L)/2$] [140].

Intravenous injections were performed by fixing the mice in a restrainer and injecting a volume of 150 µL containing the formulations into the lateral tail vein. For vasodilatation, the tail was held in heated water with a maximum degree of 45 °C for 10-20 secs in order to facilitate the injection procedure.

To guarantee complete analgesia, animals were injected subcutaneously with Carprofen (5 mg/kg) prior to intramuscular injections. Subsequently, a maximum volume of 50 µL containing the formulations was applied into the *musculus biceps femoris* using a 30G cannula. For accurate injection, the left hind leg of the mice was shaved and disinfected beforehand.

On a daily basis, the well-being and weight of all experimental mice were controlled and compared with preassigned termination criteria, such as a tumor size of ≥12 mm in diameter. In case of serverely affected well-being (e.g., continuous weight loss, pain symptoms, apathy, or automutilation), mice were immediatly sacrificed by cervical dislocation.

Blood samples were collected along the performance of euthanazation, using EDTA-coated tubes for preventing coagulation. The samples were centrifuged (Eppendorf Centrifuge 5415 D) at 3000 rpm for 7 min to generate plasma which was subsequently analyzed at the *Clinic of Small Animal Medicine (Faculty of Veterinary Medicine, LMU Munich)*. Liver (*i.e*. ALT, alanine aminotransferase and AST, aspartate aminotransferase) and kidney parameters (*i.e*. Crea, creatinine and BUN, blood urea nitrogen)

were tested in order to compare the biocompatibility of formulations with the clinically approved agents or HEPES buffered glucose (HBG) as the buffer of the formulations.

3.2.1. Lipoamino bundle LNPs for efficient mRNA transfection

3.2.1.1. *In vivo* distribution of luciferase expression by mRNA LNPs

For tumor inoculation, 10^6 N2a cells in 150 µL PBS were injected subcutaneously into the left flank of 6-week-old female A/J mice. When tumors reached a size of 250-500 mm³, animals were divided into groups of three and injected intravenously with LNPs containing 1, 3 or 10 µg of Fluc mRNA (in 150 µL HBG) and formulated with LAF carriers (**1612, 1621**) or standard ionizable lipids DLin-MC3-DMA (MC3) and SM-102 after dialyses against HBG. At 20 or 6 h *post injectionem (p.i.)*, mice were euthanized and organs (lungs, liver, spleen, kidneys, heart, brain) as well as tumors were harvested, washed in PBS and frozen overnight at -80 °C. The next day, tissue samples of 100-500 mg were homogenized by a FastPrep-24™ instrument in 500 µL of Cell Culture Lysis Reagent1x each, supplemented with 1% (v/v) protease and phosphatase inhibitor cocktail. After another freezing cycle of 24 hours to ensure full cell lysis, the samples were thawed and centrifuged for 10 min at a speed of around 13,000 rpm and at 4 °C.

For the measurement of luciferase activity, 100 µL LAR buffer was added to 25 µL of the supernatant of the cell lysate in each well, supplemented with 5% (v/v) of a mixture of 10 mM luciferin and 29 mM glycylglycine, and then analyzed for 10 secs by a Centro LB 960 plate reader luminometer. Luciferase activity was presented as relative light units (RLU) per gram organ or tumor tissue respectively after background substraction (lysis buffer).

3.2.1.2. EGFP expression in immune cells of liver, spleen and lungs

The immunostaining experiment was performed with tumor-free 6-week-old female A/J mice which were randomly splitted into three groups (n=5). LNPs formulated with either SM-102 or **1621** encapsulating 3 µg of enhanced green fluorescent protein (eGFP) mRNA (in 150 µL of HBG) and HBG as

control group, were injected into the tail vein of the animals six hours prior to euthanazation.

The organs including lungs, liver and spleen were dissected, put in PBS on ice, and sent to Dr. Matthias Bros and his team at the work group led by Prof. Stefan Grabbe (*Johannes Gutenberg University; Mainz, Germany*), where single cell suspensions were prepared using different tissue-specific strategies [70]. In the next step, the organ samples were immunohistochemically stained with fluorescence-labled antibodies and living cells were identified in which eGFP expression was detected by flow cytometry. Gating strategies are provided in the following **Figure 4** and **Figure 5** conducted by Zeyn Y, Hieber C, Bros M at University of Mainz.

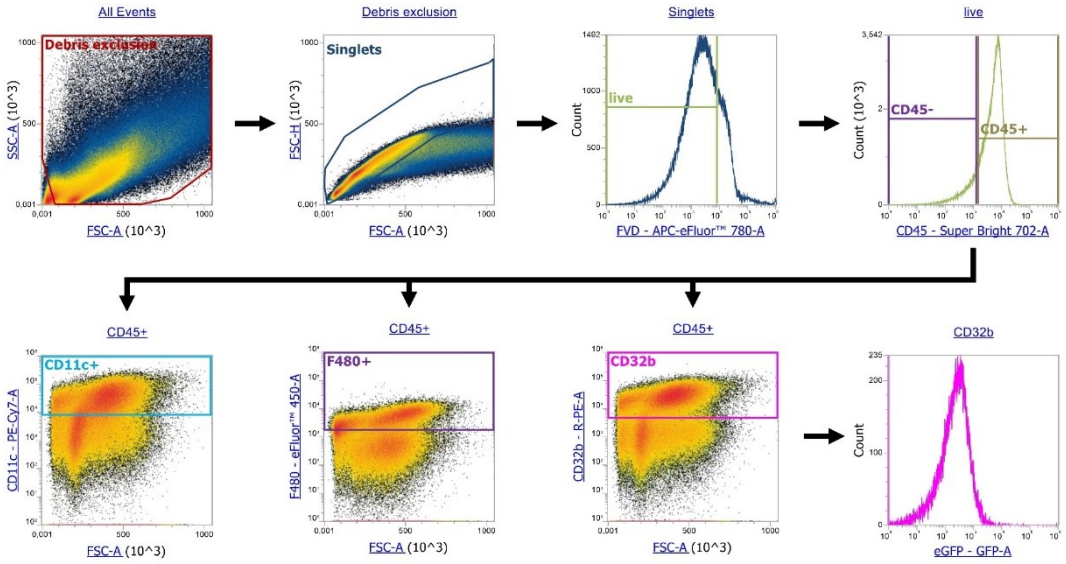

Figure 4. Gating strategy of liver NPCs (non-parenchymal cells). Debris and doublets were excluded from further analysis. Then, FVD^- and $CD45^+$ cell population (living immune cells) was discriminated into $F4/80^+$ (KC, Kupffer cells), $CD11c^+$ (DC, dendritic cells), and $CD32b^+$ (LSEC, liver sinusoidal endothelial cells). For each cell population the eGFP MFI (mean fluorescence intensity) or percentage of $eGFP^+$ cells was used as readout.

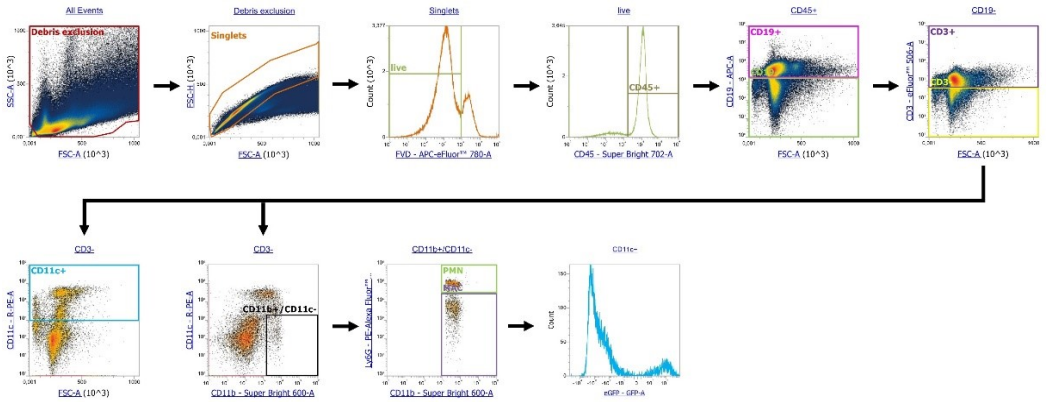

Figure 5. Gating strategy for cells of spleen and lungs, delineated by lineage marker. After exclusion of debris and doublets from further analysis, cells were gated for FVD$^-$ and CD45$^+$ cell populations (living immune cells). Next, B cells were defined as CD19$^+$. CD19$^-$ fraction was further discriminated in CD3$^+$ (T cells), and CD3$^-$ fractions. CD3$^-$ cells were gated for CD11c$^+$ (DCs) and CD11b$^+$/CD11$^-$. The CD11b$^+$/CD11$^-$ fraction was further discriminated by Ly6G$^+$ (PMN, polymorphonuclear leukocytes), and macrophages (Ly6G$^-$). For each cell population the eGFP MFI (mean fluorescence intensity) or percentage of eGFP$^+$ cells was used as readout.

3.2.1.3. Evaluation of clinical blood parameters

Blood samples were taken along the process of euthanazation (cf. **3.2.1.1.**, **3.2.1.2.**) and analyzed as described in section **3.2.** in order to compare the biocompatibility of **1612** and **1621** mRNA LNPs with gold standard SM-102 and MC3 mRNA LNPs and buffer treated (HBG) mice.

3.2.2. Targeting of liver endothelial cells with LAF siRNA LNPs

3.2.2.1. Gene silencing of coagulation factors in the liver by siVII and siVIII LNPs

To evaluate gene silencing in hepathic cells (hepatocytes and endothelial cells) *in vivo*, BALB/C mice at the age of 6- to 8 weeks were divided into groups of four. Subsequently, 150 µL of **1621** or MC3 LNP formulations in HBG, containing 5 µg of siRNA targeting either factor VII (siFVII) or factor VIII (siVIII) per animal, or HBG respectively were applied intravenously. HBG was applied as control. Fourty-eight hours *p.i*, blood samples were obtained using citrate-treated tubes and centrifuging at 1500 rpm for 10 minutes. For determination of FVII and FVIII activity in the generated plasma, the well-established chromogenic assay was performed by Mina Yazdi (PhD student at Pharmaceutical Biotechnology, LMU, Munich).

3.2.2.2. Evaluation of clinical blood parameters

Fourty-eight hours *p.i.,* blood samples were taken along the process of euthanazation (cf. **3.2.2.1.**). Analyses of plasma parameters were perforemed as described in section **3.2.** in order to compare the biocompatibility of **1621** siRNA LNPs (n=2) with positive control MC3-DLin-DMA siRNA LNPs and buffer treated (HBG) mice (n=3).

3.2.3. DMD exon skipping with xenopeptide-PMOs

3.2.3.1. Biodistribution of mRNA splicing modulation

For observing splice switching at the Duchenne muscular dystrophy (DMD) gene *in vivo*, 6-week-old BALB/C mice were injected intravenously with 150 µL of formulations containing 375 µg PMO. Therefore, the freeze-dryed formulation was reconstituted with HBG right before systemic administration and animals were divided into groups of six (PMO(Ex23) **-1395**) or five (free 3‘primary amine modified PMO(Ex23) and PMO (705) -**1395**) respectively. Mice were euthanized 48 h *p.i.* and brain, heart, lungs, liver, kidneys, spleen as welll as the *musculus quadriceps femoris* were dissected before being transferred into RNAlater solution. This step is important for stabilization while incubation overnight at 4 °C and storage at -20°C afterwards.

The further evaluations were performed by Anna-Lina Lessl (PhD student at Pharmaceutical Biotechnology, LMU, Munich) and are reported precisely in the references [135]. Using pestle and a motar as well as liquid nitrogen to prevent unfreezing, the organs were homogenized by hand. After that, mRNA isolation was achieved by using the peqGOLD Total RNA Kit and copy/complementary DNA (cDNA) was generated with the qScript cDNA synthesis kit. Furthermore, a first polymerase chain reaction (PCR) with specific primers fort he DMD_Ex20-26 gene was performed, followed by purification step (PCR purification kit) and a second nested PCR for a smaller genomic region (DMD_Ex20-24). The final analysis took place via agarose gel electrophoresis and quantification of the individual band intensities by using ImageJ software. In a last step, the bands of the lungs of animal C1 (PMO(Ex23) -**1395** treated group) were confirmed for exon 23 skipping using gel extraction and a QIAquick Gel Extraction Kit for

purification as well as (Sanger) sequencing performed by Eurofins GATC Biotech (Konstanz, Germany).

3.2.3.2. Evaluation of clinical blood parameters

The collection of blood samples and evaluation of plasma parameters was accomplished as discribed in paragraph **3.2..** For three animals being injected with PMO(Ex23) -**1395** and PMO (705)-**1395** as well as for four mice being treated with unformulated PMO(Ex23) formulations, liver and kidney values in reagard of tolerability of the injected carriers were analyzed.

3.2.4. Xenopeptide polyplexes for CRISPR Cas9 based gene editing

3.2.4.1. Pre-experiment: Luciferase expression after intramuscular injection of LAF polyplexes and LNPs

For this study, 6-weeks-old female BALB/C mice were divided into groups of four and injected intramuscularly after subcutaneous administration of Carprofen (5 mg/kg) as discribed above (**3.2.**). 50 µL of formulation contained different lipo-XPs synthesized as mRNA-LNPs (**1621**) or polyplexes (**1611, 1621, 1752, 1762**) and encapsulated 60 ng µL-1 luciferase mRNA (3 µg). After euthanazation of mice 6 h *p.i.*, organs (lungs, liver, kidneys, spleen, brain, heart), injected muscle and complementary none-injected muscle were harvested and stored at -80 °C. For evaluation of luciferase expression *ex vivo,* the samples were homogenized and analysed as already mentioned above (**3.2.1.1.**).

3.2.4.2. *In vivo* genome editing and splicing modulation by Cas9/sgRNA xenopeptides

This series of experiments also involve ed 6-weeks-old female BALB/C mice with randomly distributed groups of four and either intravenous or intramuscular injection of Cas9mRNA/sgDMD $_{Ex23}$ at a weight ratio of 1:1. Systemic application implicated 150 µL of carrier solution containing either 3 µg total RNA in **1762** polyplexes and **1621** LNPs or 10 µg total RNA in **1611** polyplexes. Intravenous injections were performed as discribed in section **3.2.** and on day 0, day 2 and day 7 of the treatment. For local administration, analgesia was guaranteed by subcutaneous injection of 5

mg/kg Carprofen beforehand (cf. **3.2.**) and single or triple applications took place on day 0, day 3 and day 14. The solution for the local treatment consisted of 50 µL of either 3 µg total RNA in **1762** polyplexes and **1621** LNPs or 10 µg total RNA in **1611** polyplexes. Seven days after the last treatment, mice were sacrificed and brain, heart, spleen as well as the *musculus biceps femoris* were dissected. In order to prevent mRNA destabilization, organs and muscle tissue were incubated in RNAlater solution for 24 h at 4 °C before freezing for long-time storage at -20 °C.

The further reworking and evaluation were performed by Janin Germer and Anna-Lina Lessl (PhD students at Pharmaceutical Biotechnology, LMU, Munich) and are represented precisely in the references [136]. Using a mortar and a pestle, each sample was homogenized manually in liquid nitrogen and split in several Eppendorf tubes in order to isolate mRNA (for the evaluation of splicing modulation) on the one hand and DNA (for the evaluation of genome editing) on the other hand.

For the isolation of mRNA and further evaluation of splicing-modulation in the physiological dystrophin gene, the peqGOLD Total RNA Kit was used following the steps oft he manufacturer´s protocol. cDNA was generated by utilizing the total RNA Kit qScript™ SuperMix according to manufacturer´s protocol. Furthermore, a first PCR was followed by a purification step (PCR purification kit) of the products and a second PCR was conducted in order to amplify the region of the exon 23 skipping precisely (cf. **3.2.2.1.**). Similar to the agarose gel electrophoresis of the PMO exon skipping experiment, the amplified cDNA sequences were quantified and the intensities of the different bands were analyzed via ImageJ. This implicates comparing the size of the additional bands with unskipped dystrophin exon 20-24 sequence at 586 bp. Also, in this experiment, purification by gel extraction using QIAqucik® Gel Extraction Kit and subsequent sanger sequencing (by Eurofins GATC Biotech (Konstanz, Germany)) of a randomly chosen sample was performed to confirm skipping of the exon 23.

For the extraction of the DNA, a QIMP DNA Mini Kit was used according to the instructions of the manufacturer´s protocol. This time, only one PCR followed by product purification was executed in order to amplify the region

surrounding the targeted sequence downstream of the exon 23. Sanger sequencing by Eurofins GATC Biotech (Konstanz, Germany) and tracking of indels by decomposition (TIDE) analysis (via web tool https://tide.nki.nl/) were utilized to identify genome editing by Cas9/sgRNA *in vivo*.

3.2.4.3. Evaluation of clinical blood parameters in comparison with monitored body weights

Along the euthanazation, blood samples of the systemically treated mice were taken and analyzed as metioned above (cf. **3.2.**), and compared to body weights of all experimental animals, monitored on a daily basis.

3.3. Statistical analysis

Results are expressed as mean + standard error of the mean (S.E.M.) if not indicated elsewise. Statistical analysis was performed by unpaired students t-test test with Welch´s correction using GraphPad Prism™ and p-values < 0.05 were considered as significant (*p < 0.05; **p < 0.01; ***p < 0.001; ns = not significant).

III. RESULTS

1. Lipoamino bundle LNPs for efficient mRNA transfection

This chapter presents the relevant thesis parts adapted from a research article published as Haase F, Pöhmerer J, Yazdi M, Grau M, Zeyn Y, Wilk U, Burghardt T, Höhn M, Hieber C, Bros M, Wagner E, Berger S. (2024) Lipoamino bundle LNPs for efficient mRNA transfection of dendritic cells and macrophages show high spleen selectivity. Eur. J. Pharm. Biopharm. 194, 95–109. [70].

Currently, LNPs represent one of the most effective non-viral delivery platforms [37]. In addition, the importance of mRNA therapeutics has increased significantly over the last decades as concerns regarding immunogenicity and stability have been addressed by chemical modification approaches [141]. For their outstanding achievements in the field of mRNA nucleoside modifications, Katalin Karikó and Drew Weissman were even awarded the Nobel Prize in 2023 [142].

Typically, LNPs are formulated with four lipidic components [81] encapsulating the payload (*e.g.* nucleic acids) as shown in **Figure 6**. The composition plays a critical role in structure, stability and function of the nanoformulation, all affecting the delivery efficiencies of the payload. As naturally occurring in eukaryotic cell membranes [143], phospholipids help packaging nucleic acids and stabilizing the LNPs. The addition of cholesterol promotes further LNP stability and integrity by modulating the membrane rigidity, allowing efficient cellular uptake and endosomal escape. PEG-lipids have multiple functions, such as prolonging the circulation time of LNPs *in vivo*, preventing aggregation, controlling the particle size, and providing ligand binding sites [144]. Although PEG lipids, as classical shielding agents, reduce interactions with cellular membrane components and effectively prevent unwanted interactions, stable PEG units must be released from the LNP surface during the cellular uptake and intracellular release of the LNP payload, whereupon they are also referred to as "sheddable"[145].

As fourth part of the lipidic composition, ionizable lipids consist of a pH-responsive head group, a linker connection and hydrophobic tails [146]. Ionizable lipids are essential for LNP formulations, providing a pH-

responsive behavior, which refers to their ability to change their charge in response to variations in pH. At physiological pH, ionizable lipids are neutral or weakly charged. In the acidic pH of endosomes, they become protonated, acquiring a positive charge. This allows nucleic acid complexation during LNP formulation and intracellular release of the encapsulated cargo after endosomal escape. In contrast to permanent cationic lipids, such as N-[1-(2,3-dioleyloxy)propyl]-N,N,N-trimethylammoniumchloride (DOTMA) or DOTAP of initial LNP formulations, ionizable lipids, such as such as 1,2-dioleoyl-3-dimethylaminopropane (DODAP) can be reversibly protonated and therefore, show higher efficiency as well as lower toxicity [37, 147]. Due to these unique advantages, they play an important role in developing LNP-based delivery systems for various applications [146, 148].

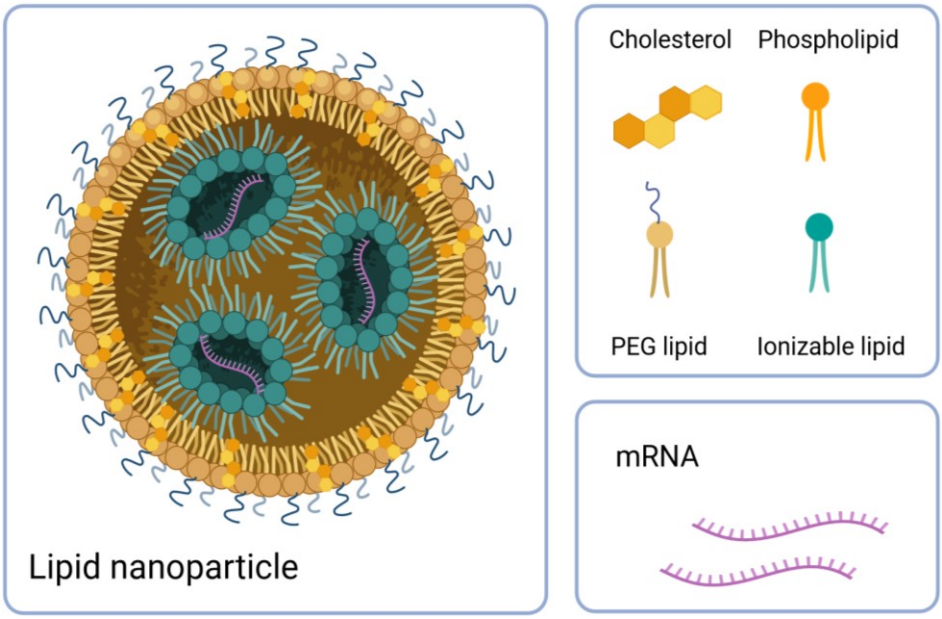

Figure 6. Schematic illustration of the lipidic motifs in mRNA LNPs. LNPs have four different lipidic components as cholesterol, phospholipid, PEG-lipid, and ionizable lipid. Figure adapted from Haase *et al*. [70] and created with Biorender.com

Despite the advantages of LNPs as a delivery system [7], endosomal escape remains still a crucial issue for LNPs as the intracellular release of even clinically approved formulations is still restricted to low values of 1-2% [149]. To address this concern, different optimization approaches have been proposed by structurally improved lipidic components, *e.g.* cholesterol-analogs [150], protonable phospholipids [151] or bioactive

molecules [152], as well as the optimization of the lipidic composition by modifying the individual ratios of LNP components [153].

In the current study, recently synthesized LAF-Stp xenopeptides (**Figure 7**), were used as ionizable components in mRNA LNP formulations. These novel-synthesized, sequence-defined oligomers show a double pH-responsiveness behavior and have already been employed in polyplexes for efficient mRNA delivery *in vitro* and *in vivo* [69]. Their attributed chameleon character refers to a pH-dependent tunable polarity of distinct building blocks, covalently connected via branching lysines for various topologies (U-shape and Bundle). On the one hand, Stp units serve as polar backbones with protonatable aminoethylene motifs. On the other hand, LAFs contain a central tertiary amine which changes the rather apolar character of the LAF upon protonation in the acidic milieu. This is evidenced by a drastic shift in the logD value, a distribution co-efficient and measure of lipophilicity, from approx. +1 (hydrophobic) at neutral pH to -1 (hydrophilic) in acidic milieu. Compared to standard ionizable lipids of DLin-MC3-DMA and SM-102 [154] with only one protonatable amine, multiple-protonatable amines within the potent LAF-Stp carriers may better regutlate the pH-responsive behavior affecting the encapsulation efficiency, cellular uptake, endosomal escape, and the delivery efficiencies.

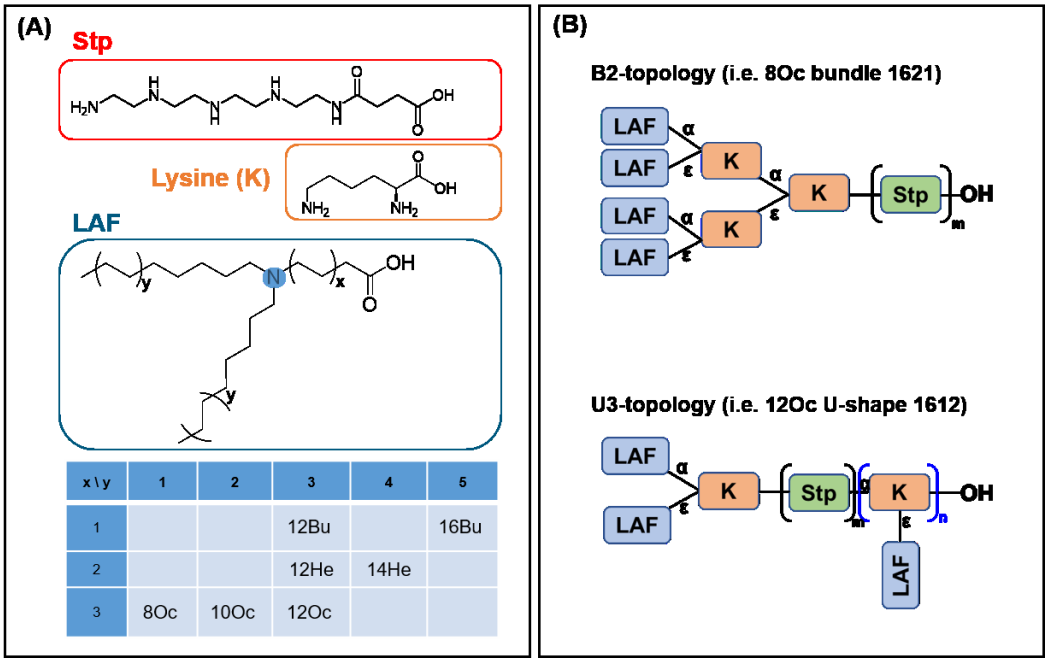

Figure 7. LAF-Stp carriers as cationizable component for LNP formulations. **(A)** Succinoyl tetraethylene pentamine (Stp; red), lysine (K) (orange) and lipo-amino fatty acid (LAF; blue) as building blocks for LAF-Stp carriers. Different LAFs comprise amino fatty acids of different carbon backbone length (Bu, 4-amonobytyric acid; He, 6-aminohexanoic acid; Oc, 8-aminooctanoic acid) with amines disubstituted with alky chains of different carbon lengths (8, octyl; 10, decyl; 12, dodecyl; 14, tetradecyl; 16, hexadecyl). By this variation, the position of the tertiary amine (blue background) can be shifted within the LAF, resulting in different LAF types. **(B)** Different topologies of LAF-Stp carriers, exemplarily shown for bundle 8Oc *1621* and U-shape 12Oc *1612*. Figures provided by Melina Grau (PhD student at Pharmaceutical Biotechnology, LMU, Munich) and adapted from Haase *et al*. [70]

In vitro screening for suitable LAF-Stp carriers [70]

Franziska Haase (PhD student at Pharmaceutical Biotechnology, LMU, Munich) evaluated the potential of LAF-Stp carriers as ionizable components in mRNA LNP formulations *in vitro*. The ratio of the four components, including cholesterol, distearoyl phosphatidylcholine (DSPC) (as phospholipid), sheddable 2-dimyristoyl-sn-glycerol-methoxy polyethylene glycol (DMG-PEG), and LAF-Stp carriers (1621 or 1612) as well as the N/P ratio (referring to the ratio of amines in the carriers to the phosphate molecules in mRNA) in the LNP formulations were optimized as shown in **Table 1.** A transfection kinetic study (**Figure 8A**) showed a fast transfection process for the most of the mRNA LNPs formulated with LAF-Stp carriers with higher efficiency at early time points compared to standard DLin-MC3-DMA and SM-102 LNPs. Moreover, the best performers such as

1621 demonstrated high efficiency in the presence of high level of serum (up to 99%) and at very low doses of mRNA in the sub-nanogram range (**Figure 8B**).

Based on the screening (**Figure 8**) data regarding the transfection kinetics and efficiency (especially in the presence of serum), suitable LAF-Stp carriers and evaluation time points could be defined for the following in vivo experiments.

	ratios		**ratios**				
	Chol/DSPC/PEG-DMG/ionizable carrier		**w/w**	**N/P (ionizable carrier/mRNA)**			
ID	**molar [mol%]**	**w/w [weight%]**	**(total carrier/ mRNA)**	**N with LAF**	**N/P**	**N w/o LAF**	**N/P**
Positive controls							
MC3	38.5/10/1.5/50	25.4/13.5/6.4/54.7	10		3	-	-
SM-102	38.5/10/1.5/50	24/12.7/6.1/57.2	22		6	-	-
Bundles							
1621	59.9/15.6/2.3/22.2	24.5/13/6.2/56.3	16	4+3	9	3	4.1
U-shapes							
1612	59.9/15.6/2.3/22.2	22.2/11.8/5.6/60.5	17	4+3	9	3	4.1

Table 1. Molar (mol%) and w/w (weight%) ratios of the lipids and ionizable carrier used in mRNA LNP formulations, and ratios between cationizable carrier to mRNA. The N/P ratio is defined either as the molar ratio of all protonatable nitrogens (LAF+Stp + any terminal amine) of the carrier to phosphate molecules of the mRNA backbone, or as the molar ratio of protonable amines of Stp+terminal amine. LAF, lipo-amino fatty acid fatty acid; N, protonatable nitrogen; Stp, succinoyl tetraethylene pentamine**.**

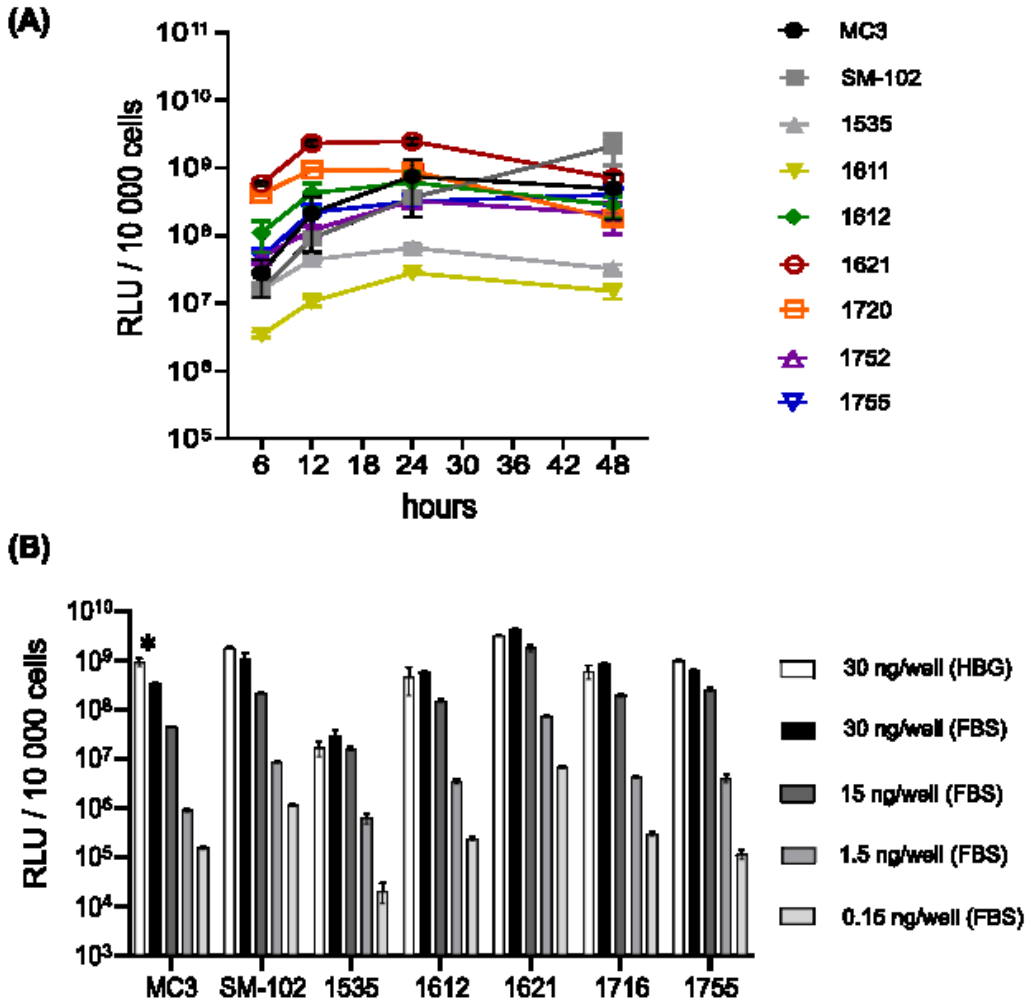

Figure 8. In vitro evaluation of luciferase expression induced by mRNA LNPs in N2a cells. (A) Luciferase expression at different time points (6, 12, 24 and 48 h) after transfection of 60 ng FLuc mRNA per well on N2a cells. **(B)** Transfection efficiency of FBS-diluted mRNA LNPs at the indicated FLuc mRNA doses in N2a cells in comparison to LNPs diluted in HBG (30 ng/well). Prior to transfection, LNPs were either diluted in HBG or with FBS at different levels (50, 75, 97,5 and 99,7 %) and then added at indicated doses into standard 10% FBS containing cell culture medium. Luciferase activity was evaluated at 6, 12, 24 and 48 h **(A)** or only at 24 h **(B)** after transfection and is shown as RLU values (n=3; mean ± SD) after background subtraction (HBG-treated control cells). These experiments were performed by Franziska Haase (PhD student at Pharmaceutical Biotechnology, LMU, Munich).

1.1. In vivo distribution of luciferase expression by mRNA LNPs

Considering the results of **Figure 8**, a selection of LAF-Stp carriers was established, including **1621** (8Oc–B2–1:4) as a bundle best performer and **1612** (12Oc-U3-1:4) as a representative U-shape to address both topology classes *in vivo*, as well as SM-102 and DLin-MC3-DMA as positive control groups.

For a primary screening of *in vivo* biodistribution of mRNA LNPs, 10 µg of luciferase mRNA encapsulated in LAF-Stp LNPs were administered intravenously in a tumor-bearing mouse model. Therefore, mice were subcutaneously inoculated with a number of 1x 10^6 N2a WT cells, split into groups of three as soon as tumors reached a size of 250-500 mm³ and injected intravenously with the chosen LNP formulations. The distribution of luciferase expression was determined 20 h *p.i.* using the commonly performed *ex vivo* luciferase assay method (**Figure 9A**). As shown in **Figure 9B**, SM-102 and DLin-MC3-DMA resulted in high expression, especially in the liver, spleen and tumor and, in the case of SM-102, also in heart tissue. Although moderate adverse reactions, such as temporarily narrowed eyelids and slowed movements, were observed after injection of **1621**, both LAF-Stp LNPs (**1621** and **1612**) led to similar efficacy in spleen and to lower expression values regarding the other organ samples.

A follow-up experiment was performed by testing the systemic injection of LNP formulations encapsulating a lower dose of luciferase mRNA (3 µg) in order to investigate dose-dependent effects *in vivo*. Moreover, **1621** was administered at a lower dose of 1 µg to further reduce toxic effects. Again, at 20 h *p.i.*, mice were euthanized and luciferase expression was measured in the harvested organs (**Figure 9C**). Despite the reduced dose, liver and tumor values remained at a comparable high level for all candidates, and only spleen expression of SM-102 decreased from 10^{10} to 10^9 RLU/ g organ. Other organs did not reveal distinct dose dependent expression. Noteworthly, there was no difference between mRNA expression in the spleen of bundle **1621** LNP-treated groups at various applied doses. No toxicity was observed for **1621** at the mRNA dose of 1 µg, while maintaining high expression efficiency in spleen.

As *in vitro* transfection kinetics of LAF-Stp structures led to the assumption of beneficial efficiencies at early-time points, a final *in vivo* study was performed using 3 µg luciferase mRNA but a shorter read-out span of only 6 h *p.i.* (**Figure 9D**). Here, SM-102 led to the highest expression amounts, primarily in liver, spleen and tumor tissue, followed by DLin-MC3-DMA with 10-fold lower liver and 50-fold lower tumor expression, but comparable spleen levels. In the case of **1612** and **1621**, transfection efficiency in the

liver could not compete with control formulations, remaining at a 100- and 10-fold lower RLU-level than SM-102 and DLin-MC3-DMA, respectively. Moreover, tumor expression mediated by **1621** and **1612** was reduced by approximately two log units as compared to the control groups. Nevertheless, both LAF-Stp carriers achieved similar high spleen expression as both positive controls (SM-102 and DLin-MC3-DMA) with no significant differences in the RLU values.

To summarize the *in vivo* findings of mRNA expression in different organs after intravenous administration of mRNA LNPs, the ionizable lipids SM-102 and DLin-MC3-DMA showed the highest transfection especially in liver and tumor tissues during the entire series of experiments. However, LNPs formulated with 12Oc U-shape **1612** as well as 8Oc bundle **1621** could mediate comparable expression in the spleen, especially at the mRNA dose of 3 µg. On top of that, both LAF-Stp carriers could attain a higher spleen/liver ratio with a 60-fold superior splenic expression for **1612** (* p = 0.0338) and even 350-fold for **1621** (** p = 0.0021) (**Figure 9D**).

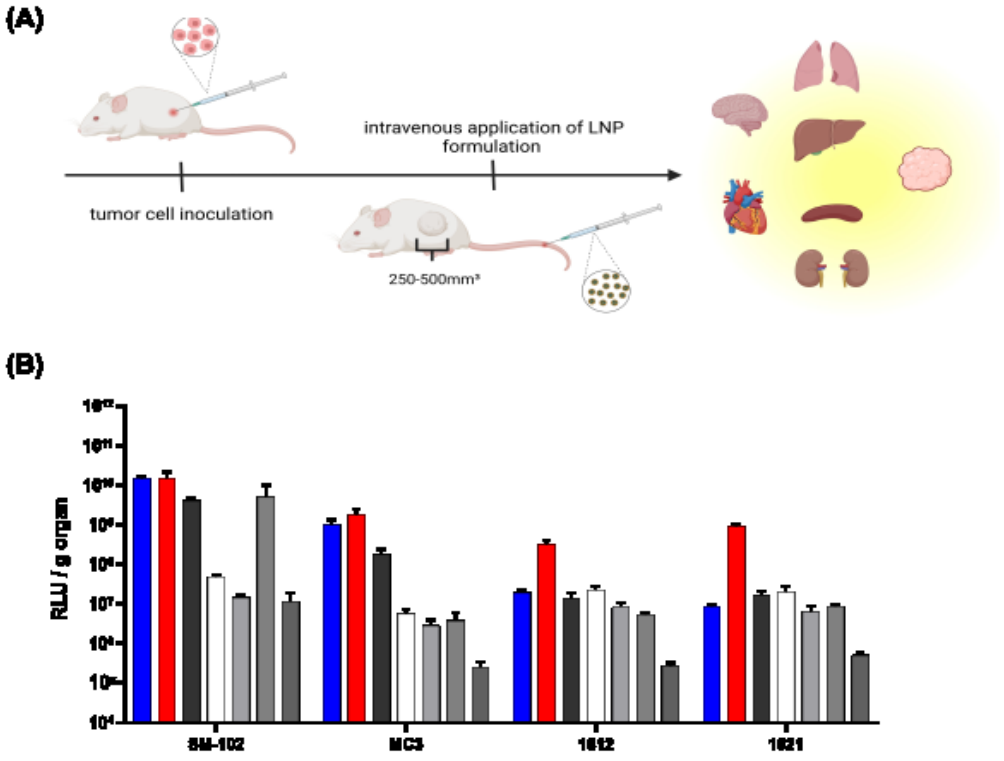

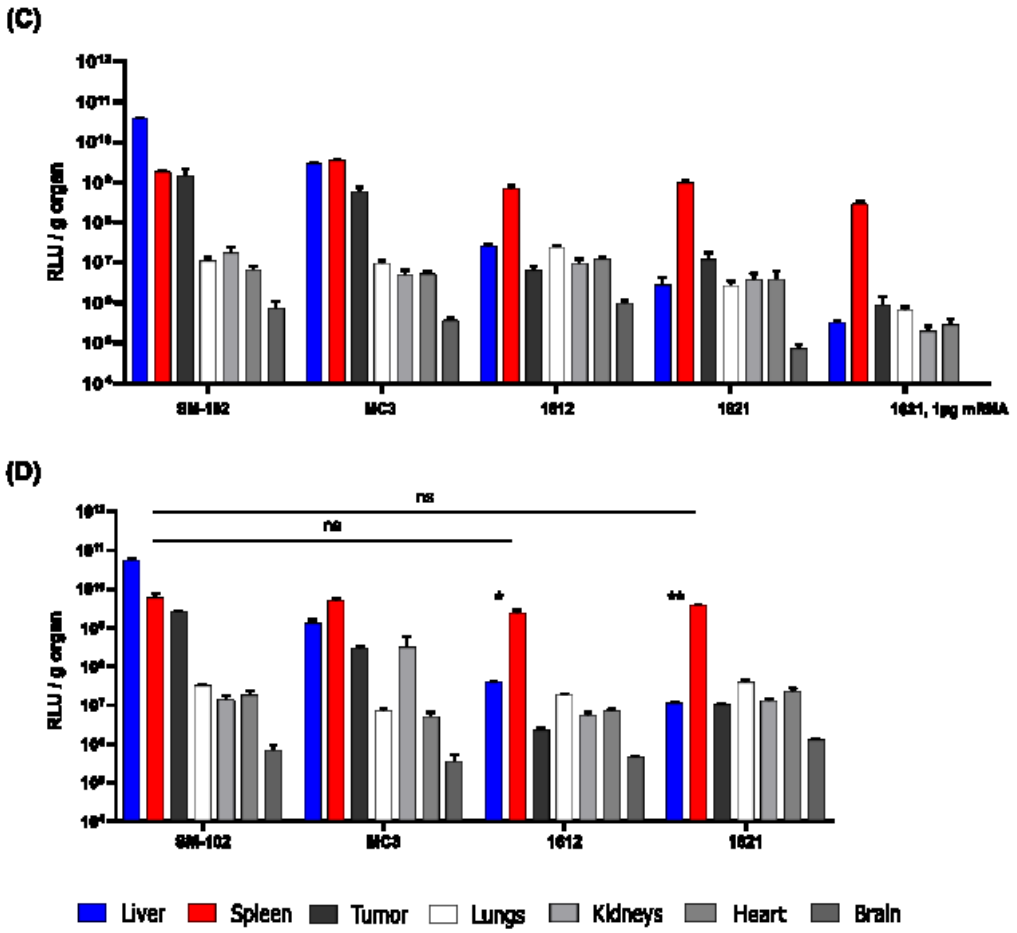

Figure 9. Luciferase expression of mRNA LNPs in different organs of N2a tumor-bearing mice. (A) Schematic illustration of the experimental procedure. A/J mice were injected with a number of 1x 10^6 N2a cells into the left flank. When the tumor sizes reached 250-500 mm^3, the selected mRNA LNPs were administered via tail vein. At the indicated time points *p.i*, the mice were euthanized and the organs were harvested. The mRNA expression was measured in the organs by luciferase assay, and the luciferase activity in RLU was determined *ex vivo* per gram (g) organ**. (B)** Ex vivo luciferase activity at 20 h after intravenous injection of LNPs containing 10 µg or **(C)** 3 µg FLuc mRNA in 150 µL HBG per mouse. LNPs were prepared by Franziska Haase (PhD student at Pharmaceutical Biotechnology, LMU, Munich) at different N/P and molar ratios (see **Table 1**). **(D)** *Ex vivo* luciferase activity at 6 h after intravenous injection of LNPs containing 3 µg mRNA. Significance between SM-102 and ***1612*** or ***1621***, in spleen expression: ns, statistically not significant. Significance between liver and spleen expression **1612**, * $p \leq 0.05$; **1621**, ** $p \leq 0.01$. Figure **(A)** created with Biorender.com.

1.2. EGFP expression in immune cells of liver, spleen and lungs

In order to investigate transfection efficacies within immune cells in the liver, spleen and lungs, **1621** was selected, according to the high luciferase expression values in spleen, compared to SM-102, to be administered intravenously as eGFP mRNA LNP. For systemic applications, tumor-free A/J mice were randomly subdivided into groups of five and injected with 3

µg of eGFP mRNA as well as HBG as a negative control. At 6 h after the treatment, animals were sacrificed, organs were harvested and delivered to Dr. Matthias Bros and his team at the work group led by Prof. Stefan Grabbe (Johannes Gutenberg University; Mainz, Germany) to be stained immunohistochemically.

The eGFP-expression in indicated cells was delineated as mean fluorescence intensity (MFI) and normalized individually to HBG-treated control groups (Ctrl) for each cell-specific organ sample. As illustrated in **Figure 10A**, SM-102 as well as **1621** LNPs induced similar moderate expression values in liver dendritic cells (DCs) and liver sinusoidal endothelial cells (LSECs), which were outperformed in macrophages (MACs) of the liver (KC, Kupffer cells) with higher level for **1621** LNPs. In the splenic immune cells, the LNPs formulated with **1621** showed rather low eGFP expression in DCs and B-cells, but could achieve moderate efficacy in MACs. In contrast, SM-102 mediated highest expression in DCs, followed by medium high expressions in MACs and only a small benefit compared to **1621** LNPs in B-cells. None of the injected LNP formulations was able to gain high expression levels in the lungs, neither in DCs nor in alveolar MACs. Yet, in polymorphonuclear neutrophils (PMN) of the lungs, a moderate efficacy was seen for both LNP formulations, in a smaller extent for **1621**. Finally, there was no eGFP expression detected in other types of immune cells (*data not shown*).

In a subsequent evaluation process, the eGFP expression in CD45-negative cells was compared with that in CD45-positive cells and presented as percentage of the gated cell population (**Figure 10B**). CD45 represents lymphocyte-related marker, common in immune cells. Thus, $CD45^-$ cells can be considered the non-immune cell population, whereas $CD45^+$ represent the immune cell fraction. SM-102 and **1621** mRNA LNPs resulted in higher transfection efficacies in $CD45^+$ (~ 3.9 - 4% of gated cell population) than in $CD45^-$ (~ 1.1-1.5 % of gated cell population) cells. However, the difference between SM-102 and **1621** in non-immune cells (~0.4 % of gated cells) of the liver outranges the difference of both carriers in immune cells (~ 0.1 % of gated cells). Considering the fact, that the liver consists of 80% hepatocytes [105] and only a small fraction of immune cells

(< 4-5 % of the total cell population) was considered, one may hypothesize that these minor differences on a single cell level, will come to higher account in regard of the entire organ (*cf*. *discussion*).

To summarize both parts of the eGFP expression study in immune cells of different organs, it is important to mention, that mRNA LNPs with **1621** succeeded especially in hepatic MACs (KCs), whereas SM-102 LNPs attained highest transfection efficacies in splenic DCs as well as MACs. Combined with the conclusions of the previous luciferase expression study, the selectivity of immune cells in the liver occurs to be higher for LNPs that were formulated with **1621** compared to SM-102 (*cf*. discussion).

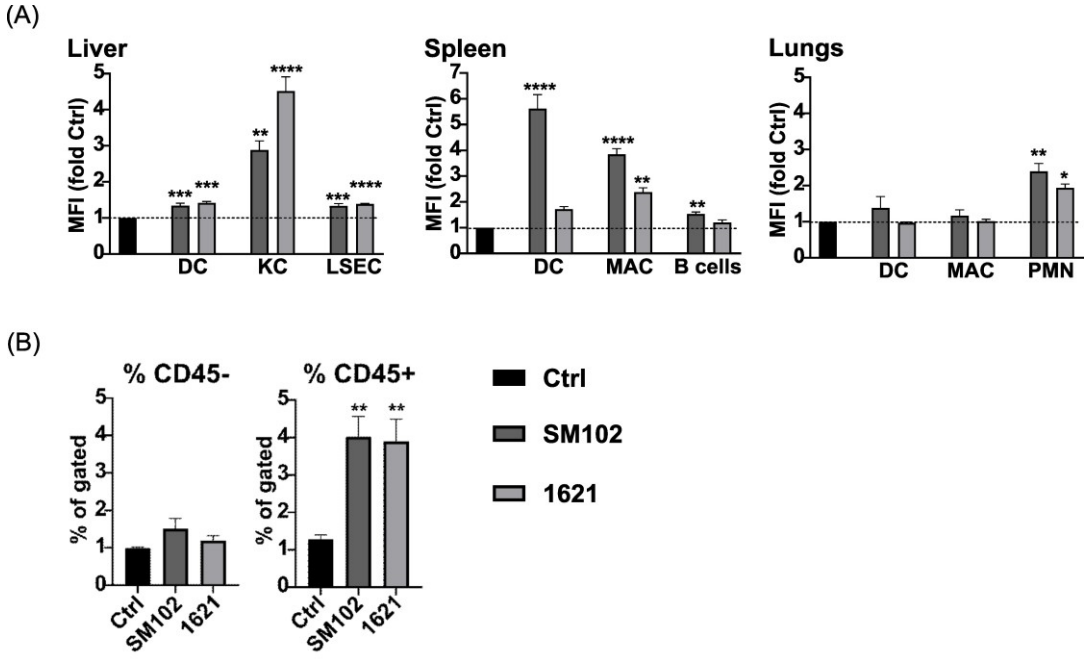

Figure 10. eGFP expression in immune cells after intravenous administration of mRNA LNPs containing 3 µg eGFP mRNA in 150 µL HBG per mouse (n=5). SM-102 (N/P 6); *1621* (N/P 9) were administered. LNP compositions are displayed in **Table 1** and gating strategies in **Figure 3** and **Figure** 4. **(A)** eGFP expression in immune cells of liver, spleen, and lungs, presented as mean fluorescence intensity (MFI) and normalized to HBG-treated controls (Ctrl). **(B)** eGFP expression in CD45-negative ($CD45^-$) vs CD45-positive cells ($CD45^+$) in the liver and presented as percentage of eGFP-positive cells within the $CD45^{-/+}$ populations. Statistical analysis was done by one-way ANOVA, Tukey test; GraphPad Prism™ 9.5.1. Significant differences vs Ctrl (HBG treated mice): * $p \leq 0.05$; ** $p \leq 0.01$; *** $p \leq 0.001$; **** $p \leq 0.0001$. DC, dendritic cells; MAC, macrophages; KC, Kupffer cells; B cells; PMN, polymorphonuclear leukocytes/neutrophils; and LSEC, liver sinusoidal endothelial cell. The evaluation of tissue samples was conducted by Zeyn Y, Hieber C, Bros M at University of Mainz.

1.3. Evaluation of clinical blood parameters

To guarantee good biocompatibility of LNP formulations in the presence of blood components, plasma samples were gathered within the previously described experiments (*cf*. section **1.1.** and **1.2.)**. In this context, **Figure 11** depicts the evaluated liver enzymes (ALT, AST,) and renal parameters (Crea, BUN) after systemic administration of applied mRNA LNPs in A/J mice. On the one hand, biochemical blood values of 12Oc U-shape **1612** and 8Oc bundle **1621** are compared to SM-102 and DLin-MC3-DMA, as gold standard ionizable lipids (**Figure 11A**). On the other hand, the **1621** group is compared to HBG as buffer control, as well as once more to SM-102 (**Figure 11B**). In both sets of the illustrated graphs, neither extremely high nor conspicuous low values in blood chemistry were measured, which indicates a good biocompatibility of the injected formulations.

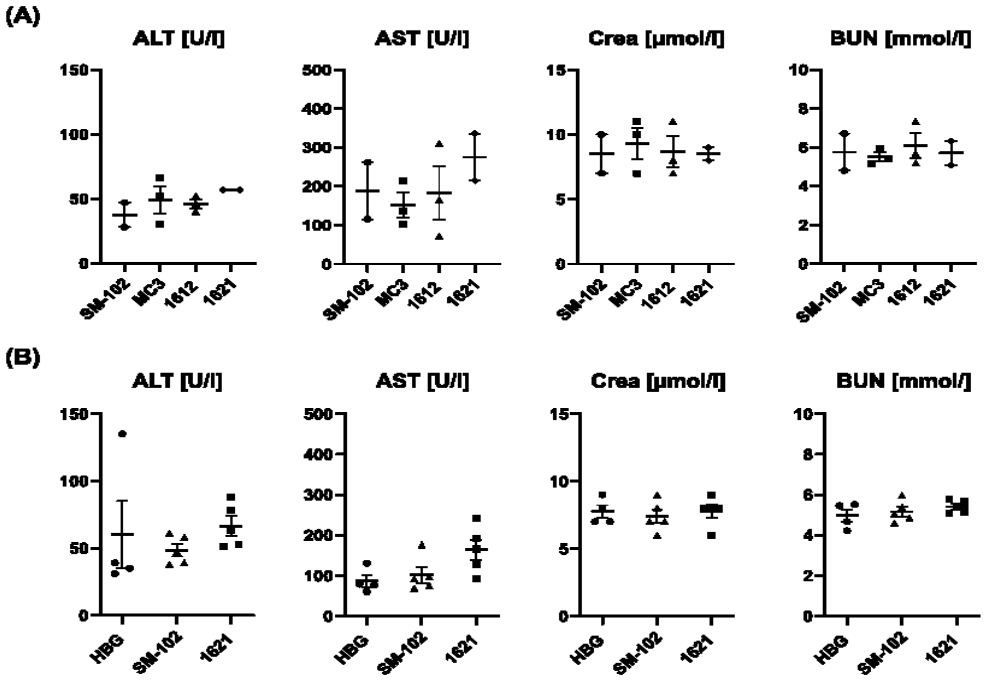

Figure 11. Evaluation of standard plasma parameters after intravenously administration of mRNA LNPs into A/J mice with or without tumors. Blood samples were taken at 6 h after injection and the parameters were evalutated in the plasma of **(A)** tumor-bearing mice injected with 3 µg FLuc mRNA and **(B)** tumor-free mice injected with 3 µg GFP mRNA. LNPs were prepared by Franziska Haase (PhD student at Pharmaceutical Biotechnology, LMU, Munich) at different N/P and molar ratios (see Table 1). **(A)** SM-102 (n=2), DLin-MC3-DMA (MC3, n=3), *1612* (n=3) and *1621* (n=2); **(B)** and SM-102 (N/P 6), *1621* (N/P 9); HBG (n=4), SM-102 (n=5), *1621* (n=5). ALT, alanine transaminase; AST, aspartate aminotransferase; Crea, creatinine; BUN, blood urea nitrogen.

2. Targeting of liver endothelial cells with LAF siRNA LNPs

This chapter presents the relevant thesis parts adapted from a research article submitted as Yazdi M, Pöhmerer J, Hasanzadeh Kafshgari M, Seidl J, Grau M, Höhn M, Vetter V, Hoch C.C, Wollenberg B., Multhoff G., Bashiri Dezfouli A, Wagner E, (2024) In Vivo Endothelial Cell Gene Silencing by siRNA-LNPs Tuned with Lipoamino Bundle Chemical and Ligand Targeting. Small, 2400643 [155].

After successful global phase 3 studies in 2018 [156], Patisiran (Onpattro) was the first clinically approved siRNA-based drug for treating hereditary transthyretin amyloidosis (hATTR) using LNP technology [100]. Here, the formulation of the Patisiran LNP consists of cholesterol, a special PEG-lipid (*see below*), DSPC and DLin-MC3-DMA as ionizable lipid, resulting in highly effective gene silencing in hepatocytes, as one of the most common target cells in the liver [37, 53]. However, targeting of other hepatic cell types has been focused in many studies in the last decades [157].

Understanding the microanatomy of the liver is crucial to get a better insight into the distinct uptake pathways by various cell types within the liver following the systemic application of LNPs. Hepatic lobules are the smallest functional subunits in which blood with high and low oxygen content from the hepatic artery and portal vein, respectively, is combined in sinusoidal vessels and finally enters in the central vein. With up to 80% of the entire cell population, hepatocytes (HCs) represent the largest fraction of highly-specialized liver cells and a common target for treating liver diseases [105]. Following the blood flow, siRNA LNPs face two major cell types of the reticuloendothelial system at first, including Kupffer cells, representing liver-resident macrophages, and LSCEs, forming the fenestrated capillary walls of liver sinusoids (**Figure 12**). To reach HCs, LNPs should cross the endothelium. An appropriate particle size is therefore essential for LNPs to overcome this barrier, passing through the fenestrae (50-200nm in diameter) of LSECs and enter the Space of Disse in which vitamin-A-containing stellate cells (SCs) are located. The endocytic mechanism of HC cell entry is attributed, at least in part, to the binding of endogenous ApoE to the surface of the LNPs [52]. For the LNP formulation of Patisiran (*see above*), this protein binding is explained by the gradual dissolution of the PEG-lipid in the blood circulation. This so-called sheddable PEG contains shorter (C14) alkyl chains and therefore dissolves rapidly from the LNP *in*

vivo [37]. Subsequently, the LNP enters hepatocytes via LDL receptor (LDLR)-specific endocytosis. [52].

In addition to HCs, targeting LSCEs is also of importance for LNP-based therapeutics, as they play an important role in hepatic pathologies, such as chronic liver diseases. These multi-functional endothelial cells, do not only build up the blood-tissue-barrier in the liver, but have moreover an enormous impact on endocytosis of blood marcomolecules via scavenger-receptors, regulating hepatic blood pressure and balancing immune system activities of the liver [158]. Effective delivery of LNPs to LSCEs can be achieved for example by a small change of the lipidic composition of Patisiran (Onpattro), resulting in negative charged particles instead of neutral mRNA LNPs [159].

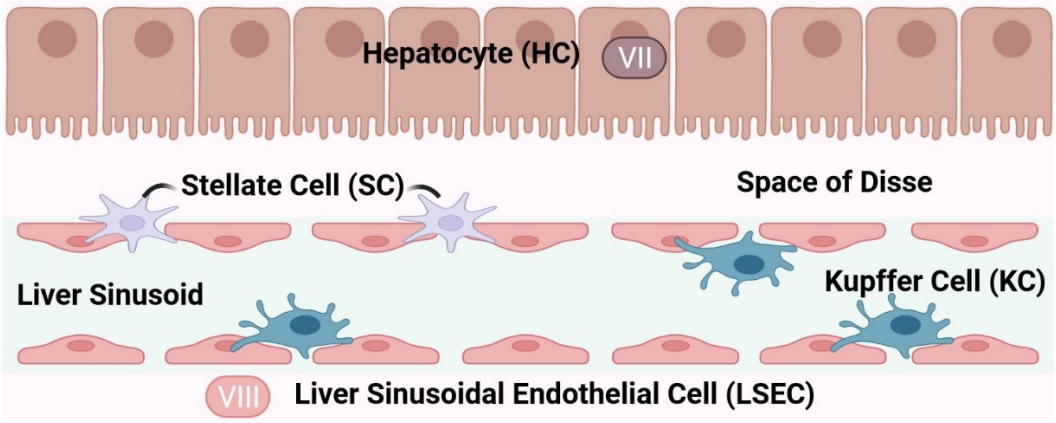

Figure 12. Schematic illustration of the liver sinusoid structure. Liver sinusoidal endothelial cells (LSCEs) build the walls of the sinusoidal capillary system and create the space of Disse between the LSCEs and Hepatocytes (HCs). Stellate cells (SCs) are located in the Space of Disse, whereas hepatic macrophages, namely kupffer cells (KCs), reside in the sinusoidal lumen. Blood coagulation factors VII and VIII are mainly attributed to distinct liver cell types (HCs and LSECs respectively). Figure created with Biorender.com.

2.1. Gene silencing of coagulation factors in the liver by siVII and siVIII LNPs

In contrast to gold standard LNP formulations with ionizable lipid SM-102, mRNA LNPs, containing best performing LAF-Stp-carrier **1621**, targeted hepatic cells (KCs and LSCEs) in the previous study (cf. **1.2**). In order to investigate whether **1621** LNP target LSECs in a higher level than HCs, we changed the cargo to siRNA in the current study to silience factor VII (FVII)

[160] in HCs and FVIII in LSECs [161]. DLin-MC3-DMA-based LNP was selected as a highly potential system to deliver siRNA into HCs [53].

The experimental setup was established on the systemic application of siRNA LNPs into healthy BALB/C mice, divided into groups of four beforehand. The LNPs were formulated either with **1621** or DLin-MC3-DMA (MC3) to deliver 5µg of siRNA (siFVII or siFVIII) per mouse. Thus, five different treatment groups were set up, including HBG as a negative control. Afterwards, euthanazation was performed 48 hours *p.i.* and citrated plasma samples were generated (**Figure 13A**). The relative activities of FVII and FVIII, measured by Mina Yazdi (PhD student at Pharmaceutical Biotechnology, LMU, Munich) utilizing the chromogenic assay method, are demonstrated in **Figure 13B**. Regarding silencing of FVII (left chart), only minor values (~30%, $p<0.05$) could be determined for **1621**-LNPs, whereas MC3-LNPs, in accordance with published research [53], resulted in higher silencing efficiencies of ~90%, $p<0.001$). On the contrary, MC3-based LNPs could not knockdown FVIII (right chart) as high as induced by **1621** LNPs (~80%, $p<0.05$).

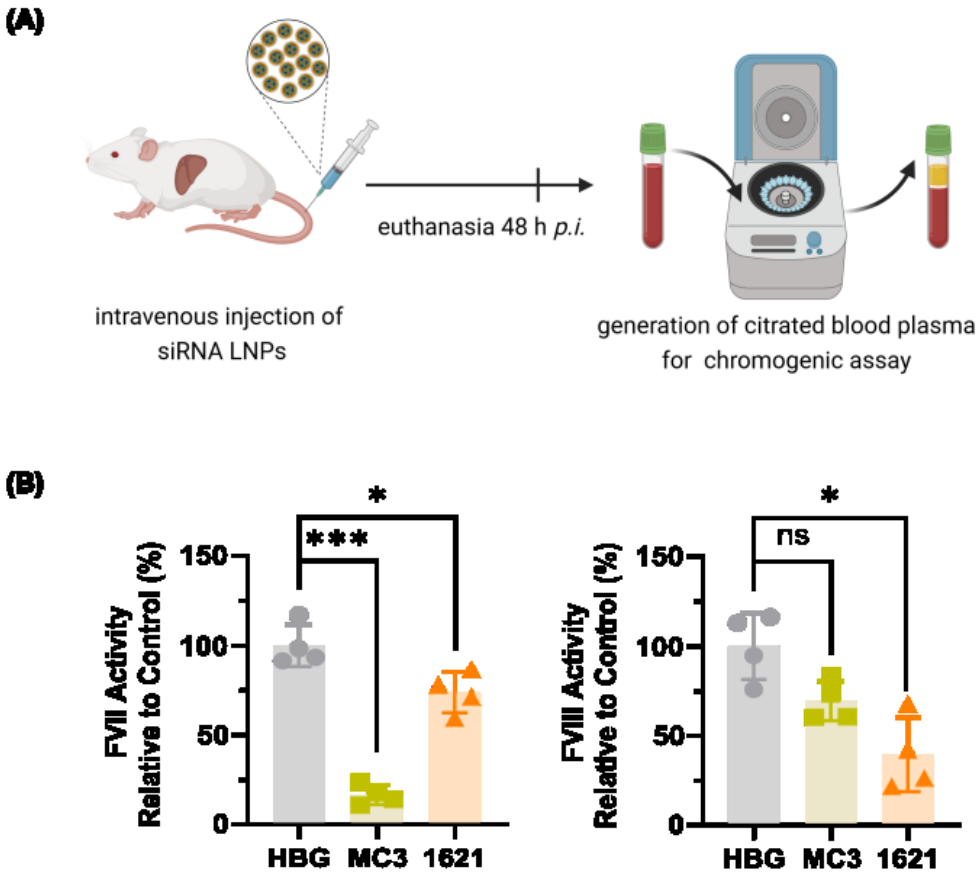

Figure 13. Selective siRNA gene silencing in LSECs and HCs. (A) LNPs formulated with DLin-MC3-DMA (MC3) or 1621 were loaded with siFVII or siFVIII (5µg siRNA /mouse). The formulations were injected into BALB/C mice via tail vein. At 48 h *p.i.*, the FVII and FVIII activities were measured in citrated plasma samples by chromogenic assay**. (B)** The FVII and FVIII activities in the plasma of treated mice are presented as percentage of the value obtained from HBG-injected mice (mean ± SD, n = 4). The evaluation of plasma samples was conducted by Mina Yazdi (PhD student at Pharmaceutical Biotechnology, LMU, Munich).

2.2. Evaluation of clinical blood parameters

For creating a valuable safety-assessment of injected **1621** LNPs compared to clinically approved MC3-formulations on the one side and nanoagent-free HBG-control solutions on the other side, biomarkers for liver damage and kidney functions were considered (**Figure 14**). Therefore, the analysis of generated blood samples did not only focus on FVII/FVIII silencing activities, but was also expanded on ALT and AST as well as BUN and Crea plasma levels. No resulting abnormalities within the measured parameters imply a good biocomopatibility of the injected siRNA formulations.

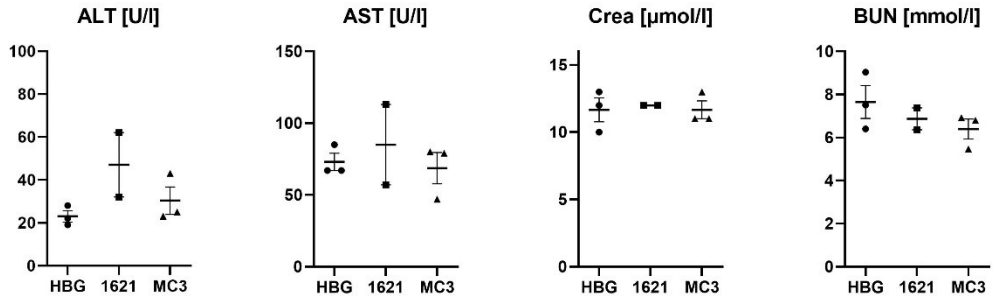

Figure 14. Evaluation of standard plasma parameters after intravenously applied siRNA-LNPs. Analysis of hepatic (ALT and AST) and renal (BUN and Crea) functions, tested in the plasma of treated mice by 1621-LNP (n=2) in comparison to MC3-LNP (n=3) and HBG-treated (n=3) groups. LNPs were prepared by Mina Yazdi (PhD student at Pharmaceutical Biotechnology, LMU, Munich) at different N/P and molar ratios (see **Table 1**). MC3, DLin-MC3-DMA; ALT, alanine aminotransferase; AST, aspartate aminotransferase; BUN, blood urea nitrogen; Crea, creatinine

3. DMD exon skipping with xenopeptide-PMOs

This chapter presents the relevant thesis parts adapted from a research article published as Lessl AL, Pöhmerer J, Lin Y, Wilk U, Höhn M, Hörterer E, Wagner E, Lächelt U. (2023) mCherry on Top: A Positive Read-Out Cellular Platform for Screening DMD Exon Skipping Xenopeptide-PMO Conjugates. Bioconjugate Chem. 34, 2263–2274.[135].

Splice-switching oligonucleotides, representing special steric block antisense oligonucleotides, interfere with splicing mechanisms of the pre-mRNA transcript and can therefore influence ribosomal protein expression in different ways [162]. By taking advantage of alternative splicing pathways, SSO *e.g.* hinder the attachment of endogenous splicing factors and consequently enhance the production of beneficial protein isoforms. However, transfection success is still limited by their poor delivery efficiency [119]. Therefore, different strategies of chemical alterations have been applied, concentrating on backbone, nucleobase or ribose sugar modifications, but also include alternative chemistries like phosphorodiamidate morpholino oligomers (**Figure 15**) [76].

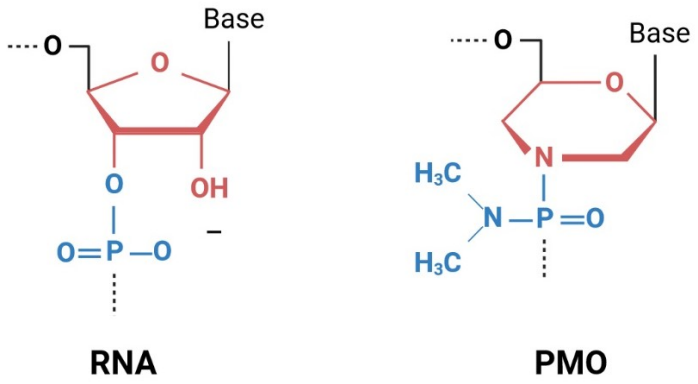

Figure 15. Schematic structures of RNA and PMO. In PMOs, ribose of the RNA is replaced with a morpholino ring (red) and the ionic phosphodiester group is substituted with an uncharged phophorodiamidate group (blue). RNA: Ribonucleic acid; PMO: Phosphorodiamidate morpholino oligomer. Figure created with Biorender.com.

To date, there are four FDA-approved PMO-therapeutics, namely Eteplirsen (Exondys 51) [163],Golodirsen (Vyondys 53) [164], Viltolarsen (Viltepso) [165], and Casimersen (Amondys 45) [166], that combined together, all base on exon skipping mechanisms for treating Duchenne muscular dystrophy. This degenerative muscular disorder is attributed to multiple nonsense or

frameshift mutations, causing alterations of the dystrophin gene, resulting in insufficient transcript levels and therefore lack of functional proteins [167, 168]. To achieve efficient restoration of dystrophin *in vivo*, low bioavailability rates and high renal clearance of intravenously applied PMOs have to be addressed [169]. Here, one common approach implements the conjugation of cell penetrating peptides (CPPs) to the uncharged PMO structure in order to enhance cellular uptake efficiencies [170, 171].

In our working group, we focus on sequence-defined XPs, containing oligo(ethylenamino) amide backbones with protonable, artificial aminio acid Stp units as well as natural amino acid motifs and fatty acid domains [62]. For PMO-delivery studies, a distinct library of the “T-shape” topology was utilized [64], as similar xenopeptide structures successfully showed efficient delivery of PMOs [67] and other therapeutic molecules *in vitro* and *in vivo* [172, 173].

In vitro studies were performed by Anna-Lina Lessl (PhD student at Pharmaceutical Biotechnology, LMU, Munich). Initially, different XPs were conjugated to PMOs by strain-promoted alkyne-azide cycloaddition (SPAAC, “click-reaction” [174]) of PMO–DBCO and azide-containing (N_3)- XP (**Figure 16A**). For a screening platform of XP-PMO conjugates *in vitro* that is likely to be transferred to *in vivo* conditions, Lessl et al. developed a positive reporter cell line based on the DMD *mdx* mouse model [175, 176]. Therefore, a sequence of two branching introns and enclosed exon 23 containing a nonsense mutation (*mdx DMDEx23*) was integrated in an mCherry gene of HeLa human cervical carcinoma cells. Consequently, exon skipping of the included sequence, faciliated by splice site blockade of the PMO oligonucleotides, can regenerate the functional reporter protein expression (**Figure 16B**). This specific artificial 5’ splice site (donor splice site) was created according to the physiological splice site of the DMD intron 23 and therefore ameliorates i*n vitro* and *in vivo* discrepancies. For a subsequent screening, PMO formulations coupled with preselected T-shape oligomers were transfected on the newly generated HeLa mCherry-DMDEx23 cell line and in a next step, fluorescence expression of the reporter protein was detected via flow cytometry (**Figure 16C**).

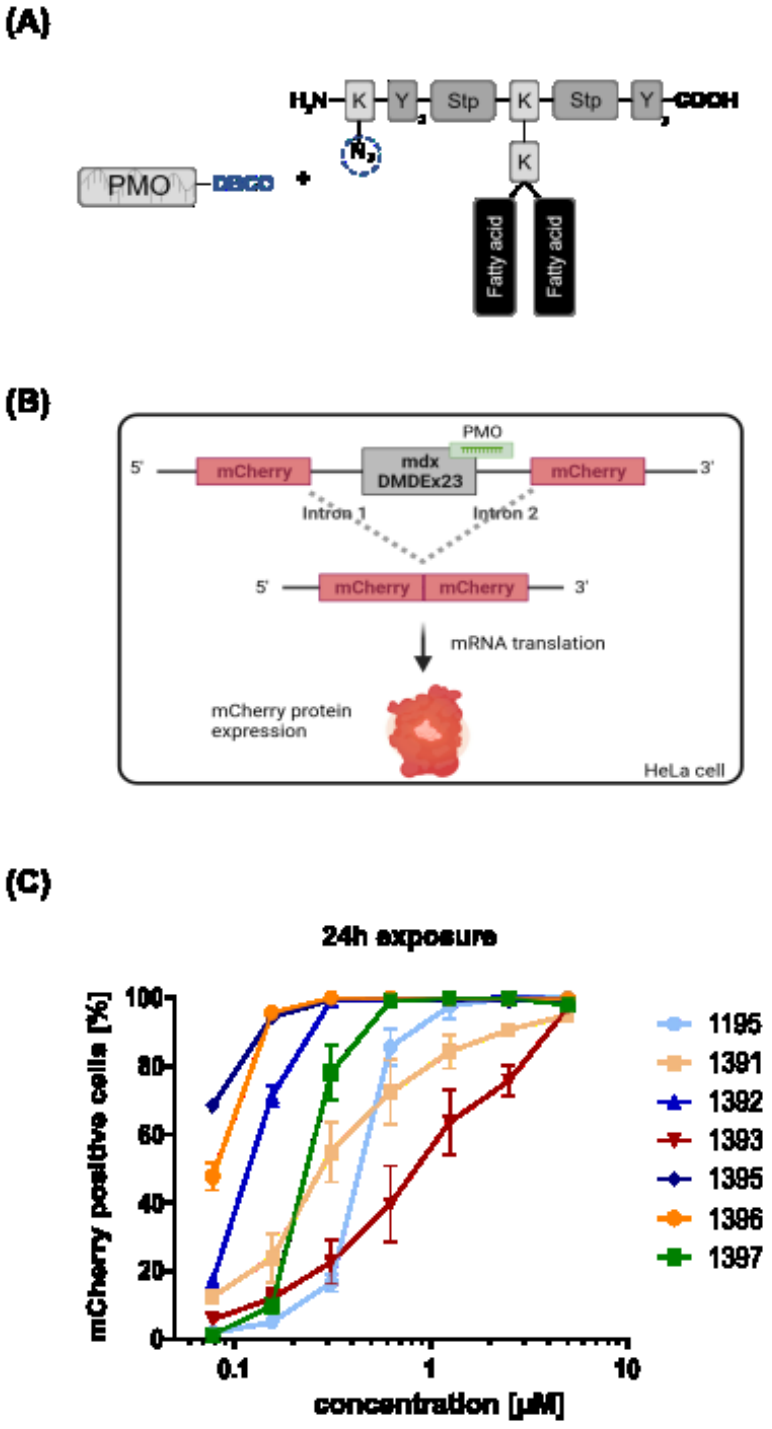

Figure 16. ***In vitro*** **establishment of the PMO conjugate structure.** **(A)** Schematic illustration of the conjugation of PMO-DBCO and azide-containing XP. **(B)** Structure of the HeLa mCherry-DMDEx23 reporter system and its mechanism in the presence of PMO. **(C)** Splice-switching activity in HeLa mCherry-DMDEx23 cells after 24 h exposure to PMO(Ex23)-XP 1:3 formulations (0,078 to 2.5 µM PMO) and subsequent incubation in fresh medium for 24 h. Figure (B) created with Biorender.com. The *in vitro* experiment (**Figure 16C**) was performed and evaluated by Anna-Lina Lessl (PhD student at Pharmaceutical Biotechnology, LMU, Munich).

3.1 Biodistribution of mRNA splicing modulation

In vitro prescreening of best perfoming formulations had identified PMO-**1395** conjugates as most adequate for systemic applications to animals (**Figure 17A**). As the incorporation of hydrophobic domains into T-shapes had been shown to be beneficial for carrier properties [65], two bound oleic acids and tyrosine tripeptides are primarily responsible for the stability of **1395**. Hence, PMO(Ex23)-**1395** as well as PMO (705)-**1395** and unformulated PMO(Ex23), containing 375 µg of PMO respectively, were administered into the tail vein of BALB/C mice, divided into groups of five (**Figure 17B**). Fourty-eight hours *p.i.*, mice were euthanized and organs (brain, spleen, kidney, liver, lungs and heart) as well as muscle tissues (*musculus quadriceps femoris*) were harvested for analysis of the DMD mRNA exon 23 splicing modulation by reverse transcription–PCR (RT-PCR) *ex vivo*.

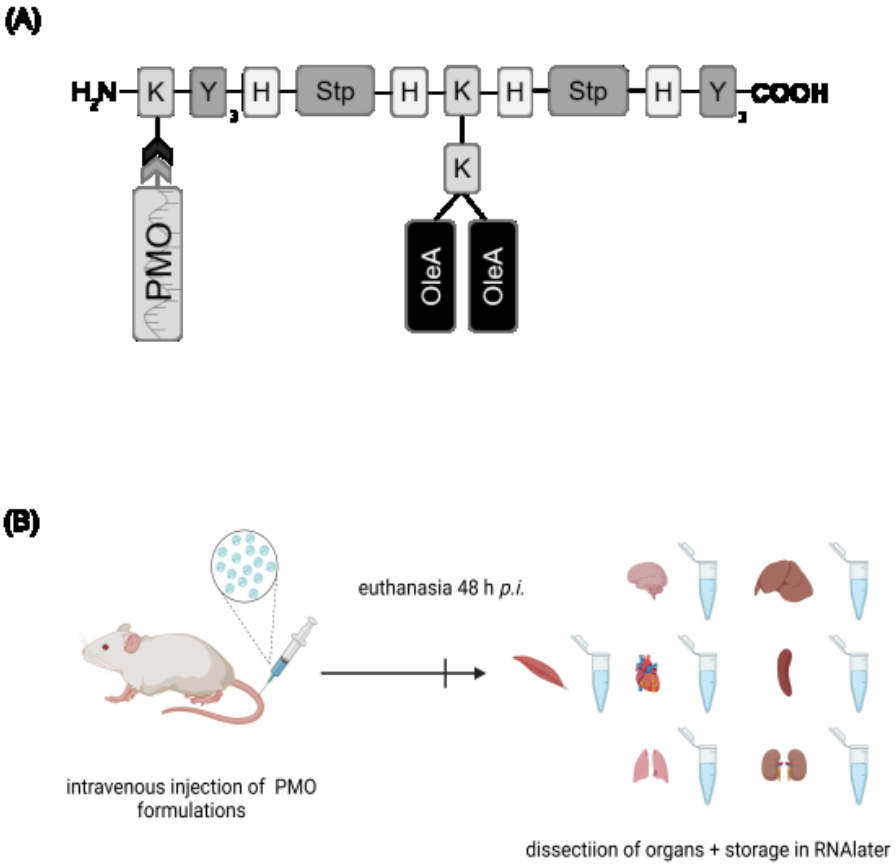

Figure 17. **Schematic illustration of the *in vivo* administration of PMO-XPs. (A)** Best performer **1395** is conjugated to PMO. **(B).** Mice were euthanized 48 h after injection of PMO formulations. Organs were harvested and stored in RNAlater. K, lysin; Y, tyrosine; H, histidine; Stp, succinoyl tetraethylene pentamine; FA, fatty acid; OleA, Oleic Acid (C18:1). Figure (B) created with Biorender.com.

As depicted in **Figure 18**, the results of gel electrophoresis are represented on the left side and corresponding ratios of splicing modulations on the right side. For the latter, intensities of the skipped exon 23 bands were measured with the ImageJ software and set into comparison with the intensities of unskipped exon 20-24 sequences. In contrast to other formulations, no splicing modulation was found in the first treatment group of PMO (705)-1395 (**Figure 18A**). As a negative control, the PMO (705) oligonucleotide does not attach to the DMD mRNA sequence and hence, only full-length bands of exon 20-24 could be detected. Whereas, PMO(Ex23), without peptide conjugation, induced only minor splicing modulation rates in *e.g*. kidneys, the formulation succeeded in exon skipping of dystrophin mRNA in skeleton muscles (**Figure 18B**) which corresponds to literature [177]. The click-connection to a preselected xenopeptide moreover, induced higher splicing rates in various organ samples except from muscle tissue. PMO(Ex23)-**1395** yielded in irregularly distributed exon skipping, especially in spleen, liver and lungs and moderately in brain, kidneys and heart (**Figure 18C**). In order to create a general overview of organ specific splicing modulation, the average exon skipping rates of each treatment group are summarized in **Figure 19A**. Thereby, not only minor splicing modulation of dystrophin mRNA in brain and heart occurred within the formulated PMO(Ex23)-**1395** administration, also higher exon skipping activities in kidneys, spleen, lungs and especially liver tissue. However, it is important to mention, that previous observed splicing modulation of the muscle, was only achieved by the free PMO(Ex23) formulation and could not be seen for the PMO(Ex23)-**1395** treated group. For confirmation of accurate exon skipping, the PCR products of one randomly selected PMO(Ex23)-**1395** administered mouse were extracted after gel electrophoresis (**Figure 19B**) and verified via Sanger sequencing, for the desired skipped exon 23 sequence (**Figure 19C**).

To summarize the biodistribution study of splicing modulation *in vivo*, PMO(Ex23)-**1395** resulted in moderate skipping rates of dystrophin exon 23 for spleen, kindneys, liver and lungs as well as, to minor extent, also for brain and heart. Compared to unconjugated PMO(Ex23), this clearly highlights an efficient PMO-XP formulation with potent shifting of muscle-

related splicing modulation to extramuscularly-attributed exon skipping of the dystrophin gene which represents an approach to expanding the application possibilities for potential therapeutics.

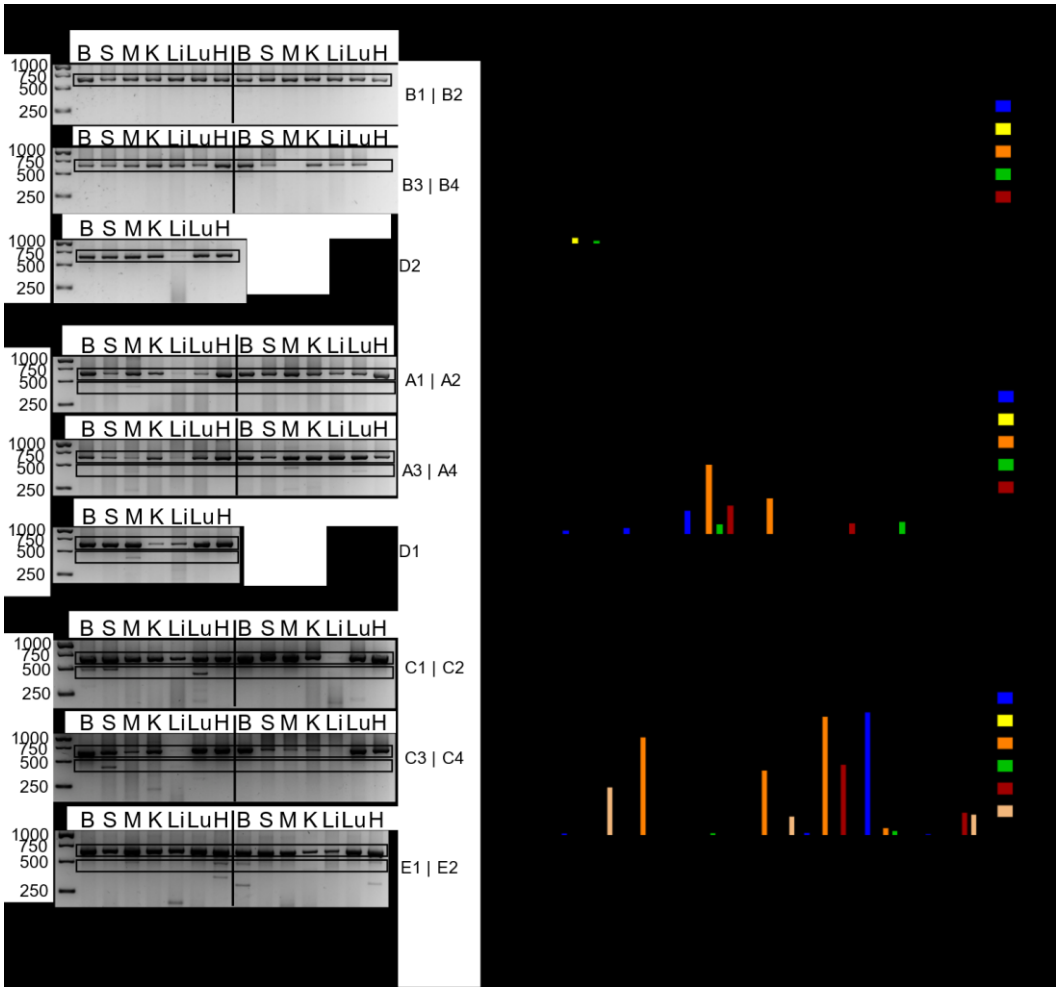

Figure 18. In vivo splicing modulation of dystrophin mRNA in BALB/C mice determined by RT-PCR. Total RNA was extracted from homogenized organs 48 h after intravenous injection of PMO formulations (375 µg PMO) and nested RT-PCR was conducted to amplify DMD Ex20-24. **A)** PMO (705)-1395 1:3 (n=5), **B)** naked unmodified PMO(Ex23) (n=5), and **C)** PMO(Ex23)-1395 1:3 (n=6). Single organs are indicated as “B, brain; S, spleen; M, quadriceps femoris muscle; K, kidneys; Li, liver; Lu, lung; H, heart. Ratios of splicing modulation were determined using ImageJ software and shown on the right side of each data set. The evaluation and graphical illustration of experiments was conducted by Anna-Lina Lessl (PhD student at Pharmaceutical Biotechnology, LMU, Munich).

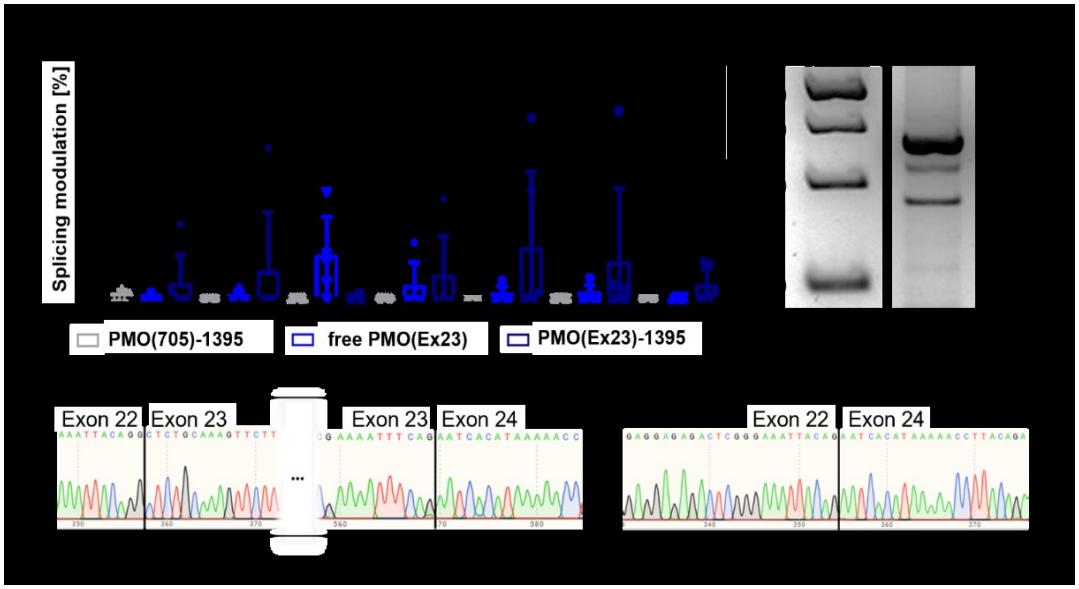

Figure 19. Summary of *in vivo* mRNA splicing modulation in BALB/C mice. A) Comparison of dystrophin mRNA splicing modulation in different organs of BALB/c mice determined *ex vivo* by RT-PCR 48 h after intravenous injection of PMO(Ex23) -**1395**, PMO (705) -**1395** formulations or unformulated PMO(Ex23). Total RNA was extracted from homogenized organs and nested RT-PCR were conducted to amplify DMD Ex20-24. (PMO (705) -**1395**, n=5; free PMO(Ex23) -DBCO, n=5; PMO(Ex23) -**1395**, n=6). All formulations contained 375 µg PMO. **B)** Exemplary gel electrophoresis result showing splicing modulation in the lung of animal C1 treated with PMO(Ex23) -**1395. C, D)** Sanger sequencing of gel extracted bands corresponding to approx. 633 bp **(C)** and 420 bp **(D)** fragments. Expected sequences of complete DMD Ex20-24 (~633 bp, **C**) and afterDMD exon 23 skipping (~420 bp, **D**) were found. The evaluation and graphical illustration of experiments was conducted by Anna-Lina Lessl (PhD student at Pharmaceutical Biotechnology, LMU, Munich).

3.2. Evaluation of clinical blood parameters

Intravenous injections of *in vitro* tested nanoagents may involve unexpected side effects in a living organism. In order to ensure tolerability of the applied PMO formulations, representative blood samples were taken in the process of euthanazation 48 h *p.i.* For analysis of liver enzymes and kidney function, ALT and AST levels as well as creatinine and BUN values were examined in the blood plasma. Compared to the free PMO(Ex23) and PMO (705)-**1395** formulations, none of the measured value of PMO(Ex23)-**1395** showed a remarkable discrepancy. With respect to all plasma parameters investigated, the mean values of PMO(Ex23)-**1395** yielded in the lower range, indicating a generally superior biocompatibility (**Figure 20**).

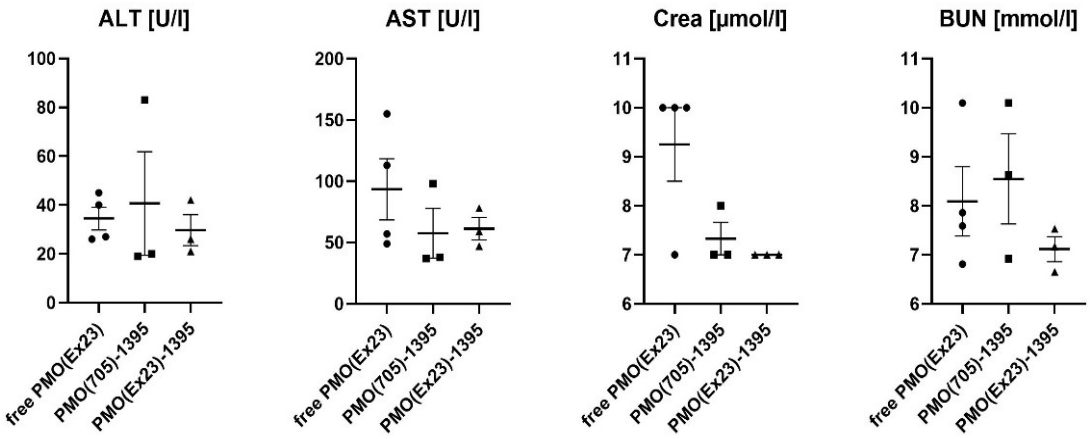

Figure 20. Evaluation of standard plasma parameters after intravenously administered PMO formulations. Blood samples were taken 48 hours after injections with applied PMO(Ex23)-**1395** (n=3), PMO (705)-**1395** (n=3) and unformulated PMO(Ex23) (n=4), containing 375 µg of PMO in 150 µL formulation. ALT, alanine transaminase; AST, aspartate aminotransferase; Crea, creatinine; BUN, blood urea nitrogen

4. Xenopeptide polyplexes for CRISPR Cas9 based gene editing

This chapter presents the relevant thesis parts adapted from a research manuscript submitted as Germer J., Lessl AL, Pöhmerer J, Grau M, Weidinger E, Höhn M, Yazdi M, Cappelluti M.A, Lombardo A, Lächelt U, Wagner E (2024) Lipo-Xenopeptide Polyplexes for CRISPR Cas9 Based Gene Editing at Ultra-Low Dose Targeting. Journal of Controlled Release, 370, 239-255 [136].

Direct targeting of eukaryotic DNA mutations has been a desirable aim in the field of genome therapies for decades. Artificial enzymes like zinc finger nucleases (ZFNs) or transcription activator-like effector nucleases (TALENs) were introduced as genome editor systems for applications in various studies and also clinical trials [178, 179]. However, the invention of the CRISPR-Cas9 mechanism in 2012 [180], represents a breakthrough technology for straightforward and cost-effective gene editing [7, 181]. This mechanism is based on a complex of the endonuclease Cas9 and a specific guide RNA for direction to the intranuclear DNA target site. Here, a double strand break is induced at a distinct locus upstream the specific proto-spacer adjacent motif (PAM) sequence [182] which subsequently promotes endogenous repair mechanisms (*see below*).

For efficient *in vivo* delivery of the Cas9 system, virus-like vectors, *e.g.* adeno-associated virus vectors [183], have been utilized, although immune responses of the host organism [184] and weak loading capacities restrict the development of therapeutic applications [185]. That is why, non-viral carriers were introduced with a superior safety profile, lower costs of production and higher encapsulation efficiencies [7]. Besides polymer-based nanoparticles [186], lipid-like vectors promised high *in vivo* applicability of co-delivered Cas9mRNA and sgRNA already at early stage [187] and proved their superior efficiency with the clinical approval of lipid nanoparticles in SARS-CoV-2 mRNA vaccines [72, 188]. Because of its transient expression and reduced risk of genomic integration, mRNA is supposed to result in reduced off-target effects as well as lower adverse reactions regarding the host´s immune system [189]. Moreover, in contrast to plasmid DNA, intranuclear delivery is not required for ribosomal translation of the Cas9mRNA and high expression levels of Cas9 protein are already achieved at early time points [187, 190]. Our own working group recently established a new generation of sequence-defined lipo-

xenopeptide carriers with double pH-responsive LAF subunits which already proved their *in vivo* efficiency in mRNA polyplex formulations [69] as wells as in equal LNPs systems [70]. Based on this and in consideration of successful delivery of Cas9/sgRNA RNPs with former generations of similar vectors [68], further progress can be expected by loading these synthetic carriers with Cas9mRNA/sgRNA.

In somatic mammalian cells, there are generally two mayor strategies for genome editing of the assembled CRISPR Cas9 complex after nuclear entry [191] which are illustrated in **Figure 21**. The aforementioned double strand break in the genomic DNA sequence is followed by either non-homologous end joining (NHEJ) or, in presence of a suitable DNA template, by homology directed repair (HDR). NHEJ represents an error-prone, direct linkage mechanism of the disconnected DNA strands, including random insertions or deletions (INDELs). This can be reflected in either frameshift mutations or target gene knockouts and occurs in most post-mitotic eukaryotic cells [192]. On the other side, an accurate repair strategy can be mediated by the insertion of a defined DNA sequence between homologous sequences of the target DNA, following the HDR pathway [193].

More recently, next-generation applications for CRISPR-Cas9 technology have emerged, including base and prime editing for even more precise genome modification without causing DSBs [194, 195].

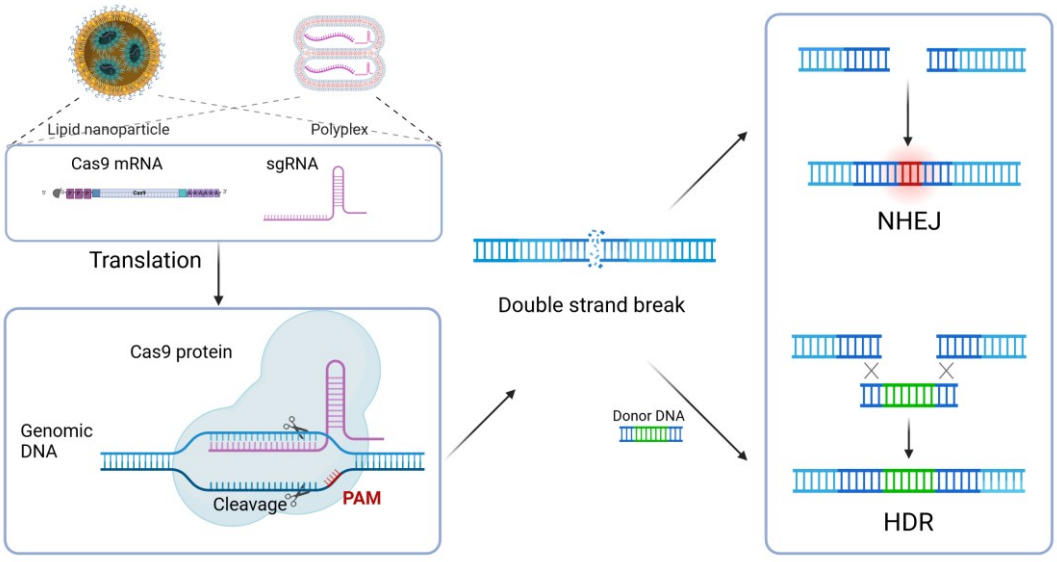

Figure 21. Schematic illustration of RNA-based genome editing strategies of the CRISPR/Cas9 system. Cas9mRNA, compacted in either LNPs or polyplexes

respectively, leads to ribosomal translation of the Cas9 protein. Subsequently, the intranuclear DNA target site is recognized by a specific sgRNA and the Cas9 endonuclease mediates a double strand break (DSB) upstream the proto-spacer adjacent motif (PAM). Afterwards, two major endogenous repair mechanisms take place: non-homologous end joining (NHEJ) resulting in frame shift mutations and target gene knockout, or homology directed repair (HDR) introducing target gene knock-ins by inserting a defined DNA template with homologous ends, *e.g.* co-delivered by the applied carrier. Figure created with Biorender.com.

For an initial characterization of potent lipo-xenopeptides *in vitro*, Janin Germer (PhD student at Pharmaceutical Biotechnology, LMU, Munich) evaluated the transfection efficiencies of Cas9 mRNA/sgDMD$_{Ex23}$ polyplexes on the same reporter model that was previously designed for screening of PMO-conjugates [135]. Here, the ratio of splice modulation in HeLa mCherry-DMD$_{Ex23}$ cells with different dosis of carriers are represented in **Figure 22A** and compared with the same transfection efficiencies including prior incubation of FBS (**Figure 22B**). Skipping of the mutated DMD exon 23 is presumably referred to restored splicing mechanisms after excluding termination codons of the dystrophin genome via NHEJ instead of precise genetic modification by the HDR pathway [196]. Applying a specific sgRNA (sgDMD $_{Ex23}$) codelivered with Cas9mRNA, faciliates precise targeting of the reporter cell genome and subsequently inducing a DSB in the vicinity of dystrophin exon 23. Therefore, small INDELs generated in the disrupted mCherry-DMD $_{Ex23}$ genome after the NHEJ repair mechanism are most likely to be responsible for rebuilding detectable mCherry reporter protein expression [196].

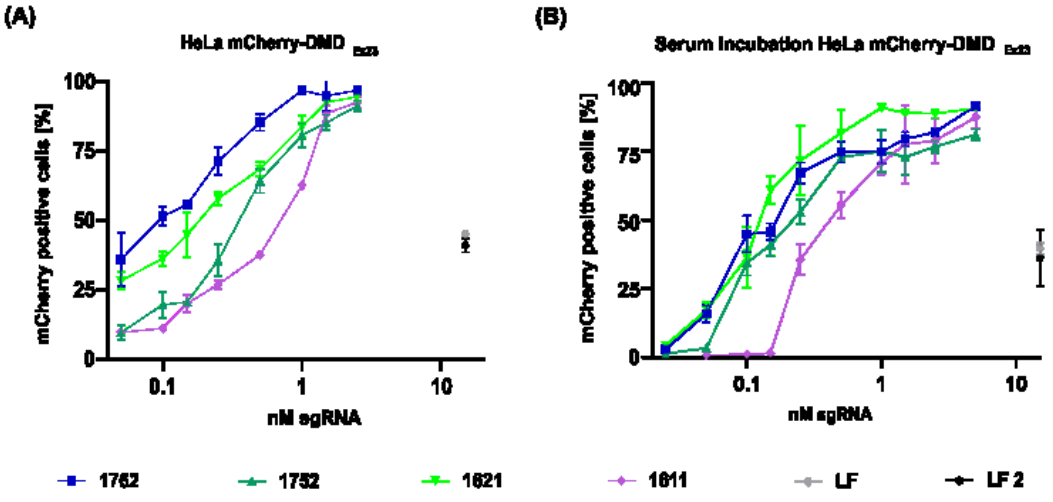

Figure 22. *In vitro* performance of Cas9 polyplexes on a HeLa mCherry-DMD$_{Ex23}$ cells. Dose titration of best performing LAF-Stp carriers forming Cas9 polyplexes containing Cas9 mRNA and sgRNA at weight ratio 1:1. N/P ratio of

bundle and U1 carriers was 24 and 18, respectively. **(A)** *In vitro* exon skipping evaluation on in HeLa mCHerry-DMD_{Ex23} with 50 pM – 2.5 nM $sgDMD_{Ex23}$. Positive controls were presented by Lipofectamine™ Messenger MAX™ lipoplexes (LF, LF2) used for transfection of Cas9 mRNA and sgRNA according to both manufacturer's protocol options resulting in a concentration of 15 nM sgRNA. **(B)** *In vitro* performance of LAF polyplexes in presence of full serum. Samples were diluted in full serum (25 pM– 0.5 nM $sgDMD_{Ex23}$, 98 % serum; 1-2.5 nM, 90 % serum) and transfected at indicated low doses in HeLa mCHerry-DMD_{Ex23}. (n=3, mean ± SD). These experiments were performed and evaluated by Janin Germer (PhD student at Pharmaceutical Biotechnology, LMU, Munich).

4.1. Pre-experiment: Luciferase expression after intramuscular injection of LAF polyplexes and LNPs

In order to evaluate local administration of novel lipo-xenopeptide carriers equally to the already established systemic application of luciferase mRNA polyplexes [69] and LNPs [70] *in vivo*, a pre-experiment was performed at first. Therefore, tumor-free BALB/C mice, subdivided into groups of four, were intamuscluarly injected with polyplexes or LNP formulations containing 3 µg of luciferase mRNA and subsequently euthanized 6 h *post injectionem*. As previous *in vitro* studies of luciferase mRNA polyplexes promoted (*data not shown*), 12Oc **1611** was selected as best performing U-shape as well as 12Bu **1752** and 10Oc **1762** as representative bundle topologies. Only 8Oc **1621** was inserted in both delivery vectors, as component of LNPs, in direct comparison to positive control SM-102 LNP, as well as in mRNA polyplexes. The experimental setup and the evaluation of luciferase expression, measured in the injected left *musculus biceps femoris* is represented in **Figure 23**. For this experimental series, LNPs were formulated with cholesterol, sheddable DMG-PEG and 1,2-dioleoyl-sn-glycero-3-phosphoethanolamine (DOPE) as phospholipid, according to *Cheng et al*. [197], to enhance nucleic acid compaction, endosomal escape and subsequently transfection efficiency of the LNPs. Both injected LNP formulation resulted in remarkably high luciferase activity with over 10^{10}RLU/g in muscle tissue and no significant difference between the gold standard SM-102 and lipo-XP carrier **1621**. Moreover, luciferase expressions of polyplex formulations could not reach equal levels, but achieved up to 100-fold lower values (10^8-10^9 RLU/g muscle), compared to injected LNPs. 10Oc **1762**, however, reached the highest activity among

administered mRNA polyplexes with a small, but no significant difference to the benchmark formulation of SM-102 LNPs. Additionally, luciferase expression analysis of further harvested organ samples outlines a concrete accumulation of **1621** LNP in the injected muscles (**Figure 24**), in contrast to organ efficacy levels lower than 10^5-10^7 RLUs. Simultaneously for polyplex formulations, expression values in other organs persisted to be 100- to 100- fold lower compared to the injected muscle and over all, in 60% of the measurements, values did not even lay in the range of detection sensivity.

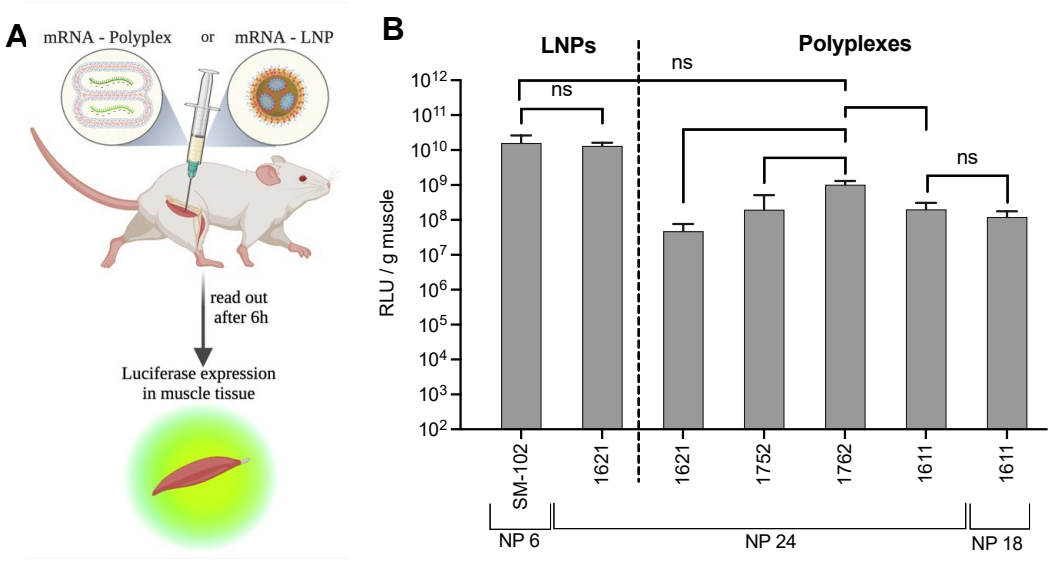

Figure 23. Luciferase expression in muscular tissue after local injection of LAF containing mRNA polyplexes and mRNA LNPs. All LAF-formulations were compared to LNP containing SM-102 at a definite molar ratio (**Table 1**) and at N/P 6 as gold standard. **(A)** Treatment schedule. **(B)** Luciferase activity in RLU was determined ex vivo per gram (g) muscle at 6 h post injection (n=4; mean ± SD). **1621** LNPs were formulated by Janin Germer (PhD student at Pharmaceutical Biotechnology, LMU, Munich) according to *Cheng et al*. [197] with a molar ratio of 47.6:23.8:4.8:23.8 mol% 130 (cholesterol: DOPE: PEG-DMG:**1621**) at the N/P ratio of 24. Significance between 1762 containing polyplexes and all other polyplexes: ** $p \leq 0.01$, Significance between 1762 containing polyplexes or LNP 1621 and SM-102: statistically not significant. * $p \leq 0.05$; ** $p \leq 0.01$; *** $p \leq 0.001$; **** $p \leq 0.0001$; ns, statistically not significant. Intramuscular injections into the left *musculus biceps femoris* were performed in cooperation with Ulrich Wilk (former vetPhD student at Pharmaceutical Biotechnology, LMU, Munich). The graphical illustration was provided by Janin Germer (PhD student at Pharmaceutical Biotechnology, LMU, Munich).

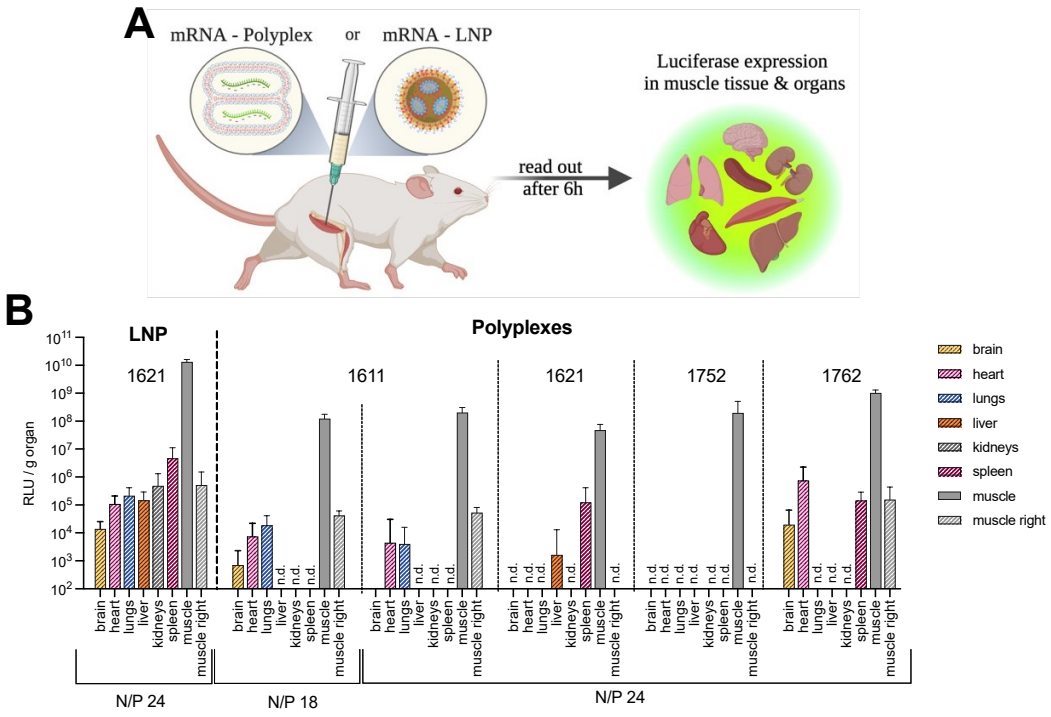

Figure 24. *In vivo* luciferase activity of LAF-Stp mRNA polyplexes and mRNA LNPs in other organs after intramuscular injection. (A) Schematic illustration of the treatment procedure. **(B)** Ex vivo luciferase assay of the organs of BALB/C mice. Luciferase activity in RLU was determined ex vivo per gram (g) organ at 6 h *post injectionem*. Performance of **1621** mRNA LNP indicated N/P ratio and a molar ratio of 47.6:23.8:4.8:23.8 mol% 130 (Chol: DOPE: PEG-DMG:1621). Performance of mRNA polyplexes with indicated N/P ratio 6 hours after intramuscular injection. (n=4; mean ± SD). n.d.: not detectable signal. Muscle right: contralateral, non-injected muscle. Intramuscular injections into the left *musculus biceps femoris* were performed in cooperation with Ulrich Wilk (former vetPhD student at Pharmaceutical Biotechnology, LMU, Munich). The graphical illustration was provided by Janin Germer (PhD student at Pharmaceutical Biotechnology, LMU, Munich).

4.2. *In vivo* genome editing and splicing modulation by Cas9/sgRNA xenopeptides

Based on the findings of the previous luciferase expression study together with the results of the aforementioned *in vitro* exon skipping experiments, best performing lipo-xenopeptide carriers **1611**, **1762** and **1621** were either administered as Cas9mRNA/sgRNA polyplexes or, in regard of **1621,** as cationizable components of Cas9mRNA/sgRNA LNPs. In the following, systemic and intramuscular injections of **1611** polyplexes, loaded with 10 µg total RNA, and **1762** polplexes or **1621** LNPs, loaded with 3 µg total RNA, were analyzed. Therefoe, exon skipping efficiencies on the one hand, and editing capacities on a genomic level on the other hand were evaluated.

It is crucial to mention, that the previously established reporter system by Lessl et al. [135] based on the widely-used DMD mdx model [198], can be transferred from *in vitro* to *in vivo* conditions as the PMO(Ex23) was designed on specific sequences occurring in the vicinity of the dystrophin exon 23 also in wild type mice. As far as the co-delivery of Cas9mRNA and sgRNA is concerned, applying a specific sgRNA (sgDMD $_{Ex23}$) [196] enables equal targeting of the splice site downstream the murine dystrophin exon 23 and elicits genome editing capacities as well as splicing modulation in consequence.

Intravenous injections of Cas9mRNA/sgDMD$_{Ex23}$

For systemic administration, tumor-free BALB/C mice were split into four groups (n=4) with injections of **1611** and **1762** polyplexes as well as **1621** LNPs starting on the first day. In total, three treatments were carried out at specific time points (day 0, 2, 7) over a period of seven days and euthanazation was conducted on day 14. The fourth group of untreated mice served as a negative control and was simultaneously sacrificed on the same day as treated animals. Consequently, organs with attributed dystrophin expression [199], *i.e.* brain, heart and muscle (*musculus biceps femoris*) were harvested for incubation in RNAlater, grinded in liquid nitrogen and subjected to biomolecular evaluation operated by Janin Germer (PhD student at Pharmaceutical Biotechnology, LMU, Munich). On the one side, evaluation of splicing modulation included mRNA isolation, RT-PCRs and electrophoretic separation of the amplificated sequences. On the other side, analyses of genomic alteration were represented by Sanger Sequencing and TIDE evaluation (**Figure 25**).

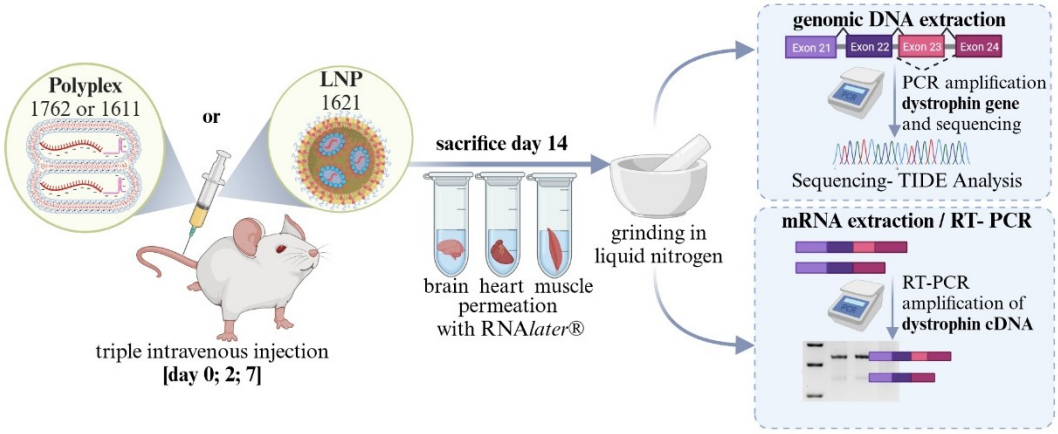

Figure 25. Treatment scheme of triple intravenously injected BALB/C mice, sample preparation and biomolecular evaluation. Systemic injection of **1762** polyplexes and **1621** LNPs containing either 3 µg total RNA or systemic injection of 10 µg total RNA in **1611** polyplexes trice, on day 0,2, and 7. Total RNA and genomic DNA was extracted from homogenized organs 7 days after last injection. For the evaluation of splicing modulation, a nested RT-PCR was conducted to amplify DMD Ex20-24. The RT-PCR product was analyzed on a 2 % agarose gel and ratios of splicing modulation were determined using ImageJ Software. For the analysis of the gene editing efficiency a PCR was performed to amplify the region surrounding exon 23. PCR products were purified and sequenced via Sanger sequencing. The sequencing results were evaluated using the TIDE analysis tool. Graphical illustration and molecular evaluation conducted by Janin Germer (PhD student at Pharmaceutical Biotechnology, LMU, Munich).

As summarized in **Figure 26A**, splicing modulation of the DMD exon 23 was observed in all treatment groups with significant differences to the negative control group (untreated animals). Therefore, gel electrophoresis bands of skipped exon23 sequences and of full-length DMD-Ex20-24 (**Figure 27**) were analyzed regarding their intensities by using the ImageJ software and yielding ratios are represented by the column chart (**Figure 26A**). Here, exon skipping in the brain was detected among all treated animals and notably discovered in samples of the polyplex **1762** group (mean value of 13.1% ± 4.4% SD). In contrast to the administered LNP formulation, polyplexes mediated significantly lower rates of splicing modulation in the heart, whereas **1621** LNPs elicited moderate values of 5.7% ± 1.1 % (mean ± SD). Unexpected low activites of exon skipping in muscle tissue were achieved by **1621** LNPs and only **1611** polyplexes could reach almost 10% of splicing modulation (mean value of 13.1% ± 4.4% SD). At this point, it should be noted, that relevant differences between the splicing modulation ratios of individual animals in each group were obvious regarding muscle and brain evaluation of exon skipping events.

Further biomolecular procedures of gene editing assessments, namely Sanger sequencing and TIDE analysis, are exemplarly demonstrated in **Figure 28** and resulting activities are illustrated in **Figure 26B**, versus the rates of splicing modulation (**Figure 26A**). Here, total efficiencies of genome editing generally remained at a lower level than corresponding exon skipping values. Although solely 2,5% - 4,7 % genetic alterations were evident in injected groups, differences were considered as significant compared to untreated animals (<0,7%). Finally, effects of the systemically applied Cas9mRNA/sgDMD$_{Ex23}$ polyplexes and LNPs appeared clearly on a mRNA level and also at moderate extent on a genomic basis, achieving moderate splicing values and lower gene editing efficiencies that are summarized in **Table 2.**

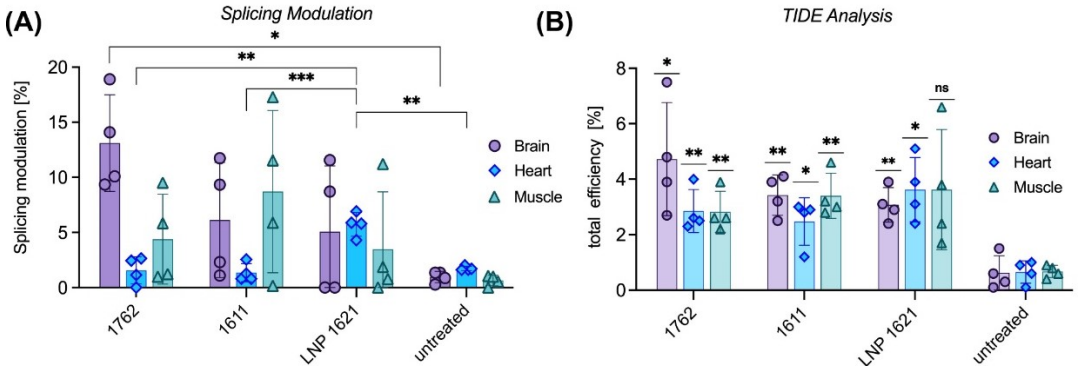

Figure 26. Evaluation of *in vivo* mRNA splicing modulation (A) and genome editing (B). DMD mRNA splicing modulation and genome editing in different organs of BALB/C mice after triple injections of Cas9 polyplexes or Cas LNP solution containing Cas9 mRNA and sgDMD$_{Ex23}$ at weight ratio 1:1. **(A)** Evaluation of splicing modulation, after triple intravenous treatment with either **1762** (N/P 24) polyplexes, **1611** (N/P 18) polyplexes or **1621** (N/P 24) LNPs. Individual band intensities were quantified and put into relation to the band of full-length DMD-Ex20-24 with a size of 568 bp by using the ImageJ software. The complete gel electrophoresis data are provided in **Figure 27**. **(B)** Evaluation of gene editing efficiency after triple intravenous application of **1762** polyplexes and **1621** LNP containing 3 µg total RNA and 1611 polyplexes containing 10 µg total RNA. Exemplary Sanger-sequences evaluation and TIDE analysis. (n=4, mean ± SD) are shown in **Figure 28**. Asterisks indicate statistical significance between treated organ to untreated control. * $p \leq 0.05$; ** $p \leq 0.01$; *** $p \leq 0.001$; ns, statistically not significant. Graphical illustration and molecular evaluation conducted by Janin Germer (PhD student at Pharmaceutical Biotechnology, LMU, Munich).

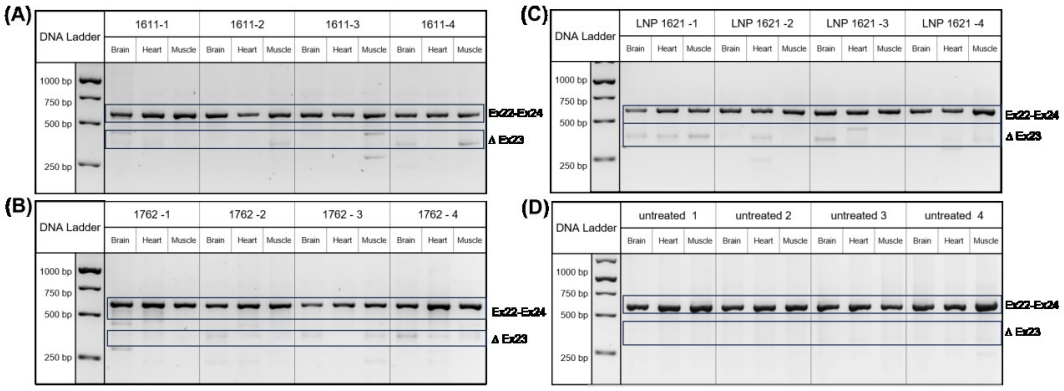

Figure 27. *In vivo* mRNA splicing modulation in BALB/C mice after triple injection with Cas9 polyplexes and Cas9 LNP. Total RNA was extracted from homogenized and nested RT-PCR was conducted to amplify DMD Ex20-24. The dystrophin expressing organs brain, heart and muscle tissue were analyzed after systemic application of Cas9 polyplexes formed with LAF **(A) 1611** at N/P 18 (10 µg total RNA); **(B) 1762** at N/P 24 (3 µg total RNA); **(C) 1621** at N/P 24 (3 µg total RNA) and **(D)** untreated treated animals (n=4) as negative control. Graphical illustration and molecular evaluation conducted by Janin Germer (PhD student at Pharmaceutical Biotechnology, LMU, Munich).

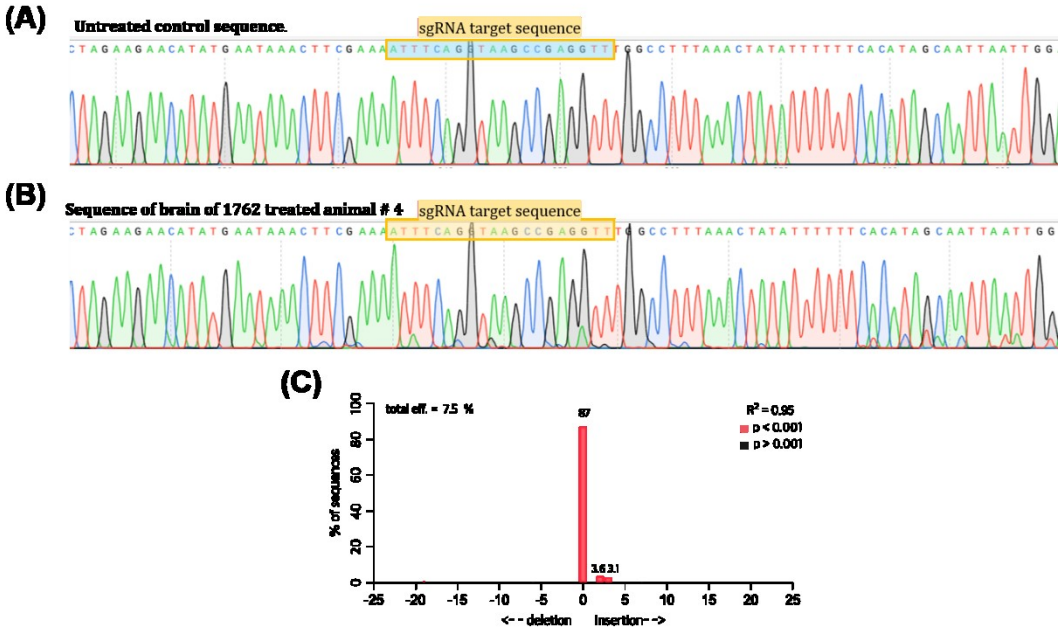

Figure 28. Exemplary Sanger sequencing and TIDE Analysis of the genomic dystrophin sequence after treatment with Cas9mRNA/sgDMD$_{Ex23}$ formulations. Total genomic DNA was extracted from homogenized organs and PCR were conducted to amplify the genomic region surrounding the dystrophin exon 23. PCR products were purified, Sanger-sequenced and evaluated by TIDE (Tracking of Indels by Decomposition) analysis. **(A)** Exemplary sequence showing the section around the sgDMD$_{Ex23}$ targeted genomic region of an untreated animal. **(B)** Exemplary sequence showing the section around the sgDMD$_{Ex23}$ targeted genomic region of the brain in animal # 4 treated with Cas9/sgDMD$_{Ex23}$ polyplexes formed with carrier **1762**. Histogram shows aberrant small peaks around and downstream the cut site. **(C)** TIDE Analysis result of indel spectrum for the

sequence shown in **(B).** Graphical illustration and molecular evaluation conducted by Janin Germer (PhD student at Pharmaceutical Biotechnology, LMU, Munich).

		Splicing modulation		Genomic evaluation		Splicing modulation		Genomic evaluation		Splicing modulation		Genomic evaluation	
	No	**(%)**	**mean ± SD**	**(%)**	**mean ± SD**	**(%)**	**mean ± SD**	**(%)**	**mean ± SD**	**(%)**	**mean ± SD**	**(%)**	**mean ± SD**
		brain				**heart**				**muscle**			
1762	**#1**	9.4	13.1 ± 4.4	2.7	4.7 ± 2.0	1.1	1.6 ± 1.2	2.3	2.9 ± 0.8	8.8	9.0 ± 5.1	2.6	2.8 ± 0.7
	#2	14.1		4.8		2.6		2.5		16.4		2.2	
	#3	10.1		3.9		0.0		2.6		5.6		2.6	
	#4	18.9		7.5		2.4		4.0		5.4		3.9	
1611	**#1**	11.7	6.1 ± 5.2	4.1	3.4 ± 0.7	2.6	1.4 ± 0.8	2.8	2.5 ± 0.9	0.2	8.7 ±7.4	2.8	3.4 ± 0.8
	#2	2.3		3.9		0.8		2.9		5.9		4.6	
	#3	1.1		2.5		1.3		1.2		17.3		3.2	
	#4	9.3		3.2		0.8		3.0		11.6		3.0	
1621- LNP	**#1**	11.6	5.1 ± 6.0	3.1	3.1 ± 0.6	5.9	5.7 ± 1.1	5.1	3.6 ± 1.2	11.2	3.5 ±5.2	6.6	3.6 ±2.2
	#2	0.0		2.4		5.8		3.1		0.8		2.4	
	#3	8.7		3.9		6.9		2.4		0.0		1.7	
	#4	0.0		2.9		4.3		3.9		1.9		3.8	
untreated	**#1**	1.3	1.0 ± 0.5	0.3	0.6 ± 0.6	1.6	1.7 ± 0.2	0.1	0.7 ± 0.4	1.1	0.7 ± 0.5	0.4	0.7 ± 0.2
	#2	0.3		0.6		1.7		1.0		0.6		0.8	
	#3	1.3		1.5		2.0		0.6		0.0		0.9	
	#4	0.9		0.1		1.6		0.9		1.0		0.6	

Table 2. *In vivo* editing of dystrophin gene after intravenous application. *In vivo* mRNA splicing modulation and genome editing in BALB/c mice after intravenous injection with Cas9 polyplexes and Cas9 LNP. Splicing modulation was determined using ImageJ Software. Genomic evaluation was performed by Sanger sequencing and subsequent evaluation of total editing efficiency with the TIDE analysis tool (https://tide.nki.nl/). All data are presented in percent for individual animals and mean ± SD (n=4). Graphical illustration and molecular evaluation conducted by Janin Germer (PhD student at Pharmaceutical Biotechnology, LMU, Munich).

Intramuscular injections of Cas9mRNA/sgDMD$_{Ex23}$

In comparison to systemic injections, equal formulations, complemented by positive control SM-102 LNPs with 3 µg of RNA in total, were applied locally in a follow-up study. To prevent localized damage to muscle fibers by the injection fluid, groups of four mice were either injected thrice in a larger period of two weeks (day 0, 3, and 14) or treated with only single intramuscular administration instead. Again, seven days after the last injection, animals were sacrificed and biomolecular evaluation of the dissected muscle tissue was conducted subsequently by Janin Germer (PhD student at Pharmaceutical Biotechnology, LMU, Munich) (**Figure 29**). Splicing modulation rates of skeletal muscles after triple injections are compared with the efficiencies of single applications on the one side (**Figure 30A**) and both are displayed next to the editing activities of the dystrophin gene in equivalent treatment groups on the other side (**Figure 30B**). An illustration of the complete gel electrophoresis evaluation is added in **Figure 31** as well as precise values of exon skipping and genomic alterations, summarized in **Table 3**.

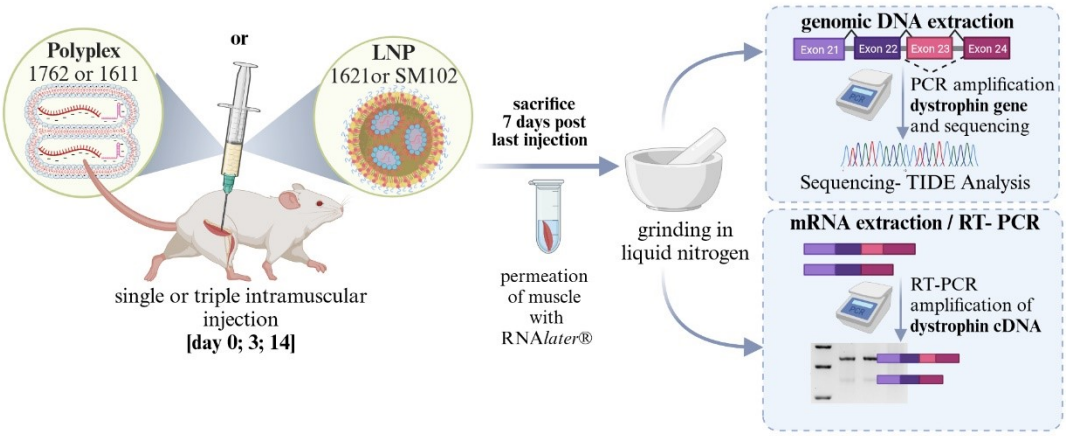

Figure 29. Injection scheme of single or triple intramuscularly injected BALB/C mice, sample preparation and evaluation. Injection volume of 50 µL nanocarrier solution containing either 3 µg total RNA in **1621** (N/P 24) LNP and **1762** polyplexes (N/P 24) or 10 µg total RNA in **1611** polyplexes (N/P 18). SM102 LNP at N/P 6 containing 3 µg total RNA in 50 µL served as gold standard. Intramuscular injections were performed in cooperation with Ulrich Wilk (former vetPhD student at Pharmaceutical Biotechnology, LMU, Munich) and Mina Yazdi (PhD student at Pharmaceutical Biotechnology, LMU, Munich). Graphical illustration and molecular evaluation conducted by Janin Germer (PhD student at Pharmaceutical Biotechnology, LMU, Munich).

Firstly, exon skipping rates of repeated applications evidently outperformed single injections in all treatment groups, reaching slightly higher in Cas9mRNA/sgRNA polyplexes than LNP formulations, and demonstrating a significant difference to the negative control (untreated mice) (**Figure 30A**). Analogous results were observed on a genomic level, implicating lower editing efficiencies over all. In a comparable manner, triple injections of lipo-xenopeptide carriers achieved higher levels of genome editing with significant differences between not injected muscle tissues and **1762** (** $p \leq 0.01$) and **1611** polplexes (**** $p \leq 0.0001$). For LNP formulations, smaller rates of genome editing were obvious, displaying a minor, not statistically significant, disparity to the negative control.

In conclusion, splicing modulations of 6,0 % - 9,3 % combined with gene editing efficiencies of 2,3 % - 3,4 % after local application ranked in the same area as exon skipping rates and editing efficiencies of the dystrophin gene past systemic application, as far as muscle samples are concerned. Single injections however, were less successful on both aspects and demonstrate the requirement of repeated treatments for efficient Cas9mRNA/sgRNA genome editing.

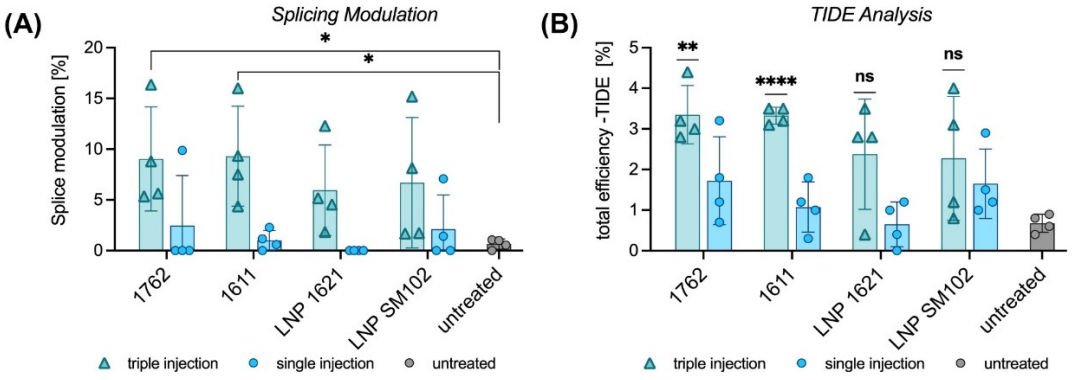

Figure 30. *In vivo* mRNA splicing modulation and genome editing in BALB/C mice (n=4) after intramuscular injection with Cas9 polyplexes and Cas9 LNP. **(A)** For the evaluation of splicing modulation, a nested RT-PCR was conducted to amplify DMD Ex20-24. The RT-PCR product was analyzed on a 2% agarose gel and ratios of splicing modulation were determined using ImageJ Software. The complete gel electrophoresis data are provided in **Figure 31**. **(B)** For the evaluation of gene editing, total genomic DNA was extracted from homogenized organs and PCR were conducted to amplify the genomic region surrounding the DMD Ex23. PCR products were purified, Sanger-sequenced and evaluated by TIDE analysis. (n=4, mean ± SD). Asterisks indicate statistical significance between treated organ

to untreated control. * p ≤ 0.05; ** p ≤ 0.01; **** p ≤ 0.0001; ns, statistically not significant. Graphical illustration and molecular evaluation conducted by Janin Germer (PhD student at Pharmaceutical Biotechnology, LMU, Munich).

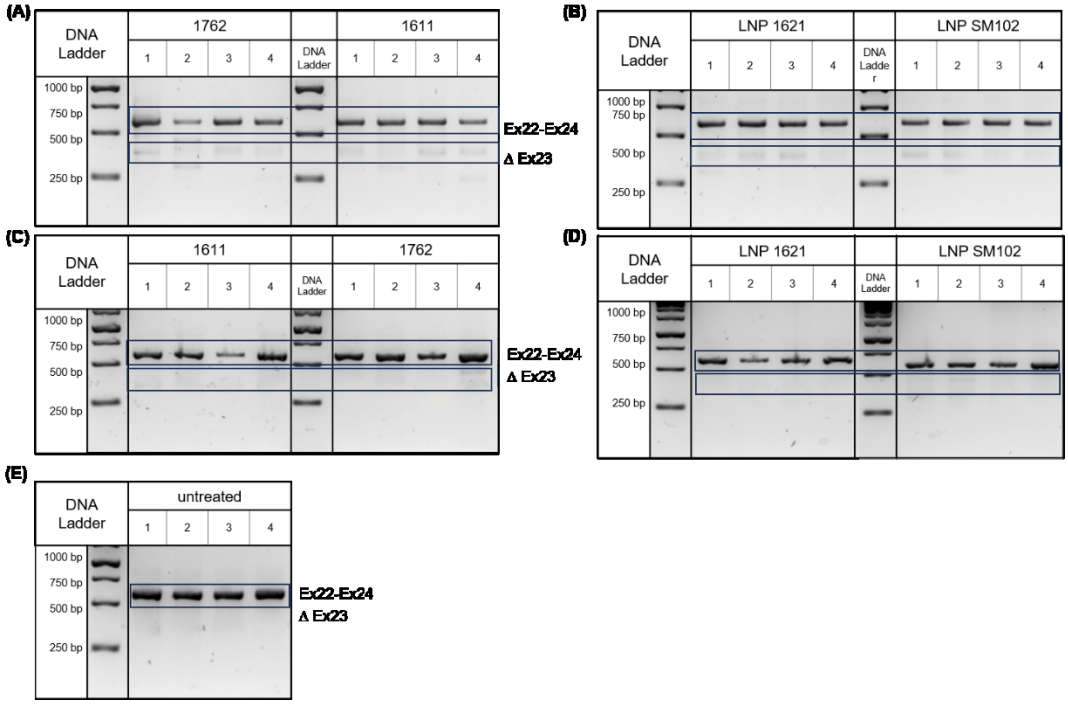

Figure 31. ***In vivo*** **mRNA splicing modulation in BALB/C mice after intramuscular injection with Cas9 polyplexes and Cas9 LNP.** Total RNA was extracted from homogenized muscle tissue 7 days after last of single or triple intramuscular injection with Cas9 polyplexes or Cas LNP containing Cas9 mRNA and sgDMD$_{Ex23}$ at weight ratio 1:1. 10 µg total RNA were applied with LAF **1611** containing Cas9 polyplexes, 3 µg total RNA was applied for all other Cas9 formulations. A nested RT-PCR was conducted to amplify DMD Ex20-24. Only the tissue of the injected muscle was analyzed after intramuscular application. **(A)**, **(B)** triple and **(C)**, **(D)** single intramuscular application Cas9 polyplexes **(A)**, **(C)** formed with LAF **1762** at N/P 24 (3 µg total RNA), LAF **1611** at N/P 18 (10 µg total RNA) and Cas9 LNPs **(B)**, **(D)** formed with LAF **1621** at N/P 24 (3 µg total RNA) and SM-102 as ionizable lipid as gold standard LNP formulation (3 µg total RNA). **(E)** untreated control group. Graphical illustration and molecular evaluation conducted by Janin Germer (PhD student at Pharmaceutical Biotechnology, LMU, Munich).

		Splicing modulation		Genomic evaluation		Splicing modulation		Genomic evaluation	
	No	**(%)**	**mean ± SD**	**(%)**	**mean ± SD**	**(%)**	**mean ± SD**	**(%)**	**mean ± SD**
		triple application				**single application**			
1762	**#1**	8.8	9.0 ± 5.1	4.4	3.4 ± 0.7	0.0	2.5 ± 4.9	1.2	1.7 ± 0.8
	#2	16.4		3.2		0.0		0.7	
	#3	5.6		2.8		0.0		1.8	
	#4	5.4		3.0		9.9		3.2	

1611	**#1**	7.5	9.3 ± 4.9	3.2	3.3 ± 0.2	1.2	1.0 ± 1.0	0.3	1.1 ± 0.6
	#2	4.4		3.1		0.6		1.8	
	#3	9.3		3.5		2.3		1.0	
	#4	16.0		3.5		0.0		1.2	
1621- LNP	**#1**	4.5	6.0 ± 4.5	2.8	2.4 ± 1.4	0.0	0.0 ± 0.0	0.0	0.7 ± 0.6
	#2	5.2		2.8		0.0		1.2	
	#3	12.3		3.5		0.0		1.0	
	#4	1.8		0.4		0.0		0.4	
SM-102 -LNP	**#1**	15.2	6.7 ± 6.4	4.0	2.3 ± 1.5	1.4	2.1 ± 3.4	1.2	1.7 ± 0.9
	#2	8.1		3.1		7.1		2.9	
	#3	1.7		1.2		0.0		1.0	
	#4	1.7		0.8		0.0		1.5	

Table 3. *In vivo* editing of dystrophin gene after intramuscular application. *In vivo* mRNA splicing modulation and genome editing in BALB/C mice after triple and single intramuscular injection with Cas9 polyplexes and Cas9 LNP. Splicing modulation was determined using ImageJ Software. Genomic evaluation was performed by Sanger sequencing and subsequent evaluation of total editing efficiency with the TIDE analysis tool (https://tide.nki.nl/). All data are presented in percent for individual animals and mean ± SD (n=4). Graphical illustration and molecular evaluation conducted by Janin Germer (PhD student at Pharmaceutical Biotechnology, LMU, Munich).

4.3. Evaluation of clinical blood parameters and monitored body weights

As already mentioned in other sections above (*cf*. sections **1.3**, **2.3**, **3.2**), administration of solely *in vitro* evaluated carrier formulations always bears a risk of inadequate tolerability *in vivo*. Especially, repeated treatments within a longer period of time could allow the immune system to react in toxic side-effects for instance. That is why, for the current Cas9mRNA/sgRNA studies, the development of body weights during the treatment as well as clinical plasma parameters seven days after the last intravenous injection need to be evaluated on a closer inspection. Blood values were only analyzed for systemically treated animals as luciferase studies of intramuscular applied mRNA carriers mainly showed a clearly accumulation of the nanoagents in injected muscle tissue (*cf*. section **4.2.**). As mice are known to have a relatively high basal metabolic rate [200],

increases and declines of their body weight during the treatment time can be a sign for injection-induced toxicity.

Systemic administration of Cas9mRNA/sgDMD$_{Ex23}$

Regarding intravenous applications of Cas9mRNA/sgDMD$_{Ex23}$, no injection-related weight loss was monitored as all treatment groups show continiously rising growth curves during the oberservation time (**Figure 32A**). Although the mean body weight of animals administered with **1762** polyplexes seem to be located below other graphs, injected mice show a higher increase of body weight with + 1,6 g difference from the last to the first day of experiment (*cf*. + 1,0 g, **1611** polyplexes; + 0,7 g, **1621** LNPs).

Moreover, with the performance of sacrificing the animals, plasma samples were obtained and evaluated in regard of renal parameters, BUN and creatinine, as well as liver enzymes, AST and ALT. As indicated in **Figure 32B**, all resulting values were within expected ranges in comparison to the untreated group, indicating good biocompatibility of the applied formulations.

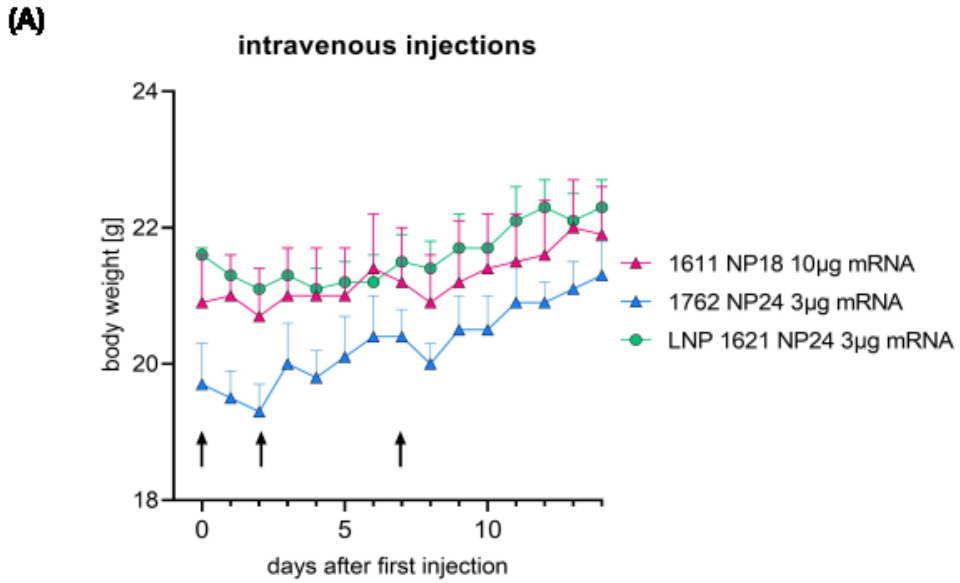

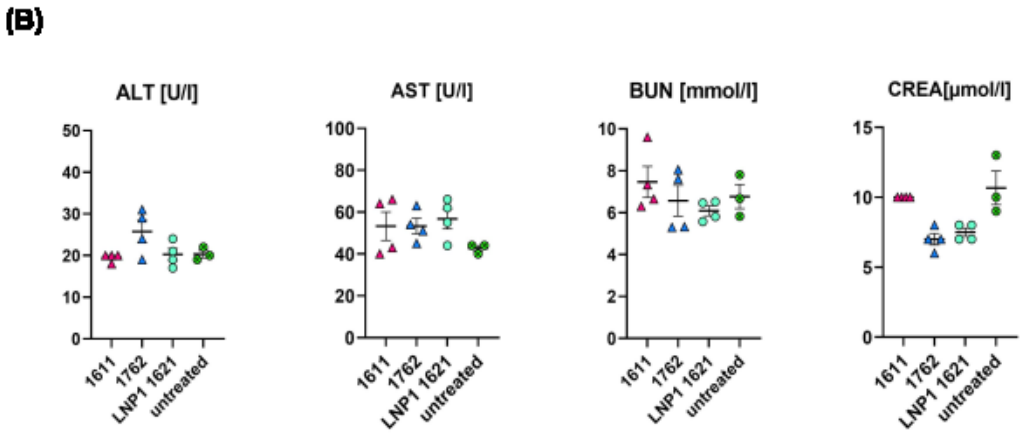

Figure 32. Evaluation of biocompatibility of intravenously applied Cas9mRNA/sgDMD$_{Ex23}$ polyplexes and LNPs. (A) Body weight of animals until their sacrifice at day 14. Arrows indicate days of injection (n=4). **(B)** Evaluation of standard plasma parameters. Blood samples were also taken on day 14. (n=4; except for untreated animals with n=3). Mice were administered trice with 150 µL nanocarrier solution containing 10 µg total RNA in **1611** polyplexes (N/P 18), 3 µg total RNA in **1762** polyplexes (N/P 24) and 3 µg total RNA in **1621** LNP (N/P 24); ALT, alanine transaminase; AST, aspartate aminotransferase; BUN, blood urea nitrogen; Crea, creatinine.

Local application of Cas9mRNA/sgDMD$_{Ex23}$

In consideration of the fact, that intramuscularly applied substances are not distributed into major blood vessels, it was desisted from analyzing plasma parameters in the locally injected treatment groups. Instead of that, observation of the body weight development indicated no visible reductions of the growth curve at the same time as injections were performed. Thus, a good tolerability of the administered polyplex and LNP fomulations is generally indicated (**Figure 33**).

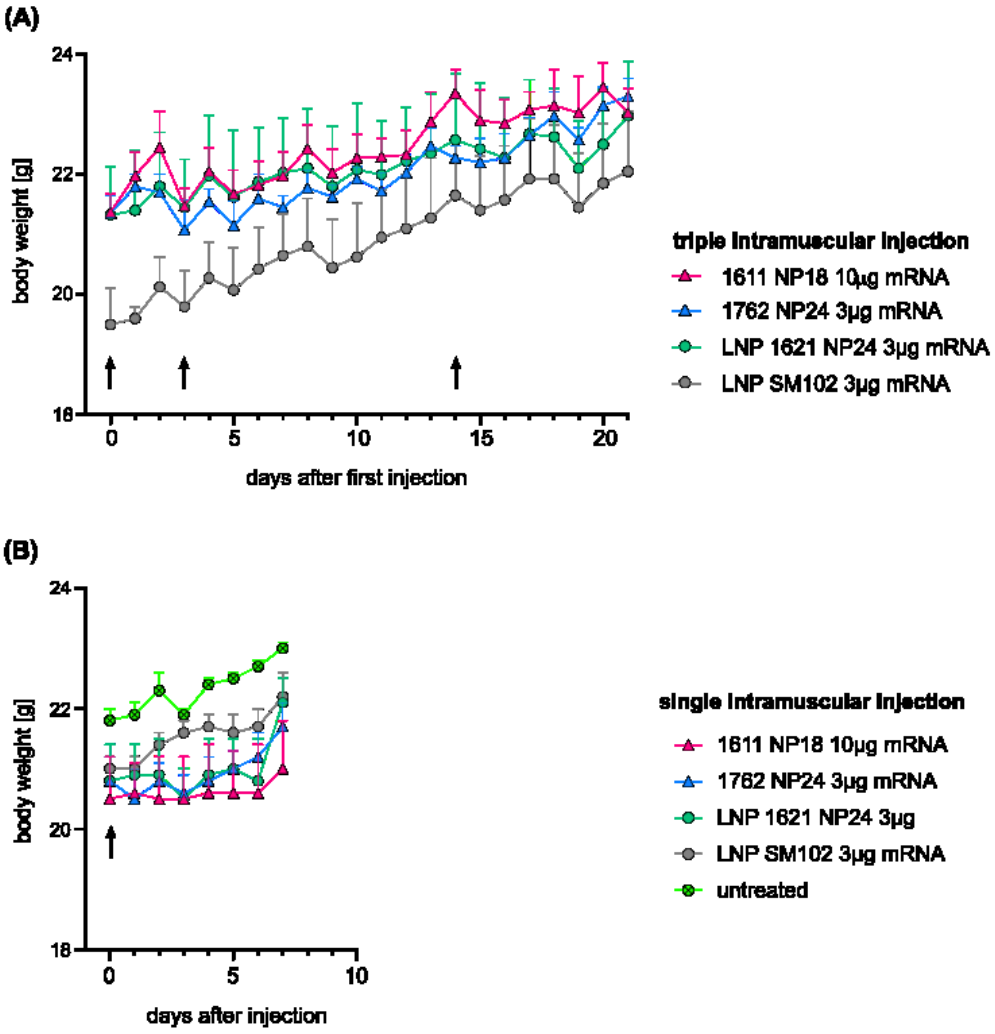

Figure 33. Body weight after intramuscular treatment of BALB/c mice with Cas9mRNA/sgDMD$_{Ex23}$ polyplexes and LNPs. (A) Triple or **(B)** single administration of 50 µL nanocarrier solution containing 10 µg total RNA in **1611** polyplexes (N/P 18) and 3 µg total RNA in **1762** polyplexes (N/P 24), in **1621** LNP (N/P 24) and in SM 102 LNP (N/P 6); each animal's body weight was monitored until their sacrifice at day 14 and arrows indicate days of injection (n=4).

IV. DISCUSSION

In the last recent years, gene therapy has experienced an enormous upswing especially regarding the field of LNP vaccines [73]. By unlocking the potential of nucleic acid medicine, gene expression can be manipulated using, *i.a.*, either gain of function or loss of function strategies, intervening at different molecular stages and exploiting the capabilities of pharmacoevolving therapies [2, 5, 12]. While this enables rapid development of adaptive therapies, clinical translation requires appropriate delivery systems to combat the hurdles of intracellular transport [13]. Although viral vectors show strong transfection efficiencies like their natural counterparts, synthetic nanocarriers overcome critical disadvantages such as immunogenicity or the risk of genomic integration [7, 27]. However, each individual non-viral approach must meet the requirements of different nucleic acid cargos and the associated individual delivery process [38, 201].

Therefore, customized synthetic vectors are designed to provide a perfect balance between extracellular stability and intracellular lability for safe and efficient transfection of the RNA payload [41]. The research of our group is based on the optimization of sequence-defined OAAs and, more recently, on a new generation of pH-sensitive lipo-xenopeptides with LAF subunits instead of classical fatty acids [69]. To date, a library of more than 1900 oligomers has been generated containing dynamic carrier building blocks based on precise SPPS and adapted to different *in vivo* conditions.

1. Lipoamino bundle LNPs for efficient mRNA transfection

This chapter presents the relevant thesis parts adapted from a research article published as Haase F, Pöhmerer J, Yazdi M, Grau M, Zeyn Y, Wilk U, Burghardt T, Höhn M, Hieber C, Bros M, Wagner E, Berger S. (2024) Lipoamino bundle LNPs for efficient mRNA transfection of dendritic cells and macrophages show high spleen selectivity. Eur. J. Pharm. Biopharm. 194, 95–109 [70].

Overcoming the endosomal barrier still represents one of the biggest obstacles in the delivery process of mRNA LNPs. Various efforts have been made to establish the perfect compromise between stable nucleic acid compaction and efficient cargo release during the intracellular delivery

process, promoted via nanocarriers with high transformable structural motifs within the delivery system. Balancing the hydrophilic-hydrophobic equilibrium as well as enhancing the pH-repsonsive lytic activity of nanocarriers represents a potent optimization approach. Our recently developed lipo-xenopeptides [69] represent such optimized carriers and were used in mRNA LNPs. Efficient endosomal escape as well as intracellular cargo release should be demonstrated.

1.1. *In vivo* distribution of luciferase expression by mRNA LNPs

In contrast to the highly exceeding transfection results *in vitro*, preselected LAF-Stp carriers **1612** and **1621** could not outperform SM-102 and DLin-MC3-DMA LNPs *in vivo*. However, expression results in splenic tissues still remained at very high luciferase detection levels even at low mRNA doses (1-3 µg) and after short time (6 h). Compared to SM-102 and DLin-MC3-DMA, **1612** and **1621** showed preferable spleen/liver ratios with high activity in the spleen as a central immune organ and lower activity in the liver. This spleen selectivity of our LAF-Stp carriers may be of particular interest to the development of mRNA LNPs for immunotherapy [202] and additionally may lower off target effects [203] upon reduced accumulation in the liver and other organs.

Another approach of spleen-selective mRNA LNP delivery was achieved by the aforementioned SORT technology [54] (*cf*. *introduction*). Here, an additional fifth anionic lipid (18PA) was included in the LNP formulation and a lower pKa value between 2 and 6 was determined which represents the apparent acid dissociation constant of a nanoparticle [153]. Compared to the current study, the spleen-selective properties of LNPs **1612** and **1621** may be due to their apparent surface pKa, as this was lowest for 12Oc U-shape **1612** at 5.1 and appeared to be most effective for bundle **1621** with a value of 6.4 [70]. According to *Jia et al.* [204] this could be explained by the different structures of the ionizable lipids, which correlate with the pKa value and consequently with the surface charge of the LNP. This may influence the formation of a protein corona in the blood circulation and also the in vivo distribution of LNPs.

1.2. EGFP expression in immune cells of liver spleen and lungs

To evaluate expression efficiencies of mRNA LNPs not only within the entire organ, but more specifically on the single cell level, eGFP mRNA was encapsulated in SM-102 and **1621** LNPs for systemic administration in mice. Subsequently, eGFP expression levels in immune cells of liver, spleen and lungs were analyzed. eGFP fluorescence in distinct immune cells was determined and showed various preferences of the applied formulations with highest amounts in hepatic MACs (KCs) for **1621** LNPs and exceeding values in splenic MACs and DCs for SM-102. This contrasting relationship between spleen and liver selectivity in terms of luciferase and eGFP expression levels could be due to the different perspective in the reporter assays performed as well as the lower proportion of immune cells in the liver compared to the spleen [205]. Including the results of the further compared relative transfection efficacies within the CD45-positve (*i.e.* immune cells) and -negative (*i.e.* non-immune cells) hepatic cell population, a preference of **1621** LNPs for immune cells rather than to hepatocytes can be hypothesized. SM-102 LNPs on the other side, transfect mainly hepatocytes and to a lower extent also immune cells of the liver, resulting in a reduced selectivity for immune cells.

1.3. Evaluation of clinical blood parameters

The natural behavior of mice does not include obvious signs of weakness, making reactions to toxic substances difficult to assess. Therefore, analyzing blood values of normal liver and kidney function was essential to evaluate acute toxicity of systemically administered nanocarriers. For both experimental parts (luciferase and eGFP mRNA LNPs) all parameters were within normal limits indicating a good tolerability of the injected formulations. However, further investigations of *e.g.* histolological sections of major organs [206] might be valuable examining whether severe tissue damages were induced by the injected nanoformulations. This would allow a broader analysis of pathophysiological processes in, *i.a.*, heart, liver, spleen, lungs and kidneys.

2. Targeting of liver endothelial cells with LAF siRNA LNPs

This chapter presents the relevant thesis parts adapted from a research article submitted as Yazdi M, Pöhmerer J, Hasanzadeh Kafshgari M, Seidl J, Grau M, Höhn M, Vetter V, Hoch C.C, Wollenberg B., Multhoff G., Bashiri Dezfouli A, Wagner E, (2024) In Vivo Endothelial Cell Gene Silencing by siRNA-LNPs Tuned with Lipoamino Bundle Chemical and Ligand Targeting. Small, 2400643 [155].

2.1. Gene silencing of coagulation factors in the liver by siVII and siVII LNPs

Based on the promising results of mRNA LNP formulations, especially with lipo-xenopeptide **1621** for efficient *in vivo* delivery to splenic tissues and hepatic immune cells, the affinity of **1621** siRNA LNPs to LSECs in the liver was examined. As biodistribution studies are known to be insufficient for evaluation of transfection efficiencies on a cellular level [207], siRNA LNPs were applied for functional FVII and FVIII gene silencing *in vivo*. Significantly lower expression of coagulation factor VIII, originating from endothelial cells, was seen for **1621**-LNPs despite a MC3- typical favorability of gene siliencing of hepatocyte-derived factor VII. It is known, that the interaction of LNPs containing different ionizable components depend on the subtypes of hepatic cells [207] and for anorganic carriers at least, also on the speed of blood flow within the hepatic sinusoid system is a major concern [208]. The preference of LSCEs over HCs by **1621** LNPs may be referred to the chemical characteristics of the employed lipo-xenopeptide. Thus, the novel lipidic composition may be beneficial for passive targeting to distinct cell types, *i.e.* LSECs, mediated by specific interactions with serum proteins and receptor-mediated uptake. However, more pharmacokinetic analyses have to be performed in order to understand the cellular pathway and structure-dependent efficiencies of **1621** siRNA LNPs.

2.2. Evaluation of clinical blood parameters

For further exceeding restricted clinical practice of previously introduced nucleic acid carriers, it is crucial to assess local and systemic toxicity concerns reported for intravenous injection of LNP formulations [209]. Therefore, evaluation of common hepatic enzymes (ALT, AST) and renal blood parameters (BUN, creatinine) confirmed neither hepatoxicity nor

splenic disfunction. Moreover, *Yazdi et al.* [155] determined several inflammatory cytokine levels of the obtained plasma specimens (*data no shown*) to appraise immunogenicity of **1621** LNPs. Whereas lipidic components of siRNA LNPs are known to induce immunogenic responses [210], all measured parameters in the current study referred to an uncritical risk of systemic application.

3. DMD exon skipping with xenopeptide-PMOs

This chapter presents the relevant thesis parts adapted from a research article published as Lessl AL, Pöhmerer J, Lin Y, Wilk U, Höhn M, Hörterer E, Wagner E, Lächelt U. (2023) mCherry on Top: A Positive Read-Out Cellular Platform for Screening DMD Exon Skipping Xenopeptide-PMO Conjugates. Bioconjugate Chem. 34, 2263–2274. [135].

In order to create a suitable screening platform for antisense oligonucleotides in the context of Duchenne muscular dystrophy, the mdx mouse model is a common approach for DMD therapeutics [211]. Therefore, *Hara et al*. e.g. utilized a vector system carrying eGFP mRNA to generate a time-efficient and mouse-sparing analyzing method of efficient exon skipping [212]. However, testing human specific ASOs requires different evaluation strategies in order to avoid mismatching target sequences. Here, incorporation of the human DMD gene in the murine genome could be an approchable resolution [213, 214].

3.1. Biodistribution of mRNA splicing modulation

In the current study, skipping efficiencies of the dystrophin exon 23 in BALB/C mice were evaluated after intravenous administration of PMO xenopeptide conjugates compared to PMO(705)-XP and PMO(Ex23). Therefore, preselected carriers were screened on a positive read-out (HeLa mCherry-DMDEx23) cell model, resulting in T-shape oligomer **1395** as a leading structure for following *in vivo* studies. The systemic application into mice revealed highly potent SSO-carriers which changed their organ-selective affinity upon peptide conjugation. In contrast to exon skipping of PMO(Ex23) in skeletal muscle, formulations with the PMO sequence but additional connection of T-shape **1395** led to a redistributed splicing rate especially in spleen, kidneys, liver and lungs. A minor effect could be achieved for brain and heart samples as well as a clear irregular distribution within the individual treatment groups. Since the freeze-dried

formulations were resuspended in HBG immediately prior the injection procedure to ensure high *in vivo* concentrations, it coud be hypothesized that the heterogeneity in efficiency is due to suboptimal reconstitution beforehand. This has to be considered for future applications to diminish high standard deviations of splicing modulation.

Another drawback in PMO induced exon skipping is the transient effect regarding therapeutic approaches. Despite their initial dose dependent efficiency [215], a sufficient long-term effect can only occur due to repeated treatments [216]. Therefore, Cas9 induced permanent editing of the mutated dystrophin gene might be a preferable alternative [217].

3.2. Evaluation of clinical blood parameters

First-time systemic applications of high dosed PMO formulations might implicate possible adverse effects *in vivo.* That is why, evaluation of blood chemistry is crucial for registration of systemic and organ-related toxicities. The plasma levels of analyzed liver enzymes (ALT, AST) and kidney function parameters (Crea, BUN) however concluded that the injected PMO-peptide conjugates offer a favorable biocompatibility profile. Due to their uncharged character and minor interaction with serum proteins, PMOs show low systemic side-effects and risks of toxicity may rather refer to hepatic and renal accumulation. As the liver attributes to high vascularization with slow blood flow in fenestrated sinusoidal capillaries, congregations of intravenously injected oligonucleotides are possible to be found in hepatic tissues. In addition, renal clearance of administered ASOs is reported to be high in a short time and reabsorption within the tubules system leads to additional concentration of oligonucleotide [119, 218].

In further evaluating the clinical translatability of the mouse model to other species, it should be noted that toxicity of peptide conjugated PMO formulations was observed in monkeys already at lower doses than in mice [219]. This may be due to the different target sequences of the oligonucleotides, which was also observed to some extent in the present study (cf. PMO(705) and PMO(Ex23) in **Figure 20**). In addition, the amphiphilic character of T-Shape **1395** (polar, hydrophilic Stp backbone

and apolar, hydrophobic fatty acids) leads to the formation of hydrophobically balanced carriers [64], which may also contribute to the improved tolerability of the peptide conjugated PMO formulations in contrast to unmodified PMO(Ex23).

4. Xenopeptide polyplexes for CRISPR Cas9 based gene editing

This chapter presents the relevant thesis parts adapted from a research manuscript submitted as Germer J., Lessl AL, Pöhmerer J, Grau M, Weidinger E, Höhn M, Yazdi M, Cappelluti M.A, Lombardo A, Lächelt U, Wagner E (2024) Lipo-Xenopeptide Polyplexes for CRISPR Cas9 Based Gene Editing at Ultra-Low Dose Targeting. Journal of Controlled Release, 370, 239-255 [136].

Permanent editing of genomic mutations, causing hereditary diseases like sickle cell anemia or Duchenne muscular dystrophy, has become an achievable goal within the progress in research of the CRISPR Cas9 technology during recent years [220]. However, safe and efficient delivery systems still require further optimization regarding therapeutic applications. Therefore, a new generation of sequence defined lipo-XPs with LAF components was recently introduced by our working group, providing potent synthetic carrier motifs for Cas9mRNA/sgRNA loaded polyplexes and LNPs [69].

4.1. Pre-experiment: Luciferase expression after intramuscular injection of LAF polyplexes and LNPs

In contrast to systemic applications of the recently developed lipo-XPs, efficiencies of intramuscularly injected carriers had not been assessed in previous studies. Therefore, either polyplexes or LNPs encapsulating luciferase mRNA and composed of best performing LAF-Stp-carriers, were administered locally into the *musculus biceps femoris* of healthy BALB/C mice. Subsequently, the *ex vivo* luciferase assay resulted in very high expression values of 10^8-10^9 RLU/g muscle tissue for mRNA polyplexes, and even higher luciferase activity levels of 10^{10} RLU/g muscle tissue for **1621** LNPs at an early read-out time point (6 h *p.i.*). Compared to the *in vivo* efficacy of systemically injected luciferase mRNA polyplexes with 10^4-10^6 RLU/g muscle tissue [69] and LNPs with 10^6-10^8 RLU/g muscle tissue [70], local application concludes to be a more effective and straightforward way for reaching the target site, preventing undesired off-target effects due

to bypassing major organs like spleen or liver. Especially for vaccination approaches, topical application of mRNA LNPs into skeletal muscles are the current gold standard method [90, 221]. Due to high infiltration of immune cells in the connective tissue at the target site as well as close-by lymph nodes, immune responses are likely to be induced by antigens encoded by the delivered mRNA [87].

4.2. *In vivo* genome and editing splicing modulation by Cas9/sgRNA xenopeptides

To further examine genome editing and splicing modulation by systemically or locally applied Cas9mRNA/sgRNA xenopeptides, the main study consisted of **1611** polyplexes**,** containing 10 µg total RNA, and **1762** polyplexes as well as **1621** LNPs, containing 3 µg total RNA (Cas9 mRNA and $sgDMD_{Ex23}$ at a weight ratio of 1:1). Intravenous injections were conducted on da 0, 2 and 7, whereas intramuscular applications followed a wider administration schedule (day 0,3,14) or were only performed once. Seven days after the last treatment, animals were euthanized, relevant organ samples (attributed to a high dystrophin expression [199]) and muscle tissues were harvested and analyzed regarding skipping activities of exon 23 in combination with editing efficiencies of the Cas9/$sgDMD_{Ex23}$ complex on a genomic basis. In direct comparison to untreated control samples, modulation of splicing efficiencies upon systemic administrated XP carriers, compacting Cas9mRNA/sgRNA, achieved highest values for brain tissues by **1762** polyplexes (13.1% ± 4.4%, mean ± SD), for muscle tissues by **1611** polyplexes (9.0% ± 5.1%, mean ± SD) and for heart tissues by **1621** LNPs (5.7 % ± 1.1 %; mean ± SD). However, on closer inspection of the individual values of the single animals, distinct differences for exon skipping in brain and muscle were obvious within each treatment group. This was not evident on a genomic level, where editing efficiencies resulted lower but evenly distributed across all formulations. Therefore, one explanation concerns possible larger deletions induced by the Cas9 system [222, 223] which remain undetectable in the TIDE analysis tool but might result in restored skipping mechanisms of the dystrophin exon 23. Furthermore, the endogenous NHEJ pathway after Cas9-induced DSBs of the DNA leads to unprecise introduction of INDEL mutations [224]. Thus,

further investigations are needed to identify the explicit sequences, occurring to be responsible for altered splicing modulation.

In contrast to systemic administrations, local application of Cas9/sgRNA polyplexes and LNPs was significantly superior regarding splicing modulation after triple injected **1762** (9.0% ± 5.1%, mean ± SD) and **1611** (9.3% ± 4.9%, mean ± SD) polyplexes compared to LNP carriers (6.0% ± 4.5%, **1621** and 6.7% ± 6.4%, **SM-102** mean ± SD) and single injected XP carriers (0.0 % - 2.5 %). As far as genome editing is concerned, equivalent treatment groups showed lower efficiencies but similar relations in terms of polyplexes (3.4% ± 0.7%, **1762** and 3.3% ± 0.2%, **1611** mean ± SD) and LNPs (2.4% ± 1.4%, **1621** and 2.3% ± 1.5%, **SM-102** mean ± SD). These results need to be compared to the exceeding luciferase expression levels of especially LNP formulations of the aforementioned pre-experiment. Here, no correlation could be observed between the distribution of intramuscularly applied LAF-Stp carriers, loaded with luciferase mRNA, and the corresponding Cas9mRNA/sgRNA formulations. Whereas local administrations of **1621** LNPs reached 100-fold higher levels of luciferase activity, genome editing and splice modulating capacities were more promising for **1762** and **1611** Cas9mRNA/sgRNA polyplexes. Additionally, gene editing performances of topical applicated Cas9mRNA/sgRNA XPs could not outperform systemic injections in a comparable manner as luciferase experiments indicated. Here, expression of luciferase resulted >100-fold lower for intravenous applied mRNA polyplexes [69] and LNPs [70] than for related intramuscularly injected mRNA carriers. Obviously, luciferase distribution of mRNA nanocarriers in various organs does not correlate with functional genome editing experiments of co-delivered Cas9mRNA/sgRNA. In the current study, single-cut efficiencies of the Cas9 endonucleases requires protein translation, formation of the RNP complex and afterwards, intranuclear delivery as prerequisites for successful genome editing. According to *Germer et al.* [136], the replacement of the sgRNA sequence with an optimized alternative, including a relatively higher on-target activity score [225] could improve genome editing abilities of the applied Cas9mRNA/sgRNA carrier systems.

4.3. Evaluation of clinical blood parameters and comparison with monitored body weights

Clinical blood parameters as well as monitored body weights of animals injected with Cas9mRNA/sgRNA polyplexes or LNPs during different treatment schedules and routes of administration demonstrated a favorable safety profile for the new generation of lipo-XP carriers. In contrast to viral vectors, our synthetic nanoparticles display a good tolerability as well as predicted low immunogenicity that are especially attributed to LNPs [189]. However, further investigations of *e.g.* muscle-related parameters such as plasma creatine kinase well as pathohistological examinations of injected muscle tissues could highlight tolerability aspects of repeated local injections.

Nevertheless, the *in vivo* conditions of the present study could be partially modified with respect to therapeutic aspects of the human DMD disease in order to improve the clinical applicability of the results. For example, *Kenjo et al.* [189] optimized an LNP formulation including dual sgRNA targeting, which was tested in the humanized *hEx45KI-mdx44* mouse model. Therefore, murine exon 45 was replaced with its human counterpart, and then exon 44 was deleted using CRISPR-Cas9 technology. This created a transgenic animal model in which pathological muscle tissue and clinical symptoms of muscle damage could be observed. Restoration of functional dystrophin was then demonstrated after repeated local applications of Cas9 mRNA/sgRNA at the RNA level and also by protein expression.

V. SUMMARY

RNA medicines *in vivo*: delivery of mRNA, siRNA, PMOs and Cas9 mRNA/sgRNA

For more than 60 years, the transfer of exogenous genes into the patient's genome has been established as an advanced field of gene therapy for the personalized treatment of life-threatening diseases. The versatility of nucleic acid medicine allows intervention in cellular processes at different molecular levels and can pursue, *i.a.,* gain-of-function and loss-of-function strategies. However, successful delivery of the DNA or RNA payload to its intracellular target site in a biological environment is a major challenge for the development of clinically translatable therapeutics. Therefore, scientific research on nanocarriers is focused either on nature-derived viral vectors with high transfection efficiency or on synthetic non-viral carriers with lower risk of immunogenicity and of genomic integration *in vivo*.

In our research group, we focus on the optimization of sequence-defined xenopeptides (XPs) for dynamic non-viral nanocarriers that meet the requirements of both, stable extracellular compaction and sufficient intracellular release of the nucleic acid payload. To date, more than 1800 different structures and topologies have been developed, most recently including aminoethylene and lipo-amino fatty (LAF) acid motifs as building blocks in lipo-XP carriers, which exhibit high efficacy at low doses *in vitro* and *in vivo* due to their pH-responsive, amphiphilic character.

The first chapter of this thesis evaluated the *in vivo* expression of lipo-XPs as components of mRNA-encapsulating lipid nanoparticles (LNPs) in various organs of tumor-bearing mice after systemic application. Commercial ionizable lipids, SM-102 of the Moderna COVID-19 vaccine and MC3-DLin-DMA of Patisiran as a treatment for hereditary amyloidosis, served as positive controls. The screening results showed a selectivity of the analyzed lipo-XP LNPs for splenic tissue, while the control carriers demonstrated a preferable expression in the liver. For further investigations in a follow-up study, the activity of best-performing structure **1621** and SM-102, was evaluated in LNPs on a cellular level. Various immune cells of liver, spleen and lungs showed favorable tropism of **1621**

LNPs to non-parenchymal cells of the liver in contrast to predominantly hepatocyte-associated expression regarding SM-102 LNPs. This suggests a potential therapeutic application of immunotherapy with reduced off-target effects of the newly synthesized lipo-XPs as LNP components.

In the second chapter of the thesis, the aforementioned LNP formulations, including the best performing lipo-XP **1621** and MC3-DLin-DMA, were applied as siRNA LNPs to tumor-free mice. The gene silencing efficiency of blood coagulation factors VII (FVII) and VIII (FVIII) was determined and showed a lower activity of hepatocyte-derived FVII for MC3-DLin-DMA LNPs and a lower activity of FVIII for **1621** LNPs, indicating a favorable selectivity for targeting non-parenchymal liver sinusoidal endothelial cells.

The third chapter of the thesis refers to the modulation of mRNA splicing by phosphorodiamidate morpholino oligomers (PMOs) and exon 23 skipping efficiency of a T-shape XP, which was previously identified as the very potent carrier **1395** for PMO(Ex23) in a Duchenne Muscular Dystrophy (DMD) reporter cell screening model. Intravenously injected PMO(Ex23) without and with **1395** conjugation showed a redistribution of splicing modulation from skeletal muscle to other organ tissues, including liver, lung and spleen.

The last chapter of this thesis focused on lipo-XP polyplexes and LNPs for the co-delivery of Cas9 mRNA/sgRNA and the efficiency of CRISPR-Cas9-based genome editing of DMD exon 23 *in vivo*. In a preliminary experiment, intramuscular injection of lipo-XP carriers with luciferase mRNA was tested, which resulted in high expression levels for especially **1621** LNPs, but also for **1762** and **1611** polyplexes. In the following main study, the best performing structures were administered with Cas9 mRNA/sgRNA both intravenously and intramuscularly and showed a significant modulation of DMD exon 23 at the genomic and mRNA level in all treatment groups compared to untreated animals.

In summary, this thesis represents the significant potential of different established synthetic nanocarriers for the *in vivo* delivery of mRNA, siRNA, PMO and CRISPR Cas9 mRNA/sgRNA.

VI. ZUSAMMENFASSUNG

RNA Medizin *in vivo*: Transfer von mRNA, siRNA, PMOs und Cas9 mRNA/sgRNA

Seit mehr als 60 Jahren hat sich der Transfer von exogenen Genen in das Genom des Patienten als fortschrittlicher Bereich der Gentherapie für die personalisierte Behandlung lebensbedrohlicher Krankheiten etabliert. Die Vielseitigkeit der Nukleinsäuremedizin ermöglicht Eingriffe in zelluläre Prozesse auf verschiedenen molekularen Ebenen und kann u.a. Strategien des Funktionsverlusts und -gewinns verfolgen. Der erfolgreiche Transport der DNA- oder RNA-Nutzlast an ihren intrazellulären Zielort in einer biologischen Umgebung ist jedoch eine große Herausforderung in der Entwicklung klinisch einsetzbarer Therapeutika. Daher konzentriert sich die wissenschaftliche Forschung zu Nanoträgern entweder auf virale Vektoren mit hoher Transfektionseffizienz oder auf synthetische nicht-virale Träger mit geringerem Risiko der Immunogenität und der genomischen Integration *in vivo.*

In unserer Fortschungsgruppe konzentrieren wir uns auf die Optimierung von sequenzdefinierten Xenopeptiden für dynamische, nicht-virale Nanocarrier, die sowohl die Anforderungen einer stabilen extrazellulären Verdichtung als auch die einer ausreichenden intrazellulären Freisetzung der Nukleinsäure-Nutzlast erfüllen. Bis heute wurden mehr als 1800 verschiedene Strukturen und Topologien entwickelt, darunter zuletzt Aminoethylene und Lipoaminofettsäure-Motive als Bausteine für Lipo-XP-Carrier, die aufgrund ihres pH-responsiven, amphiphilen Charakters eine hohe Wirksamkeit bei niedrigen Dosen *in vitro* und *in vivo* aufweisen.

Das erste Kapitel dieser Arbeit untersuchte die *In-vivo*-Expression von Lipo-XPs als Bestandteile von mRNA-verkapselnden Lipid-Nanopartikeln (LNPs) in verschiedenen Organen von tumortragenden Mäusen nach systemischer Applikation. Kommerzielle ionisierbaren Lipide SM-102 des Moderna COVID-19-Impfstoffs und MC3-DLin-DMA von Patisiran, einem Behandlungsmittel der hereditären Amyloidose, dienten als

Positivkontrollen. Die Screening-Ergebnisse wiesen eine Selektivität der untersuchten Lipo-XP LNPs für Milzgewebe auf, während die Kontrollcarrier eine bevorzugte Expression in der Leber zeigten. Für weitere Untersuchungen in einer Folgestudie wurde die Aktivität der leistungsstärksten Struktur **1621** und SM-102 in LNPs auf zellulärer Ebene bewertet. Verschiedene Immunzellen von Leber, Milz und Lunge zeigten einen günstigen Tropismus von **1621** LNPs für nicht-parenchymale Leberzellen im Gegensatz zu einer vorwiegend Hepatozyten-assoziierten Expression von SM-102 LNPs. Dieses deutet auf eine mögliche immuntherapeutische Anwendung der neu synthetisierten Lipo-XPs als LNP-Bestandteile mit reduzierten Off-Target-Effekten hin.

Im zweiten Kapitel der Arbeit wurden die oben genannten LNP-Formulierungen, einschließlich des leistungsstärksten Lipo-XPs **1621** und MC3-DLin-DMA, als siRNA-LNPs bei tumorfreien Mäusen angewendet. Die Effizienz des Gen-Silencings der Blutgerinnungsfaktoren VII (FVII) und VIII (FVIII) wurde bestimmt und zeigte eine geringere Aktivität des aus Hepatozyten stammenden FVII für MC3-DLin-DMA LNPs und eine geringere Aktivität von FVIII für **1621** LNPs, was auf eine günstige Selektivität für das Targeting von nicht-parenchymalen sinusoidalen Leberendothelzellen hinweist.

Das dritte Kapitel der Arbeit befasst sich mit Modulation des mRNA-Splicings durch Phosphorodiamidat-Morpholino-Oligomere (PMOs) und der Exon-23-Skipping-Effizienz eines T-förmigen XPs, das zuvor als sehr potenter Träger **1395** für PMO(Ex23) in einem Duchenne Muskeldystrophie (DMD) Reporterzell-Screening-Modell identifiziert wurde. Intravenös injiziertes PMO(Ex23) ohne und mit **1395**-Konjugation zeigte eine Umverteilung der Splicing-Modulation *in vivo* von der Skelettmuskulatur zu anderen Organgeweben, einschließlich Leber, Lunge und Milz.

Das letzte Kapitel dieser Arbeit befasste sich mit Lipo-XP-Polyplexen und LNPs für die gemeinsame Verabreichung von Cas9 mRNA/sgRNA und der Effizienz des CRISPR Cas9-basierten Genome Editings von DMD exon 23 *in vivo.* In einem Vorversuch wurde die intramuskuläre Injektion von Lipo-

XP-Trägern mit Luciferase mRNA getestet, die inbesondere bei **1621** LNPs, aber auch bei **1762** und **1611** Polyplexen zu hohen Expressionswerten führte. In der folgenden Hauptstudie wurden die leistungsstärksten Strukturen mit Cas9 mRNA/sgRNA sowohl intravenös als auch intramuskulär verabreicht und zeigten in allen Behandlungsgruppen eine deutliche Modulation von DMD-Exon 23 auf genomischer und mRNA-Ebene im Vergleich zu unbehandelten Tieren.

Zusammenfassend stellt diese Arbeit das bedeutende Potenzial verschiedener etablierter synthetischer Nanocarrier für die *In-vivo*-Verabreichung von mRNA, siRNA, PMO und CRISPR Cas9 mRNA/sgRNA dar.

VII. REFERENCES

1. Tatum, E., *Molecular biology, nucleic acids, and the future of medicine.* Cell Ther Transplant, 2010. **1**: p. 74-79.
2. Yamada, Y., *Nucleic Acid Drugs-Current Status, Issues, and Expectations for Exosomes.* Cancers (Basel), 2021. **13**(19).
3. Smull, C.E. and E.H. Ludwig, *Enhancement of the plaque-forming capacity of poliovirus ribonucleic acid with basic proteins.* J Bacteriol, 1962. **84**(5): p. 1035-40.
4. Oyama, S., T. Yamamoto, and A. Yamayoshi, *Recent Advances in the Delivery Carriers and Chemical Conjugation Strategies for Nucleic Acid Drugs.* Cancers (Basel), 2021. **13**(15).
5. Anguela, X.M. and K.A. High, *Entering the Modern Era of Gene Therapy.* Annu Rev Med, 2019. **70**: p. 273-288.
6. Friedmann, T. and R. Roblin, *Gene therapy for human genetic disease?* Science, 1972. **175**(4025): p. 949-55.
7. Yan, Y., et al., *Non-viral vectors for RNA delivery.* Journal of Controlled Release, 2022. **342**: p. 241-279.
8. Xie, X., et al., *Recent advances in targeting the "undruggable" proteins: from drug discovery to clinical trials.* Signal Transduction and Targeted Therapy, 2023. **8**(1): p. 335.
9. Stephenson, M.L. and P.C. Zamecnik, *Inhibition of Rous sarcoma viral RNA translation by a specific oligodeoxyribonucleotide.* Proc Natl Acad Sci U S A, 1978. **75**(1): p. 285-8.
10. Wolff, J.A., et al., *Direct gene transfer into mouse muscle in vivo.* Science, 1990. **247**(4949 Pt 1): p. 1465-8.
11. Citeline, A.S.o.G.C.T.a., *Gene, Cell, + RNA Therapy Landscape Report*. 2023.
12. Lachelt, U. and E. Wagner, *Nucleic Acid Therapeutics Using Polyplexes: A Journey of 50 Years (and Beyond).* Chem Rev, 2015. **115**(19): p. 11043-78.
13. Dowdy, S.F., *Overcoming cellular barriers for RNA therapeutics.* Nat Biotechnol, 2017. **35**(3): p. 222-229.
14. Uchida, S., et al., *Nanomedicine-Based Approaches for mRNA Delivery.* Mol Pharm, 2020. **17**(10): p. 3654-3684.
15. Sahin, U., K. Kariko, and O. Tureci, *mRNA-based therapeutics--developing a new class of drugs.* Nat Rev Drug Discov, 2014. **13**(10): p. 759-80.
16. Davidson, B.L. and P.B. McCray, Jr., *Current prospects for RNA interference-based therapies.* Nat Rev Genet, 2011. **12**(5): p. 329-40.
17. Roberts, T.C., R. Langer, and M.J.A. Wood, *Advances in oligonucleotide drug delivery.* Nat Rev Drug Discov, 2020. **19**(10): p. 673-694.
18. Arechavala-Gomeza, V., B. Khoo, and A. Aartsma-Rus, *Splicing modulation therapy in the treatment of genetic diseases.* Appl Clin Genet, 2014. **7**: p. 245-52.
19. Friedmann, T., *A brief history of gene therapy.* Nature Genetics, 1992. **2**(2): p. 93-98.

20. Martínez-Puente, D.H., et al., *Plasmid DNA for Therapeutic Applications in Cancer.* Pharmaceutics, 2022. **14**(9).
21. Chamundeeswari, M., J. Jeslin, and M.L. Verma, *Nanocarriers for drug delivery applications.* Environmental Chemistry Letters, 2019. **17**(2): p. 849-865.
22. Felgner, P.L., et al., *Nomenclature for synthetic gene delivery systems.* Hum Gene Ther, 1997. **8**(5): p. 511-2.
23. Chow, Y.T., et al., *Single Cell Transfection through Precise Microinjection with Quantitatively Controlled Injection Volumes.* Scientific Reports, 2016. **6**(1): p. 24127.
24. Wickham, T.J., et al., *Increased in vitro and in vivo gene transfer by adenovirus vectors containing chimeric fiber proteins.* J Virol, 1997. **71**(11): p. 8221-9.
25. Greber, U.F., *Virus assembly and disassembly: the adenovirus cysteine protease as a trigger factor.* Rev Med Virol, 1998. **8**(4): p. 213-222.
26. Ma, Y., R.J.M. Nolte, and J.J.L.M. Cornelissen, *Virus-based nanocarriers for drug delivery.* Advanced Drug Delivery Reviews, 2012. **64**(9): p. 811-825.
27. Bulcha, J.T., et al., *Viral vector platforms within the gene therapy landscape.* Signal Transduction and Targeted Therapy, 2021. **6**(1): p. 53.
28. Administration, F.-U.S.F.a.D. *FDA Approves First Gene Therapies to Treat Patients with Sickle Cell Disease*. FDA News Release 2023 17.02.2024]; Available from: https://www.fda.gov/news-events/press-announcements/fda-approves-first-gene-therapies-treat-patients-sickle-cell-disease.
29. Nayak, S. and R.W. Herzog, *Progress and prospects: immune responses to viral vectors.* Gene Ther, 2010. **17**(3): p. 295-304.
30. Wu, Z., H. Yang, and P. Colosi, *Effect of genome size on AAV vector packaging.* Mol Ther, 2010. **18**(1): p. 80-6.
31. Paunovska, K., D. Loughrey, and J.E. Dahlman, *Drug delivery systems for RNA therapeutics.* Nature Reviews Genetics, 2022. **23**(5): p. 265-280.
32. Cullis, P.R. and B. De Kruijff, *Lipid polymorphism and the functional roles of lipids in biological membranes.* Biochimica et Biophysica Acta (BBA) - Reviews on Biomembranes, 1979. **559**(4): p. 399-420.
33. Barenholz, Y., *Doxil®--the first FDA-approved nano-drug: lessons learned.* J Control Release, 2012. **160**(2): p. 117-34.
34. Tenchov, R., et al., *Lipid Nanoparticles─From Liposomes to mRNA Vaccine Delivery, a Landscape of Research Diversity and Advancement.* ACS Nano, 2021. **15**(11): p. 16982-17015.
35. Tros de Ilarduya, C., Y. Sun, and N. Düzgüneş, *Gene delivery by lipoplexes and polyplexes.* Eur J Pharm Sci, 2010. **40**(3): p. 159-70.
36. Lv, H., et al., *Toxicity of cationic lipids and cationic polymers in gene delivery.* Journal of Controlled Release, 2006. **114**(1): p. 100-109.
37. Cullis, P.R. and M.J. Hope, *Lipid Nanoparticle Systems for Enabling Gene Therapies.* Mol Ther, 2017. **25**(7): p. 1467-1475.

38. Scholz, C. and E. Wagner, *Therapeutic plasmid DNA versus siRNA delivery: common and different tasks for synthetic carriers.* J Control Release, 2012. **161**(2): p. 554-65.
39. Freitag, F. and E. Wagner, *Optimizing synthetic nucleic acid and protein nanocarriers: The chemical evolution approach.* Adv Drug Deliv Rev, 2021. **168**: p. 30-54.
40. Sun, Q., et al., *Integration of Nanoassembly Functions for an Effective Delivery Cascade for Cancer Drugs.* Advanced Materials, 2014. **26**(45): p. 7615-7621.
41. Berger, S., et al., *Optimizing pDNA Lipo-polyplexes: A Balancing Act between Stability and Cargo Release.* Biomacromolecules, 2021. **22**(3): p. 1282-1296.
42. Hager, S. and E. Wagner, *Bioresponsive polyplexes - chemically programmed for nucleic acid delivery.* Expert Opin Drug Deliv, 2018. **15**(11): p. 1067-1083.
43. Sakurai, F., et al., *Interaction between DNA-cationic liposome complexes and erythrocytes is an important factor in systemic gene transfer via the intravenous route in mice: the role of the neutral helper lipid.* Gene Ther, 2001. **8**(9): p. 677-86.
44. Tenzer, S., et al., *Rapid formation of plasma protein corona critically affects nanoparticle pathophysiology.* Nature Nanotechnology, 2013. **8**(10): p. 772-781.
45. Monopoli, M.P., et al., *Biomolecular coronas provide the biological identity of nanosized materials.* Nature Nanotechnology, 2012. **7**(12): p. 779-786.
46. Allen, T.M., et al., *Liposomes containing synthetic lipid derivatives of poly(ethylene glycol) show prolonged circulation half-lives in vivo.* Biochimica et Biophysica Acta (BBA) - Biomembranes, 1991. **1066**(1): p. 29-36.
47. Alconcel, S.N.S., A.S. Baas, and H.D. Maynard, *FDA-approved poly(ethylene glycol)–protein conjugate drugs.* Polymer Chemistry, 2011. **2**(7): p. 1442-1448.
48. LI, S.-D. and L. HUANG, *Surface-Modified LPD Nanoparticles for Tumor Targeting.* Annals of the New York Academy of Sciences, 2006. **1082**(1): p. 1-8.
49. Onzi, G., et al., *Passive targeting and the enhanced permeability and retention (EPR) effect.* The ADME Encyclopedia: A Comprehensive Guide on Biopharmacy and Pharmacokinetics, 2021: p. 1-13.
50. Cardoso, A.L.C., et al., *Tf-lipoplexes for neuronal siRNA delivery: A promising system to mediate gene silencing in the CNS.* Journal of Controlled Release, 2008. **132**(2): p. 113-123.
51. Wang, D., et al., *Efficient tumor-targeting delivery of siRNA via folate-receptor mediated biomimetic albumin nanoparticles enhanced by all-trans retinoic acid.* Materials Science and Engineering: C, 2021. **119**: p. 111583.
52. Akinc, A., et al., *Targeted delivery of RNAi therapeutics with endogenous and exogenous ligand-based mechanisms.* Mol Ther, 2010. **18**(7): p. 1357-64.

53. Jayaraman, M., et al., *Maximizing the potency of siRNA lipid nanoparticles for hepatic gene silencing in vivo.* Angew Chem Int Ed Engl, 2012. **51**(34): p. 8529-33.
54. Cheng, Q., et al., *Selective organ targeting (SORT) nanoparticles for tissue-specific mRNA delivery and CRISPR-Cas gene editing.* Nat Nanotechnol, 2020. **15**(4): p. 313-320.
55. He, B., et al., *Recent advances in drug delivery systems for enhancing drug penetration into tumors.* Drug Deliv, 2020. **27**(1): p. 1474-1490.
56. Zuhorn, I.S., R. Kalicharan, and D. Hoekstra, *Lipoplex-mediated transfection of mammalian cells occurs through the cholesterol-dependent clathrin-mediated pathway of endocytosis.* J Biol Chem, 2002. **277**(20): p. 18021-8.
57. Zang, X., et al., *Anti-EphA10 antibody-conjugated pH-sensitive liposomes for specific intracellular delivery of siRNA.* Int J Nanomedicine, 2016. **11**: p. 3951-67.
58. Degors, I.M.S., et al., *Carriers Break Barriers in Drug Delivery: Endocytosis and Endosomal Escape of Gene Delivery Vectors.* Accounts of Chemical Research, 2019. **52**(7): p. 1750-1760.
59. ur Rehman, Z., D. Hoekstra, and I.S. Zuhorn, *Mechanism of polyplex- and lipoplex-mediated delivery of nucleic acids: real-time visualization of transient membrane destabilization without endosomal lysis.* ACS Nano, 2013. **7**(5): p. 3767-77.
60. Bus, T., A. Traeger, and U.S. Schubert, *The great escape: how cationic polyplexes overcome the endosomal barrier.* Journal of Materials Chemistry B, 2018. **6**(43): p. 6904-6918.
61. Hartmann, L., et al., *Tailor-made poly(amidoamine)s for controlled complexation and condensation of DNA.* Chemistry, 2008. **14**(7): p. 2025-33.
62. Schaffert, D., et al., *Solid-phase synthesis of sequence-defined T-, i-, and U-shape polymers for pDNA and siRNA delivery.* Angew Chem Int Ed Engl, 2011. **50**(38): p. 8986-9.
63. Schaffert, D., N. Badgujar, and E. Wagner, *Novel Fmoc-polyamino acids for solid-phase synthesis of defined polyamidoamines.* Org Lett, 2011. **13**(7): p. 1586-9.
64. Lin, Y., et al., *Chemical Evolution of Amphiphilic Xenopeptides for Potentiated Cas9 Ribonucleoprotein Delivery.* Journal of the American Chemical Society, 2023. **145**(28): p. 15171-15179.
65. Krhac Levacic, A., et al., *Dynamic mRNA polyplexes benefit from bioreducible cleavage sites for in vitro and in vivo transfer.* J Control Release, 2021. **339**: p. 27-40.
66. Kuhn, J., et al., *Delivery of Cas9/sgRNA Ribonucleoprotein Complexes via Hydroxystearyl Oligoamino Amides.* Bioconjug Chem, 2020. **31**(3): p. 729-742.
67. Kuhn, J., et al., *Supramolecular Assembly of Aminoethylene-Lipopeptide PMO Conjugates into RNA Splice-Switching Nanomicelles.* Advanced Functional Materials, 2019. **29**(48): p. 1906432.
68. Lin, Y., et al., *Folate Receptor-Mediated Delivery of Cas9 RNP for Enhanced Immune Checkpoint Disruption in Cancer Cells.* Small, 2023. **19**(2): p. e2205318.

69. Thalmayr, S., et al., *Molecular Chameleon Carriers for Nucleic Acid Delivery: The Sweet Spot between Lipoplexes and Polyplexes.* Adv Mater, 2023. **35**(25): p. e2211105.
70. Haase, F., et al., *Lipoamino bundle LNPs for efficient mRNA transfection of dendritic cells and macrophages show high spleen selectivity.* Eur J Pharm Biopharm, 2024. **194**: p. 95-109.
71. Sahin, U., et al., *COVID-19 vaccine BNT162b1 elicits human antibody and TH1 T cell responses.* Nature, 2020. **586**(7830): p. 594-599.
72. Polack, F.P., et al., *Safety and Efficacy of the BNT162b2 mRNA Covid-19 Vaccine.* New England Journal of Medicine, 2020. **383**(27): p. 2603-2615.
73. Schoenmaker, L., et al., *mRNA-lipid nanoparticle COVID-19 vaccines: Structure and stability.* Int J Pharm, 2021. **601**: p. 120586.
74. Zhou, F., et al., *From structural design to delivery: mRNA therapeutics for cancer immunotherapy.* Exploration, 2023. **n/a**(n/a): p. 20210146.
75. Verbeke, R., et al., *Three decades of messenger RNA vaccine development.* Nano Today, 2019. **28**: p. 100766.
76. Han, G., et al., *Advances in mRNA therapeutics for cancer immunotherapy: From modification to delivery.* Adv Drug Deliv Rev, 2023. **199**: p. 114973.
77. Wojtczak, B.A., et al., *5'-Phosphorothiolate Dinucleotide Cap Analogues: Reagents for Messenger RNA Modification and Potent Small-Molecular Inhibitors of Decapping Enzymes.* J Am Chem Soc, 2018. **140**(18): p. 5987-5999.
78. Tan, L., et al., *Optimization of an mRNA vaccine assisted with cyclodextrin-polyethyleneimine conjugates.* Drug Deliv Transl Res, 2020. **10**(3): p. 678-689.
79. Anderson, B.R., et al., *Nucleoside modifications in RNA limit activation of 2'-5'-oligoadenylate synthetase and increase resistance to cleavage by RNase L.* Nucleic Acids Research, 2011. **39**(21): p. 9329-9338.
80. Heine, A., S. Juranek, and P. Brossart, *Clinical and immunological effects of mRNA vaccines in malignant diseases.* Mol Cancer, 2021. **20**(1): p. 52.
81. Lokugamage, M.P., et al., *Optimization of lipid nanoparticles for the delivery of nebulized therapeutic mRNA to the lungs.* Nature Biomedical Engineering, 2021. **5**(9): p. 1059-1068.
82. Mockey, M., et al., *mRNA-based cancer vaccine: prevention of B16 melanoma progression and metastasis by systemic injection of MART1 mRNA histidylated lipopolyplexes.* Cancer Gene Ther, 2007. **14**(9): p. 802-14.
83. Patel, A.K., et al., *Inhaled Nanoformulated mRNA Polyplexes for Protein Production in Lung Epithelium.* Adv Mater, 2019. **31**(8): p. e1805116.
84. Cabral, H., et al., *Block Copolymer Micelles in Nanomedicine Applications.* Chemical Reviews, 2018. **118**(14): p. 6844-6892.
85. Yang, Z., et al., *Large-scale generation of functional mRNA-encapsulating exosomes via cellular nanoporation.* Nat Biomed Eng, 2020. **4**(1): p. 69-83.

86. Verbeke, R., et al., *The dawn of mRNA vaccines: The COVID-19 case.* Journal of Controlled Release, 2021. **333**: p. 511-520.
87. Kim, J., et al., *Self-assembled mRNA vaccines.* Adv Drug Deliv Rev, 2021. **170**: p. 83-112.
88. Tilstra, G., et al., *Iterative Design of Ionizable Lipids for Intramuscular mRNA Delivery.* J Am Chem Soc, 2023. **145**(4): p. 2294-2304.
89. Sabnis, S., et al., *A Novel Amino Lipid Series for mRNA Delivery: Improved Endosomal Escape and Sustained Pharmacology and Safety in Non-human Primates.* Mol Ther, 2018. **26**(6): p. 1509-1519.
90. Hassett, K.J., et al., *Optimization of Lipid Nanoparticles for Intramuscular Administration of mRNA Vaccines.* Mol Ther Nucleic Acids, 2019. **15**: p. 1-11.
91. Liu, Z., et al., *Non-viral nanoparticles for RNA interference: Principles of design and practical guidelines.* Advanced Drug Delivery Reviews, 2021. **174**: p. 576-612.
92. Fire, A., et al., *Potent and specific genetic interference by double-stranded RNA in Caenorhabditis elegans.* nature, 1998. **391**(6669): p. 806-811.
93. Elbashir, S.M., et al., *Duplexes of 21-nucleotide RNAs mediate RNA interference in cultured mammalian cells.* Nature, 2001. **411**(6836): p. 494-8.
94. Lam, J.K., et al., *siRNA Versus miRNA as Therapeutics for Gene Silencing.* Mol Ther Nucleic Acids, 2015. **4**(9): p. e252.
95. Lokugamage, M.P., et al., *Constrained Nanoparticles Deliver siRNA and sgRNA to T Cells In Vivo without Targeting Ligands.* Adv Mater, 2019. **31**(41): p. e1902251.
96. Ipsaro, J.J. and L. Joshua-Tor, *From guide to target: molecular insights into eukaryotic RNA-interference machinery.* Nat Struct Mol Biol, 2015. **22**(1): p. 20-8.
97. Lai, C.F., C.Y. Chen, and L.C. Au, *Comparison between the repression potency of siRNA targeting the coding region and the 3'-untranslated region of mRNA.* Biomed Res Int, 2013. **2013**: p. 637850.
98. Kraynack, B.A. and B.F. Baker, *Small interfering RNAs containing full 2'-O-methylribonucleotide-modified sense strands display Argonaute2/eIF2C2-dependent activity.* Rna, 2006. **12**(1): p. 163-76.
99. Sledz, C.A., et al., *Activation of the interferon system by short-interfering RNAs.* Nat Cell Biol, 2003. **5**(9): p. 834-9.
100. Hoy, S.M., *Patisiran: First Global Approval.* Drugs, 2018. **78**(15): p. 1625-1631.
101. Syed, Y.Y., *Givosiran: A Review in Acute Hepatic Porphyria.* Drugs, 2021. **81**(7): p. 841-848.
102. Garrelfs, S.F., et al., *Lumasiran, an RNAi Therapeutic for Primary Hyperoxaluria Type 1.* N Engl J Med, 2021. **384**(13): p. 1216-1226.
103. Lamb, Y.N., *Inclisiran: First Approval.* Drugs, 2021. **81**(3): p. 389-395.
104. Mullard, A., *FDA approves fifth RNAi drug - Alnylam's next-gen hATTR treatment.* Nat Rev Drug Discov, 2022. **21**(8): p. 548-549.

105. Witzigmann, D., et al., *Lipid nanoparticle technology for therapeutic gene regulation in the liver.* Adv Drug Deliv Rev, 2020. **159**: p. 344-363.
106. Nair, J.K., et al., *Impact of enhanced metabolic stability on pharmacokinetics and pharmacodynamics of GalNAc–siRNA conjugates.* Nucleic Acids Research, 2017. **45**(19): p. 10969-10977.
107. Rajeev, K.G., et al., *Hepatocyte-specific delivery of siRNAs conjugated to novel non-nucleosidic trivalent N-acetylgalactosamine elicits robust gene silencing in vivo.* Chembiochem, 2015. **16**(6): p. 903-8.
108. Patel, P., et al., *Development of amino acid-modified biodegradable lipid nanoparticles for siRNA delivery.* Acta Biomaterialia, 2022. **154**: p. 374-384.
109. Khare, P., et al., *Development of Lipidoid Nanoparticles for siRNA Delivery to Neural Cells.* The AAPS Journal, 2021. **24**(1): p. 8.
110. Gehring, N.H. and J.Y. Roignant, *Anything but Ordinary - Emerging Splicing Mechanisms in Eukaryotic Gene Regulation.* Trends Genet, 2021. **37**(4): p. 355-372.
111. Black, A.J., J.R. Gamarra, and J. Giudice, *More than a messenger: Alternative splicing as a therapeutic target.* Biochimica et Biophysica Acta (BBA) - Gene Regulatory Mechanisms, 2019. **1862**(11): p. 194395.
112. Marasco, L.E. and A.R. Kornblihtt, *The physiology of alternative splicing.* Nature Reviews Molecular Cell Biology, 2023. **24**(4): p. 242-254.
113. Monani, U.R., et al., *A single nucleotide difference that alters splicing patterns distinguishes the SMA gene SMN1 from the copy gene SMN2.* Hum Mol Genet, 1999. **8**(7): p. 1177-83.
114. Goedert, M. and R. Jakes, *Mutations causing neurodegenerative tauopathies.* Biochimica et Biophysica Acta (BBA) - Molecular Basis of Disease, 2005. **1739**(2): p. 240-250.
115. Dvinge, H., et al., *RNA splicing factors as oncoproteins and tumour suppressors.* Nat Rev Cancer, 2016. **16**(7): p. 413-30.
116. Havens, M.A. and M.L. Hastings, *Splice-switching antisense oligonucleotides as therapeutic drugs.* Nucleic Acids Research, 2016. **44**(14): p. 6549-6563.
117. de Smet, M.D., C.J. Meenken, and G.J. van den Horn, *Fomivirsen - a phosphorothioate oligonucleotide for the treatment of CMV retinitis.* Ocul Immunol Inflamm, 1999. **7**(3-4): p. 189-98.
118. Moreno, P.M.D., et al., *Delivery of Splice Switching Oligonucleotides by Amphiphilic Chitosan-Based Nanoparticles.* Molecular Pharmaceutics, 2016. **13**(2): p. 344-356.
119. Godfrey, C., et al., *Delivery is key: lessons learnt from developing splice-switching antisense therapies.* EMBO Mol Med, 2017. **9**(5): p. 545-557.
120. Rosenke, K., et al., *Inhibition of SARS-CoV-2 in Vero cell cultures by peptide-conjugated morpholino oligomers.* Journal of Antimicrobial Chemotherapy, 2020. **76**(2): p. 413-417.
121. Lim, K.H., et al., *Antisense oligonucleotide modulation of non-productive alternative splicing upregulates gene expression.* Nature Communications, 2020. **11**(1): p. 3501.

122. Ledford, H. and E. Callaway, *Pioneers of revolutionary CRISPR gene editing win chemistry Nobel.* Nature, 2020. **586**(7829): p. 346-347.
123. Philippidis, A., *CASGEVY Makes History as FDA Approves First CRISPR/Cas9 Genome Edited Therapy.* Human Gene Therapy, 2024. **35**(1-2): p. 1-4.
124. Gillmore, J.D., et al., *CRISPR-Cas9 In Vivo Gene Editing for Transthyretin Amyloidosis.* N Engl J Med, 2021. **385**(6): p. 493-502.
125. Carvalho, T., *CRISPR-Cas9 hits its target in amyloidosis.* Nature medicine, 2022. **28**(12): p. 2438.
126. Ishino, Y., et al., *Nucleotide sequence of the iap gene, responsible for alkaline phosphatase isozyme conversion in Escherichia coli, and identification of the gene product.* J Bacteriol, 1987. **169**(12): p. 5429-33.
127. Lander, Eric S., *The Heroes of CRISPR.* Cell, 2016. **164**(1): p. 18-28.
128. Li, Y., et al., *Ex vivo cell-based CRISPR/Cas9 genome editing for therapeutic applications.* Biomaterials, 2020. **234**: p. 119711.
129. He, Z.Y., et al., *Non-viral and viral delivery systems for CRISPR-Cas9 technology in the biomedical field.* Sci China Life Sci, 2017. **60**(5): p. 458-467.
130. Xu, C., et al., *Targeting of NLRP3 inflammasome with gene editing for the amelioration of inflammatory diseases.* Nature Communications, 2018. **9**(1): p. 4092.
131. Abbasi, S., et al., *Co-encapsulation of Cas9 mRNA and guide RNA in polyplex micelles enables genome editing in mouse brain.* J Control Release, 2021. **332**: p. 260-268.
132. Liu, J., et al., *Fast and Efficient CRISPR/Cas9 Genome Editing In Vivo Enabled by Bioreducible Lipid and Messenger RNA Nanoparticles.* Adv Mater, 2019. **31**(33): p. e1902575.
133. Miller, J.B., et al., *Non-Viral CRISPR/Cas Gene Editing In Vitro and In Vivo Enabled by Synthetic Nanoparticle Co-Delivery of Cas9 mRNA and sgRNA.* Angew Chem Int Ed Engl, 2017. **56**(4): p. 1059-1063.
134. Wei, T., et al., *Lung SORT LNPs enable precise homology-directed repair mediated CRISPR/Cas genome correction in cystic fibrosis models.* Nat Commun, 2023. **14**(1): p. 7322.
135. Lessl, A.L., et al., *mCherry on Top: A Positive Read-Out Cellular Platform for Screening DMD Exon Skipping Xenopeptide-PMO Conjugates.* Bioconjug Chem, 2023. **34**.
136. Germer, J., et al., *Lipo-Xenopeptide Polyplexes for CRISPR/Cas9 based Gene editing at ultra-low dose.* Journal of Controlled Release, 2024. **370**: p. 239-255.
137. inotiv. *A inbred mice A/JOlaHsd*. 2024 21.02.2024]; Available from: https://www.inotivco.com/model/a-jolahsd?selctry=The+Netherlands&ctry.
138. labs, j. *BALB/cJRj Mouse*. 2011 21.01.2024]; Available from: https://janvier-labs.com/en/fiche_produit/balb-cjrj_mouse/.
139. Justiz, B.d. *Tierschutzgesetz (TierSchG) §11*. 2022 21.02.2024]; Available from: https://www.gesetze-im-internet.de/tierschg/__11.html.

140. Faustino-Rocha, A., et al., *Estimation of rat mammary tumor volume using caliper and ultrasonography measurements.* Lab Anim (NY), 2013. **42**(6): p. 217-24.
141. Kormann, M.S.D., et al., *Expression of therapeutic proteins after delivery of chemically modified mRNA in mice.* Nature Biotechnology, 2011. **29**(2): p. 154-157.
142. *The Nobel Prize. Press Release: The Nobel Assembly at Karolinska Institutet.* . 2023 27.02.2024]; Available from: https://www.nobelprize.org/prizes/medicine/2023/press-release/.
143. Ahmed, K.S., et al., *Liposome: composition, characterisation, preparation, and recent innovation in clinical applications.* J Drug Target, 2019. **27**(7): p. 742-761.
144. Eygeris, Y., et al., *Chemistry of Lipid Nanoparticles for RNA Delivery.* Accounts of Chemical Research, 2022. **55**(1): p. 2-12.
145. Zhao, C., et al., *"Sheddable" PEG-lipid to balance the contradiction of PEGylation between long circulation and poor uptake.* Nanoscale, 2016. **8**(20): p. 10832-10842.
146. Rietwyk, S. and D. Peer, *Next-generation lipids in RNA interference therapeutics.* ACS nano, 2017. **11**(8): p. 7572-7586.
147. Sun, D. and Z.R. Lu, *Structure and Function of Cationic and Ionizable Lipids for Nucleic Acid Delivery.* Pharm Res, 2023. **40**(1): p. 27-46.
148. Kulkarni, J.A., et al., *On the Formation and Morphology of Lipid Nanoparticles Containing Ionizable Cationic Lipids and siRNA.* ACS Nano, 2018. **12**(5): p. 4787-4795.
149. Gilleron, J., et al., *Image-based analysis of lipid nanoparticle-mediated siRNA delivery, intracellular trafficking and endosomal escape.* Nat Biotechnol, 2013. **31**(7): p. 638-46.
150. Kim, J., et al., *Engineering Lipid Nanoparticles for Enhanced Intracellular Delivery of mRNA through Inhalation.* ACS Nano, 2022. **16**(9): p. 14792-14806.
151. Liu, S., et al., *Membrane-destabilizing ionizable phospholipids for organ-selective mRNA delivery and CRISPR–Cas gene editing.* Nature Materials, 2021. **20**(5): p. 701-710.
152. Ding, F., et al., *Boosting ionizable lipid nanoparticle-mediated in vivo mRNA delivery through optimization of lipid amine-head groups.* Biomaterials Science, 2021. **9**(22): p. 7534-7546.
153. Kimura, S. and H. Harashima, *On the mechanism of tissue-selective gene delivery by lipid nanoparticles.* J Control Release, 2023. **362**: p. 797-811.
154. Lam, K., et al., *Unsaturated, Trialkyl Ionizable Lipids are Versatile Lipid-Nanoparticle Components for Therapeutic and Vaccine Applications.* Advanced Materials, 2023. **35**(15): p. 2209624.
155. Yazdi, M., et al., *In Vivo Endothelial Cell Gene Silencing by siRNA-LNPs Tuned with Lipoamino Bundle Chemical and Ligand Targeting.* Small, 2024. **n/a**(n/a): p. 2400643.
156. Adams, D., et al., *Patisiran, an RNAi Therapeutic, for Hereditary Transthyretin Amyloidosis.* N Engl J Med, 2018. **379**(1): p. 11-21.
157. Kim, M., et al., *Engineered ionizable lipid nanoparticles for targeted delivery of RNA therapeutics into different types of cells in the liver.* Science advances, 2021. **7**(9): p. eabf4398.

158. Gibert-Ramos, A., et al., *The Hepatic Sinusoid in Chronic Liver Disease: The Optimal Milieu for Cancer.* Cancers (Basel), 2021. **13**(22).
159. Pattipeiluhu, R., et al., *Anionic Lipid Nanoparticles Preferentially Deliver mRNA to the Hepatic Reticuloendothelial System.* Adv Mater, 2022. **34**(16): p. e2201095.
160. Akinc, A., et al., *A combinatorial library of lipid-like materials for delivery of RNAi therapeutics.* Nat Biotechnol, 2008. **26**(5): p. 561-9.
161. Shahani, T., et al., *Human liver sinusoidal endothelial cells but not hepatocytes contain factor VIII.* J Thromb Haemost, 2014. **12**(1): p. 36-42.
162. Kole, R., A.R. Krainer, and S. Altman, *RNA therapeutics: beyond RNA interference and antisense oligonucleotides.* Nature Reviews Drug Discovery, 2012. **11**(2): p. 125-140.
163. Mendell, J.R., et al., *Eteplirsen for the treatment of Duchenne muscular dystrophy.* Annals of Neurology, 2013. **74**(5): p. 637-647.
164. Servais, L., et al., *Long-Term Safety and Efficacy Data of Golodirsen in Ambulatory Patients with Duchenne Muscular Dystrophy Amenable to Exon 53 Skipping: A First-in-human, Multicenter, Two-Part, Open-Label, Phase 1/2 Trial.* Nucleic Acid Therapeutics, 2022. **32**(1): p. 29-39.
165. Clemens, P.R., et al., *Long-Term Functional Efficacy and Safety of Viltolarsen in Patients with Duchenne Muscular Dystrophy.* Journal of Neuromuscular Diseases, 2022. **9**: p. 493-501.
166. Wagner, K.R., et al., *Safety, tolerability, and pharmacokinetics of casimersen in patients with Duchenne muscular dystrophy amenable to exon 45 skipping: A randomized, double-blind, placebo-controlled, dose-titration trial.* Muscle & Nerve, 2021. **64**(3): p. 285-292.
167. Duan, D., et al., *Duchenne muscular dystrophy.* Nat Rev Dis Primers, 2021. **7**(1): p. 13.
168. García-Rodríguez, R., et al., *Premature termination codons in the DMD gene cause reduced local mRNA synthesis.* Proc Natl Acad Sci U S A, 2020. **117**(28): p. 16456-16464.
169. Le, B.T., et al., *Thiomorpholino oligonucleotides as a robust class of next generation platforms for alternate mRNA splicing.* Proceedings of the National Academy of Sciences, 2022. **119**(36): p. e2207956119.
170. Gan, L., et al., *A cell-penetrating peptide enhances delivery and efficacy of phosphorodiamidate morpholino oligomers in mdx mice.* Mol Ther Nucleic Acids, 2022. **30**: p. 17-27.
171. López-Vidal, E.M., et al., *Deep Learning Enables Discovery of a Short Nuclear Targeting Peptide for Efficient Delivery of Antisense Oligomers.* JACS Au, 2021. **1**(11): p. 2009-2020.
172. Truebenbach, I., et al., *Combination Chemotherapy of L1210 Tumors in Mice with Pretubulysin and Methotrexate Lipo-Oligomer Nanoparticles.* Mol Pharm, 2019. **16**(6): p. 2405-2417.
173. Klein, P.M., et al., *Folate receptor-directed orthogonal click-functionalization of siRNA lipopolyplexes for tumor cell killing in vivo.* Biomaterials, 2018. **178**: p. 630-642.

174. Kaushal, J., et al., *Click chemistry in the synthesis of catalytically relevant organoselenium compounds: development and applications of catalysts for organic synthesis.* New Journal of Chemistry, 2022. **46**(31): p. 14757-14781.
175. Dunckley, M.G., et al., *Modification of splicing in the dystrophin gene in cultured Mdx muscle cells by antisense oligoribonucleotides.* Hum Mol Genet, 1998. **7**(7): p. 1083-90.
176. Bulfield, G., et al., *X chromosome-linked muscular dystrophy (mdx) in the mouse.* Proc Natl Acad Sci U S A, 1984. **81**(4): p. 1189-92.
177. Lehto, T., et al., *Cellular trafficking determines the exon skipping activity of Pip6a-PMO in mdx skeletal and cardiac muscle cells.* Nucleic Acids Res, 2014. **42**(5): p. 3207-17.
178. Osborn, M.J., et al., *TALEN-based Gene Correction for Epidermolysis Bullosa.* Molecular Therapy, 2013. **21**(6): p. 1151-1159.
179. Muenzer, J., et al., *CHAMPIONS: A phase 1/2 clinical trial with dose escalation of SB-913 ZFN-mediated in vivo human genome editing for treatment of MPS II (Hunter syndrome).* Molecular Genetics and Metabolism, 2019. **126**(2): p. S104.
180. Jinek, M., et al., *A programmable dual-RNA-guided DNA endonuclease in adaptive bacterial immunity.* Science, 2012. **337**(6096): p. 816-21.
181. Cerci, B., et al., *Clinical trials and promising preclinical applications of CRISPR/Cas gene editing.* Life Sci, 2023. **312**: p. 121204.
182. Jiang, F. and J.A. Doudna, *CRISPR–Cas9 Structures and Mechanisms.* Annual Review of Biophysics, 2017. **46**(1): p. 505-529.
183. Ran, F.A., et al., *In vivo genome editing using Staphylococcus aureus Cas9.* Nature, 2015. **520**(7546): p. 186-191.
184. Liu, Q., et al., *Virus-like nanoparticle as a co-delivery system to enhance efficacy of CRISPR/Cas9-based cancer immunotherapy.* Biomaterials, 2020. **258**: p. 120275.
185. Li, C. and R.J. Samulski, *Engineering adeno-associated virus vectors for gene therapy.* Nature Reviews Genetics, 2020. **21**(4): p. 255-272.
186. Chen, G., et al., *A biodegradable nanocapsule delivers a Cas9 ribonucleoprotein complex for in vivo genome editing.* Nature Nanotechnology, 2019. **14**(10): p. 974-980.
187. Jiang, C., et al., *A non-viral CRISPR/Cas9 delivery system for therapeutically targeting HBV DNA and pcsk9 in vivo.* Cell Research, 2017. **27**(3): p. 440-443.
188. Baden, L.R., et al., *Efficacy and Safety of the mRNA-1273 SARS-CoV-2 Vaccine.* New England Journal of Medicine, 2020. **384**(5): p. 403-416.
189. Kenjo, E., et al., *Low immunogenicity of LNP allows repeated administrations of CRISPR-Cas9 mRNA into skeletal muscle in mice.* Nature Communications, 2021. **12**(1): p. 7101.
190. Yang, P., et al., *Nano-vectors for CRISPR/Cas9-mediated genome editing.* Nano Today, 2022. **44**: p. 101482.

191. Scully, R., et al., *DNA double-strand break repair-pathway choice in somatic mammalian cells.* Nature Reviews Molecular Cell Biology, 2019. **20**(11): p. 698-714.
192. Takata, M., et al., *Homologous recombination and non-homologous end-joining pathways of DNA double-strand break repair have overlapping roles in the maintenance of chromosomal integrity in vertebrate cells.* The EMBO Journal, 1998. **17**(18): p. 5497-5508.
193. Lin, Y., E. Wagner, and U. Lachelt, *Non-viral delivery of the CRISPR/Cas system: DNA versus RNA versus RNP.* Biomater Sci, 2022. **10**(5): p. 1166-1192.
194. Gaudelli, N.M., et al., *Programmable base editing of A•T to G•C in genomic DNA without DNA cleavage.* Nature, 2017. **551**(7681): p. 464-471.
195. Anzalone, A.V., et al., *Search-and-replace genome editing without double-strand breaks or donor DNA.* Nature, 2019. **576**(7785): p. 149-157.
196. Long, C., et al., *Postnatal genome editing partially restores dystrophin expression in a mouse model of muscular dystrophy.* Science, 2016. **351**(6271): p. 400-3.
197. Cheng, Q., et al., *Dendrimer-Based Lipid Nanoparticles Deliver Therapeutic FAH mRNA to Normalize Liver Function and Extend Survival in a Mouse Model of Hepatorenal Tyrosinemia Type I.* Adv Mater, 2018. **30**(52): p. e1805308.
198. Nelson, C.E., et al., *In vivo genome editing improves muscle function in a mouse model of Duchenne muscular dystrophy.* Science, 2016. **351**(6271): p. 403-7.
199. Petkova, M.V., et al., *Characterization of a DmdEGFPreporter mouse as a tool to investigate dystrophin expression.* Skeletal Muscle, 2016. **6**(1): p. 25.
200. Brzęk, P., et al., *Significance of variation in basal metabolic rate in laboratory mice for translational experiments.* J Comp Physiol B, 2022. **192**(1): p. 161-169.
201. Zu, H. and D. Gao, *Non-viral Vectors in Gene Therapy: Recent Development, Challenges, and Prospects.* Aaps j, 2021. **23**(4): p. 78.
202. Waldmann, T.A., *Immunotherapy: past, present and future.* Nature Medicine, 2003. **9**(3): p. 269-277.
203. Jones, D., *Silencing the sceptics.* Nature Reviews Drug Discovery, 2004. **3**(12): p. 997-997.
204. Jia, Y., et al., *Lipid Nanoparticles Optimized for Targeting and Release of Nucleic Acid.* Advanced Materials, 2023. **n/a**(n/a): p. 2305300.
205. Bronte, V. and M.J. Pittet, *The spleen in local and systemic regulation of immunity.* Immunity, 2013. **39**(5): p. 806-18.
206. Yang, T., et al., *Efficient hepatic delivery and protein expression enabled by optimized mRNA and ionizable lipid nanoparticle.* Bioactive Materials, 2020. **5**(4): p. 1053-1061.
207. Sago, C.D., et al., *Cell Subtypes Within the Liver Microenvironment Differentially Interact with Lipid Nanoparticles.* Cellular and Molecular Bioengineering, 2019. **12**(5): p. 389-397.

208. Tsoi, K.M., et al., *Mechanism of hard-nanomaterial clearance by the liver.* Nature Materials, 2016. **15**(11): p. 1212-1221.
209. Sato, Y., et al., *Highly specific delivery of siRNA to hepatocytes circumvents endothelial cell-mediated lipid nanoparticle-associated toxicity leading to the safe and efficacious decrease in the hepatitis B virus.* Journal of Controlled Release, 2017. **266**: p. 216-225.
210. Abrams, M.T., et al., *Evaluation of Efficacy, Biodistribution, and Inflammation for a Potent siRNA Nanoparticle: Effect of Dexamethasone Co-treatment.* Molecular Therapy, 2010. **18**(1): p. 171-180.
211. Aoki, Y., et al., *Bodywide skipping of exons 45-55 in dystrophic mdx52 mice by systemic antisense delivery.* Proc Natl Acad Sci U S A, 2012. **109**(34): p. 13763-8.
212. Hara, Y., et al., *Novel EGFP reporter cell and mouse models for sensitive imaging and quantification of exon skipping.* Scientific Reports, 2020. **10**.
213. Veltrop, M., et al., *A dystrophic Duchenne mouse model for testing human antisense oligonucleotides.* PLOS ONE, 2018. **13**(2): p. e0193289.
214. t Hoen, P.A., et al., *Generation and characterization of transgenic mice with the full-length human DMD gene.* J Biol Chem, 2008. **283**(9): p. 5899-907.
215. Goemans, N.M., et al., *Systemic administration of PRO051 in Duchenne's muscular dystrophy.* N Engl J Med, 2011. **364**(16): p. 1513-22.
216. Verhaart, I.E., et al., *The Dynamics of Compound, Transcript, and Protein Effects After Treatment With 2OMePS Antisense Oligonucleotides in mdx Mice.* Mol Ther Nucleic Acids, 2014. **3**(2): p. e148.
217. Moretti, A., et al., *Somatic gene editing ameliorates skeletal and cardiac muscle failure in pig and human models of Duchenne muscular dystrophy.* Nat Med, 2020. **26**(2): p. 207-214.
218. Engelhardt, J.A., *Comparative Renal Toxicopathology of Antisense Oligonucleotides.* Nucleic Acid Therapeutics, 2016. **26**(4): p. 199-209.
219. Moulton, H.M. and J.D. Moulton, *Morpholinos and their peptide conjugates: therapeutic promise and challenge for Duchenne muscular dystrophy.* Biochim Biophys Acta, 2010. **1798**(12): p. 2296-303.
220. Abdelnour, S.A., et al., *The Potential of CRISPR/Cas9 Gene Editing as a Treatment Strategy for Inherited Diseases.* Front Cell Dev Biol, 2021. **9**: p. 699597.
221. Liang, F., et al., *Efficient Targeting and Activation of Antigen-Presenting Cells In Vivo after Modified mRNA Vaccine Administration in Rhesus Macaques.* Mol Ther, 2017. **25**(12): p. 2635-2647.
222. Kosicki, M., et al., *Cas9-induced large deletions and small indels are controlled in a convergent fashion.* Nature Communications, 2022. **13**(1): p. 3422.
223. Kosicki, M., K. Tomberg, and A. Bradley, *Repair of double-strand breaks induced by CRISPR–Cas9 leads to large deletions and*

complex rearrangements. Nature Biotechnology, 2018. **36**(8): p. 765-771.
224. Sander, J.D. and J.K. Joung, *CRISPR-Cas systems for editing, regulating and targeting genomes.* Nature Biotechnology, 2014. **32**(4): p. 347-355.
225. Doench, J.G., et al., *Rational design of highly active sgRNAs for CRISPR-Cas9–mediated gene inactivation.* Nature Biotechnology, 2014. **32**(12): p. 1262-1267.

VIII. APPENDIX

1. Publications

Lin, Y., Wilk, U., Pöhmerer, J., Hörterer, E., Höhn, M., Luo, X., Mai, H., Wagner, E., Lächelt, U., **Folate Receptor-Mediated Delivery of Cas9 RNP for Enhanced Immune Checkpoint Disruption in Cancer Cells.** Small 2023, 19, 2205318.

Thalmayr, S.; Grau, M.; Peng, L.; Pöhmerer, J.; Wilk, U.; Folda, P.; Yazdi, M.; Weidinger, E.; Burghardt, T.; Höhn, M.; Wagner, E.; Berger, S. **Molecular Chameleon Carriers for Nucleic Acid Delivery: The Sweet Spot Between Lipoplexes and Polyplexes.** Adv. Mater. 2023, 35, 2211105

Lessl AL, Pöhmerer J, Lin Y, Wilk U, Höhn M, Hörterer E, Wagner E, Lächelt U. **mCherry on Top: A Positive Read-Out Cellular Platform for Screening DMD Exon Skipping Xenopeptide-PMO Conjugates**. Bioconjugate Chem. 2023, 34, 2263–2274

Zeyn, Y, Hobernik, D, Wilk, U, Pöhmerer, J, Hieber, C, Medina-Montano, C, Rohrig, N, Strahle, C. F, Thoma-Kress, A. K, Wagner, E, Bros, M, Berger, S. **Transcriptional Targeting of Dendritic Cells Using an Optimized Human Fascin1 Gene Promoter** Int J Mol Sci. 2023, 24, 16938

Haase F, Pöhmerer J, Yazdi M, Grau M, Zeyn Y, Wilk U, Burghardt T, Höhn M, Hieber C, Bros M, Wagner E, Berger S. **Lipoamino bundle LNPs for efficient mRNA transfection of dendritic cells and macrophages show high spleen selectivity**. Eur. J. Pharm. Biopharm. 2024, 194, 95–109

Germer J., Lessl AL, Pöhmerer J, Grau M, Weidinger E, Höhn M, Yazdi M, Cappelluti M.A, Lombardo A, Lächelt U, Wagner E **Lipo-Xenopeptide Polyplexes for CRISPR Cas9 Based Gene Editing at Ultra-Low Dose Targeting.** Journal of Controlled Release 2024, 370, 239-255

Yazdi M, Pöhmerer J, Hasanzadeh Kafshgari M, Seidl J, Grau M, Höhn M, Vetter V, Hoch C.C, Wollenberg B., Multhoff G., Bashiri Dezfouli A, Wagner

E. **In Vivo Endothelial Cell Gene Silencing by siRNA-LNPs Tuned with Lipoamino Bundle Chemical and Ligand Targeting**. Small 2024, 2400643

Köhler B, Brieger E, Brandstätter T, Hörterer E, Wilk U, Pöhmerer J, Jötten A, Paulitschke P, Broedersz C.P, Zahler S, Rädler J. O, Wagner E, Roidl A. **Unravelling the metastasis-preventing effect of miR-200c *in vitro* and *in vivo*.** Molecular Oncology 2024 (*Manuscript accepted for publication*)

2. Abstracts

Thalmayr, S.; Grau, M.; Peng, L.; Pöhmerer, J.; Wilk, U.; Folda, P.; Yazdi, M.; Weidinger, E.; Burghardt, T.; Höhn, M.; Wagner, E.; Berger, S. **Molecular Chameleon Carriers for Nucleic Acid Delivery: The Sweet Spot Between Lipoplexes and Polyplexes.** ASGCT 26th Annual Meeting 2023, Los Angeles, CA, United States of America, May 2023

Yazdi M, Pöhmerer J, Kafshgari MH, Seidl J, Grau M, Höhn M, Hoch C.C, Wollenberg B., Multhoff G., Dezfouli AB, Wagner E**. In Vivo Endothelial Cell Gene Silencing by siRNA-LNPs Tuned with Lipoamino Bundle Chemical and Ligand Targeting.** DG-GT Annual Meeting 2024, Munich, Germany, March 2024

Germer J., Lessl AL, Pöhmerer J, Grau M, Höhn M, Weidinger E, Yazdi M, Cappelluti M.A, Lombardo A, Lächelt U, Wagner E **Lipo-Xenopeptide Polyplexes for CRISPR Cas9 Based Gene Editing at Ultra-Low Dose Targeting.** DG-GT Annual Meeting 2024, Munich, Germany, March 2024

IX. ACKNOWLEDGEMENTS

First of all, I would like to thank Prof. Dr. Ernst Wagner for giving me the opportunity to write my thesis at his Chair of Pharmaceutical Biology and Biotechnology. It was an honor to be mentored in such a supportive way and to be entrusted with the supervision of the animal facility as well as the coordination of the *in vivo* experiments. I am very thankful to have been part of many great collaborations on interesting research topics.

Moreover, I would like to thank Prof. Dr. Eckhard Wolf for his supervision on behalf of the Faculty of Veterinary Medicine.

I would also like to thank my amazing colleagues who have created a great working atmosphere and have become a group of friends that I will definitely miss in the future. Thank you, Elisa and Uli, for welcoming me into your little veterinary family and teaching me all the important tasks. From the moment I started working, it was very easy to integrate into your team. Thank you for all the advice you have given me along the way and the pleasure of getting to know your unique personalities.

Thank you, Mina, for being such a great coworker in our small animal facility over the past year. I admired your scientific work, great advice and personality to keep going in the most stressful situations. Thank you very much, Simone, for all your advice and support during my research and finally the writing of my dissertation.

A big thank you goes to my better half, Oliver, who has supported me all my life and especially in the last difficult years and months with his loving nature.
I would also like to thank my mother, Christa, who has dedicated her life to my future. Without you I would not have been able to achieve all this.

The last two thank-yous are sent to heaven, where two great men are watching from above. Thank you, Markus, for the warm and funny way you took care of our animals, and thank you, Papa, for the inspiration you gave me for my academic journey. I hope I was able to fulfill our dream and I wish you could be here to celebrate with me.